# University of Glasgow

Taylor, William Alexander (2023) *Contactless artificial intelligence-enabled radio frequency sensing for healthcare applications.* PhD thesis.

https://theses.gla.ac.uk/83473/

# Contactless Artificial Intelligence-enabled Radio Frequency Sensing for Healthcare Applications

William Alexander Taylor

Submitted in fulfilment of the requirements for the
Degree of Doctor of Philosophy

School of Engineering
College of Science and Engineering
University of Glasgow



January 2023

# Abstract

Human motion detection is getting considerable attention in the field of Artificial Intelligence (AI) driven healthcare systems. Human motion detection can be used to provide remote healthcare solutions for vulnerable people by identifying particular movements such as falls, gait and breathing/heart disorders. This can allow people to live more independent lifestyles with the safety of being monitored if more direct care is needed. At present contact-based devices can provide real-time monitoring by deploying devices on a person's body. However, placing devices on a person's body all the time can be uncomfortable. Elderly people are also at risk of forgetting to wear devices. additionally, contact-based devices also require removal for recharging due to battery requirements. This thesis details the work that has been undertaken in the field of non-contact monitoring of human movements and vital signs. There is current research looking at using camera and radar technology to monitor vulnerable people within the home however, these techniques come with some disadvantages. Camera technology in the home has privacy concerns as people can feel uncomfortable being watched and radar technology introduces new technology into the home. This thesis explores the use of Radio Frequency (RF) signals to sense human movements and vital signs. RF signals are currently present in many homes as Wi-Fi networks already emit RF signals through the home. As people move around these signals, signal propagation is affected. Channel State Information (CSI) describes how a signal propagated from the transmitter to the receiver. This thesis takes the CSI and employs Machine Learning (ML) techniques to associate patterns observed in the CSI with specific movements. This principle is used to develop a real-time monitoring system that can detect what movements have occurred. The results of this thesis have shown to be able to differentiate between different activities using RF signals with over 90 % accuracy. This thesis serves as a proof of concept for contactless fall and vital sign detection systems that can assist elderly and vulnerable people to live independently without the need to wear monitoring devices.

# Contents

# List of Tables

# List of Figures

# List of Abbreviations

AI - Artificial Intelligence

ADLs - Activities of Daily Living

BiLSTM - Bi-directional Long Short-Term Memory

BPM - Beats Per Minute

BVP - Blood Volume Pulse

CNN - Convolutional Neural Network

COVID19 - COronaVIrusDisease 2019

CSI - Channel State Information

CT - Computed Tomography

DNN - Deep Neural Network

DTW - Dynamic Time Warping

DWT - Discrete Wavelet Transform

EWMA - Exponentially Weighted Moving Average

FFT - Fast Fourier Transformer

FMCW - Frequency-Modulated Continuous-Wave

FN - False Negative

FP - False Positive

GLCM - Grey Level Cooccurrence Matrix

GLRLM - Grey Level Run Length Matrix

GLSZM - Grey Level Size Zone Matrix

GPU - Graphic Processing Unit

GRU - Gated Recurrent Unit

HMM - Hidden Markov Model

HITL - Human-In-The-Loop

HMP - Human Motion Primitives

IR-UWB - Impulse-Radio Ultra-Wideband

IMU - Inertial Measurement Unit

KNN - K Nearest Neighbour

LDA - Linear Discriminant Analysis

LDP - Local Directional Patterns

LSTM - Long Short-Term Memory

MEMS - Micro Electromechanical System

ML – Machine Learning

NAN - Not A Number

NHS - National Health Service

NI – National Instruments

OFDM - Orthogonal Frequency Division Multiplexing

PCA – Principal Component Analysis

RF - Radio Frequency

ReLU - Rectified Linear Unit

RGB - Red Green and Blue

RSA - Rivest-Shamir-Adleman

RNN - Recurring Neural Networks

SDRs - Software-Defined Radios

SFS - Sequential Forward Selection

SARS-CoV-2 - Severe Acute Respiratory Syndrome Coronavirus 2

SVM - Support Vector Machine

TN - True Negative

TP - True Positive

UWB - Ultra Wide Band

USRP - Universal Software-defined Radio Peripheral

WHO - world health organisation

# List of Publications

This section lists papers authored within the duration of PhD study since December 2019. The list details the authors, title of the work, the publishing body and the status of the papers:

**Journal**:

1. Taylor, W., Shah, S. A., Dashtipour, K., Zahid, A., Abbasi, Q. H., & Imran, M. A. (2020). An intelligent non-invasive real-time human activity recognition system for next-generation healthcare. Sensors, 20(9), 2653. doi:https://doi.org/10.3390/s20092653. (Published)

2. Taylor, W., Abbasi, Q. H., Dashtipour, K., Ansari, S., Shah, S. A., Khalid, A., & Imran, M. A. (2020). A Review of the State of the Art in Non-Contact Sensing for COVID-19. Sensors, 20(19), 5665. doi: https://doi.org/10.3390/s20195665. (Published)

   Taylor, W., Dashtipour, K., Shah, S. A., Hussain, A., Abbasi, Q. H., & Imran, M. A. (2021). Radar sensing for activity classification in elderly people exploiting micro-doppler signatures using machine learning.
   Sensors, 21(11), 3881. doi: https://doi.org/10.3390/s21113881 (Published)

3. W. Taylor, M. Z. Khan, A. Tahir, A. Taha, Q. H. Abbasi and M. A. Imran, "An Implementation of Real-Time Activity Sensing Using Wi-Fi: Identifying Optimal Machine-Learning Techniques for Performance Evaluation," in IEEE Sensors Journal, vol. 22, no. 21, pp. 21127-21134, 1 Nov.1, 2022, doi: 10.1109/JSEN.2022.3201973.

4. W. Taylor, A. Taha, A. Tahir, A. Hussain, Q. H. Abbasi & M. A. Imran. WiFi Monitoring System for Vulnerable People with Encryption and Alert System. Computer Methods and Programs in Biomedicine Update. (Under Review)

**Conference**:

1. W. Taylor, S. A. Shah, K. Dashtipour, J. L. Kernec, Q. H. Abbasi, K. A. K.Arshad and M. A. Imran (2022). Wireless Sensing for Human Activity Recognition Using USRP. In: Ur Rehman, M., Zoha, A. (eds) Body Area Networks. Smart IoT and Big Data for Intelligent Health Management. BODYNETS 2021. Lecture Notes of the Institute for Computer Sciences, Social Informatics and Telecommunications Engineering, vol 420. Springer, Cham. https://doi.org/10.1007/978-3-030-95593-9_5

2. W. Taylor, A. Taha, K. Dashtipour, S. A. Shah, Q. H. Abbasi and M. A. Imran, "RF Based Real Time Human Motion Sensing," 2021 IEEE International Symposium on Antennas and Propagation and USNC-URSI Radio Science Meeting (APS/URSI), 2021, pp. 2044-2045, doi: 10.1109/APS/URSI47566.2021.9703954.

3. W. Taylor, A. Taha, K. Dashtipour, S. A. Shah, Q. H. Abbasi and M. A. Imran, "AI-based Real-time Classification of Human Activity using Software Defined Radios," 2021 1st International Conference on Microwave, Antennas & Circuits (ICMAC), 2021, pp. 1-4, doi: 10.1109/ICMAC54080.2021.9678242.

4. W. Taylor, A. Taha, A. Tahir, S. A. Shah, Q. H. Abbasi and M. A. Imran, "Novel Contactless Sensing Technique for Real-time Human Activity Detection," 2022 IEEE International Symposium on Antennas and Propagation and USNC-URSI Radio Science Meeting (AP-S/URSI), 2022, pp. 1562-1563, doi: 10.1109/AP-S/USNC-URSI47032.2022.9886894.

5. W. Taylor, A. Taha, A. Tahir, Q. H. Abbasi and M. A. Imran, (2022). "Real-Time Contactless WiFi Based Room Detection of Sitting and Standing Human Motions". In 2022 29th IEEE International Conference on Electronics Circuits and Systems (IEEE ICECS 2022)

# Acknowledgements

# Declaration

University of Glasgow

**University of Glasgow**
*College of Science and
Engineering*

I declare that the thesis does not include work forming part of a thesis presented successfully for another degree [unless explicitly identified and as noted below].

I declare that this thesis has been produced in accordance with the University of Glasgow's Code of Good Practice in Research.

I acknowledge that if any issues are raised regarding good research practice based on review of the thesis, the examination may be postponed pending the outcome of any investigation of the issues.

Signature: _____

Date: ____10/01/2023_____

**This completed statement must be bound into the submitted copies of the soft-bound thesis.**

# Statement of Copyright

The copyright of this thesis rests with the author. No quotation from it should be published without the author's prior written consent and information derived from it should be acknowledged.

# Chapter 1

# Introduction

## 1.1 General Background

In recent years, home healthcare through the use of different technologies has gained much attention for its ability to improve the lives of people who require special care [1]. Special care is required by a large number of people such as the elderly population. The elderly population is on the increase and this results in a decrease in the capacity of nursing homes [2, 3].

## 1.2 Problem Statement

The elderly population is set to increase to 2.1 billion in the year 2050 according to statistics from the United Nations [4]. With this expected increase in the elderly population, it will have even more strain on caregivers so dependencies on technology to support care will be needed to maintain support [5]. This presents a need to develop systems which can be used to ease the dependencies of care homes and caregivers by allowing technologies to take on the extra burden. Other advantages include allowing elderly and vulnerable people to be able to remain in their own homes and thus allowing greater independence and quality of life for these individuals.

## 1.3 Aims and Objectives

The aim of this thesis is to develop a non-invasive, contactless, AI-enabled Radio Frequency (RF) sensing system for real-time healthcare monitoring of human activities and vital signs. All the studies conducted in this thesis have been done after acquiring ethical approval from the college of science and engineering at the University of Glasgow. The objectives of this research are:

1. To investigate the existing systems in place to monitor human motion and vital signs.

2. To investigate machine learning techniques that can be used to classify data relating to human motion and vital signs.

3. To integrate artificial intelligence algorithms into the RF sensing system and to evaluate the performance and accuracy of the non-invasive, contactless, AI-enabled RF sensing system in a clinical setting.

4. To utilise available data in a range of experiments with varying parameters to produce results for analysis.

5. To design and develop an RF sensing system that can accurately measure human activities in real-time. Allowing vulnerable people to live independently within their homes without the need to wear sensors or have routine healthcare visits.

6. To design and develop an RF sensing system that can accurately measure vital signs such as heart rate and respiration rate without the need for physical contact.

7. To identify potential applications and benefits of the RF sensing system in various medical settings, such as hospitals, primary care clinics, and home healthcare environments.

## 1.4 Contributions

This thesis has proposed the use of RF sensing in real-time for healthcare applications. The key contributions are listed below:

1. Investigate the accuracy and computational cost of a range of machine-learning algorithms in the context of real-time radio frequency sensing.

2. Proposal of a real-time radio frequency sensing system that can accurately detect if a single subject is performing sitting, standing, or walking. Which serves as a proof of concept for fall detection.

3. Proposal of a real-time radio frequency sensing system that can accurately detect the breathing and heart rates of multiple subjects.

## 1.5 Thesis Organisation

This thesis is organised into the following chapters:

**Chapter 2** will list the current technologies and literature related to the field of human motion and vital sign detection.

**Chapter 3** reviews the way in which contactless sensing technologies can be used to detect COronaVIrusDisease 2019 (COVID-19). The chapter compares technologies such as CT Scanning, Radar, and RF sensing. The chapter concludes with the findings that although technologies such as CT scanning are highly accurate, the cost is high. Technologies such as Radar and RF sensing can be implemented at a fraction of the cost and provide high results.

**Chapter 4** details how ML techniques can be applied for image classifications of radar micro-Doppler signatures. The chapter makes use of traditional ML algorithms and deep learning neural network algorithms The radar images contained the movements of walking, sitting down, standing up, picking up an object, drinking water, and falling. The findings of the chapter show that through various data processing techniques, ML can accurately differentiate between different movements from the captured radar micro-Doppler signatures.

**Chapter 5** makes use of RF signals using a Universal Software-defined Radio Peripheral (USRP) to create wireless communication. A subject then performs sitting and standing between the transmitter antenna and the receiver antenna. The Channel State Information (CSI) data is then collected and ML algorithms are used to perform binary classification between sitting and standing classes, The ML algorithms used are Random Forest, K Nearest Neighbours (KNN), Support Vector Machine (SVM), neural network Model and an ensemble of all the algorithms together. The performance of each algorithm is analysed. the best-performing algorithm using the CSI data, Random Forest is used on a benchmark dataset using wearable technology and performed better using the CSI data.

**Chapter 6** develops a real-time monitoring system using RF signals. Data is collected for a person moving, remaining still and the area unoccupied. An (Artificial Intelligence ) AI model is created using a series of tested machine-learning algorithms. The AI model is created using the algorithm which performs the fastest and most accurately. The AI model is then used in a real-time system which continuously performs classification on a stream of data. Allowing the system to detect the movements of a person in real-time and if the person is remaining still or left the monitoring area.

**Chapter 7** builds on the previous chapter by developing a more advanced system which can detect specifically if a subject is standing or sitting using RF signals. This is achieved by using an overlapping function on the incoming CSI data. The data stream is overlapped by 80 % to ensure that any movements can be centred in the classification window. Techniques are used to filter windows to allow for a movement in the CSI to be centred. This ensures that the whole movement from start to finish is in the window so that an AI model can successfully classify the movement in the CSI data. If a movement is detected in the centre of the window then the

AI model can be used to classify if the data is sitting or standing. This allows for CSI data to be constantly fed into the running system and as movements occur the system can classify what movement occurred in real-time.

**Chapter 8** further develops the idea of a real-time RF-based monitoring system by adding functions to encrypt and store the data for storage on the cloud. As a monitoring system will observe people's movements it will be classified as sensitive data. This chapter encrypts data before storing it on the cloud. Then a central web server can download and decrypt the data for processing. This chapter introduces an additional classification of walking and a feature to email a desired recipient if no movements occur within a predefined time frame.

**Chapter 9** looks at further applications of using RF signals as a real-time monitoring system. As RF signals can be used to detect larger body movements such as sitting, standing or falling, this chapter looks at detecting smaller movements of the chest with the aim of vital sign estimation. The chapter details the experimental setup of how RF signals can be used to detect breathing and heart rates for multiple people. The breathing and heart rates detected using RF signals are compared to wearable sensors serving as ground truth with good results.

**Chapter 10** concludes the thesis and details future work to be considered for expanding the work discussed throughout the thesis.

# Chapter 2

# Literature Review

Human motion detection is an important area of research in the field of healthcare systems. Eventually, more and more sectors of the healthcare industry will begin to use technology [6, 7]. Motion detection is the process of using technology to extract the features of human movement [8, 9, 10]. Human motion detection can be used for the monitoring of patients and vulnerable people such as the elderly or young children [11, 12]. Motion detection can be used to detect if a human falls within the home. The World Health Organisation (WHO) reports that falls can cause around 646 thousand deaths and over 37 million serious injuries [13, 14]. If falls were able to be detected then family members or professional caregivers can be alerted of the person in distress and this can help to mitigate any injuries sustained or any potential fatalities [15]. Other examples of monitoring can be used for early detection and pre-emptive intervention of individuals suffering from Alzheimer's disease as the behaviour symptoms can be caused by the disease [16].

## 2.1 Contact-based

Techniques Human motion can be detected by the use of contact-based devices such as mobile devices or smart watches using accelerometers [17, 18]. Some types of contact-based devices include accelerometers and Strain sensors.

### 2.1.1 Accelerometers

Accelerometers are devices that can track human motion. Accelerometers are embedded into wearable devices or smartphones that subjects carry on their person [19]. This can be advantageous if the subject already owns a capable mobile device but can be expensive to provide a mobile device. contact-based devices can be in the form of smartwatches with accelerometers embedded. The accelerometers work together with gyroscopes to be able to determine the orientation of the subject's body [20]. The data received from the accelerometers can be applied to

ML algorithms to classify the human motion taking place [21].

### 2.1.2   Strain sensors

Strain sensors are an example of a contact-based device that can monitor body signals such as physical, chemical, and biological signals [22]. The strain sensors take the mechanical movements of a body and convert them into electrical signals [23]. Strain sensors need to be flexible with a large stretchability to be able to meet the demands of human motion detection [24]. Current strain sensor technology can monitor human joint motion, speaking, and deep breathing in real-time [25]. One of the challenges with using strain sensors to detect human motion is to obtain high performance while still being comfortable for the subject to wear [26]. Research in this field looks at the fabrication of these devices to ensure that high performance can be obtained while remaining comfortable to the subjects [27]. The strain sensors make use of graphene oxide. To ensure the comfort of the sensors the graphene oxide can be immersed into the polyester fabric and cotton fabric [28]. Other research looks to develop these strain sensors so that they can be produced with low production costs [29]. The strain sensors need to be designed specifically for what they aim to detect. This will include a wearable sleeve for arm movement or a glove for hand movement [30]. Strain sensors are also affected by environmental conditions such as temperature, humidity, and surrounding magnetic materials [31].

### 2.1.3   Current Literature using contact-based

Techniques Chin et al. [32] collected a range of human activities where the test subjects were using contact-based accelerometers on their wrists. The dataset collected by these activities was then run through the ML algorithms Random Forest, KNN, and SVM. The results found that SVM had the highest results of 91.5%.

Jalal et al. [33] used a benchmark dataset of 14 indoor human activities. The benchmark dataset was collected using triaxial accelerometer sensors. The research included separating static activities from dynamic activities. The paper then went on to apply the Random Forest algorithm for ML classification. The static results scored higher at 92.16% with the dynamic activities scoring 80.0% with an average result of 85.17%. The work conducted in [34] used contact-based smartwatches with accelerometers to monitor the movement of ping-pong players. The watch recorded data of 8 different motions on how the test subjects moved the ping-pong paddle including forehand attack, forehand flick, backhand flick, etc. The data was then processed using 7 ML algorithms including Random Forest, SVM, KNN, and decision trees. The research found Random Forest to be the best performance with an accuracy score of 97.80%.

The work of [11] made use of accelerometers to detect human activity. They used the Human Motion Primitives (HMP) dataset which includes 14 activities collected from acceleration-measuring devices attached to the wrists of humans. They used Random Forest for accuracy and

achieved an accuracy score of 79.58%.

The authors in [35] developed a real-time activity monitoring system using wristbands paired with mobile devices. The work makes use of data fusion to combine data from both wristbands and mobile devices. Data fusion provides a contingency for when subjects forget to wear the wristband, it is still possible that the subject will have their mobile device on their person and vice versa. The work included a diverse dataset of many different activities which is possible by using the many sensors included in the mobile device and the wristbands. The smartphone is also able to identify the location of the person and thus provides the presence or non-presence of the person.

## 2.2 Contactless Techniques

Contact-based techniques can work well if the conditions are met. One of the main concerns is if a subject is wearing their device however if the subject does not wear the device then the system is rendered useless. Elderly people are classed as a vulnerable group and fall detection can provide great benefit to them. Elderly people are at more risk of dementia and Parkinson's disease, which can affect their memory. This increases the probability that the subject will forget to wear their monitoring device. There also leaves the issue of comfort where a subject may find the contact-based device uncomfortable while sitting at home. Non-interference methods can be used to solve these issues. Non-interference methods are techniques used to monitor human motion without interfering with the person's body which is the case with contact-based sensors.

### 2.2.1 Camera Technology

Camera technology can be used to record individuals. ML can be applied to the frames of the footage to establish if an individual has fallen [36]. This method will allow the subject to not have to wear any devices while being monitored. The ML aspect removes the need for a human to be observing the video footage which can prevent the subject from feeling that they are being watched. This type of system can achieve high accuracy [37]. These types of systems can be expensive. To decrease the costs of the systems, devices such as a low-cost Raspberry Pi device with a camera can be used to obtain good performance compared to more expensive ones. Cameras have the disadvantage of having privacy concerns as most people are uncomfortable with cameras watching over them.

### 2.2.2 Radar Technology

Current research has also made use of radar technology to detect human activity [38, 39, 40]. Radar can provide contactless activity detection ensuring the privacy of subjects [41]. Radar sensing systems make use of the Doppler information to be able to detect human activities such

as falling incidents [42]. The Doppler information is known as the Doppler effect. The Doppler effect is when the radar signal echoes off the human body performing a movement and from this, the velocity of the target can be seen and this allows radar imaging techniques to commence [43]. These radar images are known as spectrograms. Spectrograms contain all the phase and amplitude information collected by the radar of time [44]. The changes in the Doppler effect when a subject performs certain movements can be captured and stored as spectrograms and then labelled for training in ML applications [45].

**Current Literature using Radar Technology**

The following section provides details about state-of-the-art work in the field of human activity recognition using radar sensing technology in conjunction with ML methods that have been applied for classification purposes. The work of [46] used a frequency-modulated continuous-wave (FMCW) radar system to look at the Doppler, temporal changes and radar cross sections to collect data of falling and other fall-related activities such as stepping, jumping, squatting, walking, and jogging from 3 participants. The data was then run through 10-fold cross-validation with KNN achieving a high accuracy result of 95.5%. This work demonstrates that wireless waves through the use of radar systems can be used to classify human motion through changes in frequencies. The work of [47] collected and published radar spectrograms of human activities. The activities included walking, standing, sitting, picking up an object, drinking water, and falling. The paper used SVM, KNN, and GoogleNet algorithms to classify the collected spectrograms. The results produced using these algorithms were 78.25 % accuracy for SVM, 77.15 % accuracy for KNN, and 74.70 % accuracy for GoogleNet. The collected dataset was then published for further research. The paper [48] used radar spectrograms of activities like walking, falling sitting down, and bending down. The spectrograms were used for image classification and images were converted to Grey-scale for data pre-processing. The algorithms Deep Neural Network (DNN) and SVM were applied to the pre-processed data. DNN achieved an accuracy result of 87.00 % while SVM achieved an accuracy score of 78.00 %. Research in [49] used spectrograms as image classification using Grey-scale. The images were then classified using the SVM algorithm. The paper developed Sequential Forward Selection (SFS) for feature selection. The results of the classification achieved between 92.00 % and 95.00 % accuracy depending on the number of features used. The paper [50] used algorithms stacked Recurrent Neural Network (RNN) with Long Short-Term Memory (LSTM) and deep Convolutional Neural Network (CNN) to classify 6 human motions using Radar Doppler Images. The 6 motions were boxing, hand clapping, hand waving, piaffe, jogging, and walking. The results achieved in these experiments found that the stacked RNN with LSTM achieved 92.65 % accuracy with the Deep CNN achieving 82.33 % accuracy. Erol, B. and Amin, M. [51] used spectrograms and range maps of human motion and fused them for classification. The spectrogram results are similar to the experiments conducted in this thesis. The paper investigated five human motions namely bending, falling,

sitting, kneeling, and walking. The spectrogram experiment used obtained a result of 82.24 % accuracy using KNN with Principal Component Analysis (PCA). With fusion methods of the spectrograms and range maps the paper was able to achieve a result of 93.94 % using KNN with PCA. The work of [52] used Impulse-Radio Ultra-wideband (IR-UWB) radar to capture 12 kinds of motions. The data processing used KNN to define the features in the spectrograms. Then the power spectrum and Doppler shifts are extracted then it is sent to a CNN algorithm for classification. This was run using 5-fold cross-validation and achieved up to 98 % for detecting the human motions. The paper [53] used IR-UWB radar with CNN to be able to identify between falling and Activities of Daily Living (ADLs). This work used binary classification and focused on differentiating between the falling motion and any other type of activity around the home. The CNN algorithm was able to provide an accuracy score of 96.35 %. [54] made use of Ultra Wide Band (UWB) radars to create a dataset that contained 10 subjects aged between 22 and 39 years old, performing 15 different activities. The data was collected while other people were still active in the building behind walls. This is to simulate a realistic care home where other residents will reside in neighbouring apartments. The experiment achieved an accuracy score of 80 % using the Random Forest algorithm. The work of [55] used UWB radar for 7 subjects carrying out 4 activities namely walking, sitting, standing, and simulated falling. The collected data was run using 10-fold cross-validation and found the KNN performed the best with a result of 94.90 % accuracy. [56] used UWB radars to collect data for binary classification of falling and non-falling events. Data was collected using 10 volunteers in 3 different locations within a proposed apartment. They validated their results by using the leave one subject out method and found that the achieved accuracy was 90.00 % using a CNN-LSTM architecture deep learning model. The paper [57] detailed how falls in the homes of elderly people can be detected by using UWB radar technology. This, therefore, provides a contactless sensing fall detection system, and the results of the paper show that this proposed approach can be applied in real-time by streaming incoming data from the UWB device. The paper aims to distinguish between normal activities and falling. The system is beneficial for fall detection but is not designed to provide broader monitoring of elderly people's activities which may be indicative of a fall risk rather than providing notification of a fall that occurs when harm may have already been caused to the individual. This thesis aims to make use of the cheaper more available Wi-Fi technology compared to this work using radar technology.

### 2.2.3 RF Technology

Using RF signals is a method of detection where the subject is not required to wear any devices. This removes the problem of subjects having to remember to wear devices and avoids any discomfort. This is known as a non-intrusive method of detection. It works by observing the state of the wireless connection between devices such as Wi-Fi signals within a home. As the signals travel through the atmosphere they will propagate differently depending on the objects in the

room. These objects can include humans and the signals will propagate differently depending on the positioning of the body. Wi-Fi records the information of the signal propagation and this is called CSI. The CSI is used from Wi-Fi to look at the amplitude of the RF signals while the human moves in between the RF signal transmission [58, 59]. The CSI describes how the wireless signal propagates between the transmitting node and receiving node [60]. This data can be exploited to detect changes during a specific human motion such as the example of a fall occurring. Wi-fi is considered superior due to its low cost and extensive coverage in homes already [61]. Another advantage of using Wi-Fi is that it eliminates the need for excessive equipment which can feel invasive and the additional equipment can be expensive and require maintenance [60]. By implementing systems to only use the smallest amount of equipment, costs are kept down as well as ease of installation.

**Current Literature using RF Technology**

The paper [62] made use of the CSI of Wi-Fi Orthogonal Frequency Division Multiplexing (OFDM) signals for the classification of 5 different arm movements. The human-made different arm movements while standing between a Wi-Fi router and a laptop send wireless signals to each other. The CSI was then captured and ML was applied to the collected data. The ML algorithm chosen was the LSTM algorithm, which was able to achieve a high accuracy result of 96%.

Nipu et al. [63] used CSI to try and identify a specific person. The experiment conducted had different people walk through two devices while data is transmitted and stored the CSI while that person walked through the RF signals. Principle Component Analysis (PCA) is used to remove any noise from the CSI. The aim was to identify the individual that was walking through the devices. The experiment used 5 individuals who then walked through the devices 20 times. This builds a total of 100 CSI samples. The Butterworth Low Pass filter was also used for noise cancellation of the CSI samples. The paper used 7-time domain features for feature extractions. These features were skewness, mean, maximum, kurtosis, median and energy, and highest FFT(fast Fourier transformation) peaks. This reduced the computational times without affecting the results. ML algorithms, Random Forest, Hidden Markov Model (HMM) SVM, KNN and Boosted Decision Tree were then applied to this dataset for supervised ML. The performance of the algorithms was measured by accuracy. The confusion matrix was also presented. Four experiments were carried out with increasing group sizes. The first experiment had binary classification between two people and then increased the multi-classification until all 5 people were included in the dataset. The experiments found that the algorithms scored higher when only 2 people were used in a binary classification experiment. The Random Forest algorithms scored the highest with 97.5% accuracy with only binary classification. The Boosted Decision Tree had higher accuracy than the rest of the multiclass experiments however accuracy dropped for both algorithms as the number of people increased. This shows that one of the key challenges is

being able to classify more classes with high accuracy.

Tan et al. [64] used USRP devices to detect human movement and vital signs. This is achieved by monitoring the signal propagation as the subject moves between the USRP devices. The Paper [65] was able to identify differences in the positions of patients lying in a bed. The research was aimed at helping patients who are in bed for long periods from developing bedsores from staying too long in one position. The results showed clear differences in the CSI when patients lay in different positions.

Wi-Fi signals were used in the work of [66] to detect the number of people behind a wall. They used ML to classify the CSI to establish if there is a person behind a wall and if so how many. The experiments included collecting data for no people behind the wall, one person, two persons, three persons, and four persons present. Experiments showed the Decision Tree to be the most accurate algorithm for ML. The paper [67] used the CSI of the activities of running, walking, sleeping, and no activity for ML classification. The work developed an algorithm that was able to make classifications on CSI on different time windows. As a human subject walked into the room the CSI was recorded for a different amount of time windows. Then the classifier only had to deal with small amounts of data when making classifications. This allows for real-time classification to identify if someone is walking in the room. The experiments included walking in 5 different motions to confirm the algorithm can detect the walking motion.

The work of [68] experimented with various filters for noise reduction in the CSI data. Namely the mean filter, Butterworth low-pass filter, median filter, and threshold filter. The results found that the Butterworth low-pass filter performed the best. The mean filter fails to filter out abnormalities and the median filter and threshold filter ignore noise at higher frequencies. The Butterworth low-pass filter low pass filter successfully preserves the integrity of the data by removing the noise without changing the size and waveform of the data.

The work of [69] found that the use of a sensitive pilot carrier was able to help in the detection of human activities.

Similar work on healthcare was done in [70, 71, 72]. The authors of [73] used RF sensing to detect four people performing activities. The work was able to have the highest accuracy of 91.25 % accuracy when using a single subject. This thesis will seek to implement real-time sensing using a single subject.

Aziz Shah, Syed, et al. [74] made use of contactless sensing using Wi-Fi for real-time classification of human activities picking up an object; walking; sitting on a chair; jogging, and leaving a room. The work takes the amplitude of the Wi-Fi subcarriers and converts them to scalogram images and passes these images through deep learning algorithms. The deep learning provided an accuracy result of 91.1 %. The paper mentions the use of real-time but does not detail the process of how a real-time approach is carried out. One of the main focuses of this thesis is the privacy factor of activity classification. This thesis expands on the ideas detailed in this work and implements a working real-time system to provide continuous monitoring.

Zhang, Daqing, et al. [75] present a real-time fall sensing system using CSI of RF signals. The classifications are made using SVM. The set-up uses a camera to serve as ground truth while the CSI stream records the data being collected. The data is then labelled using the camera footage as a reference. This shows that the data is collected in real-time and classifications are made on the real-time data. The paper does not detail how long it takes for a classification to be made following all the data processing steps detailed in the paper. Therefore this thesis seeks to provide an analysis of ML algorithms to select an appropriate algorithm to provide a real-time classification of new incoming data.

The authors of [76] made use of RF signals to sense sitting down, standing up, and static stand activities in real-time. The paper made use of Linear Discriminant Analysis (LDA) and SVM ML algorithms. The authors of this paper considered the timing component of the algorithms concerning the sample rate. The results concluded the AI model created could make classifications within 300 milliseconds with an accuracy of 70 %. The work of this thesis will seek to increase the accuracy of a real-time system by reducing the complexity of detected movements and keeping the classification time in milliseconds.

The paper [77] made use of Wi-Fi to sense that social distancing is present in elevators and office space with an accuracy of 92 % for the elevator and 97 % in the office space. This is achieved by using the CSI to calculate the number of occupants within an elevator and office space. The paper made use of description features of the CSI amplitude like the work of this thesis. The features the authors used to describe the CSI amplitude were mean, standard deviation, median absolute difference, minimum value, maximum value, skewness, kurtosis, and entropy. The paper did not compare the difference in results between using describing features against the full CSI amplitude data which the work of this thesis looks to add to the current literature.

The authors of [78] recorded the timings of each algorithm in the application of detecting diseases by use of medical records as datasets. The algorithms tested in this paper were SVM, KNN and Random Forest. Results showed that on average SVM was the fastest at classifying the data. This thesis provides a similar analysis in the field of activity detection using RF sensing.

Current literature takes the CSI and applies ML to it and records the results. The only related work close to real-time classification is the work of [79]. This work identifies between no activity and walking. This is a lot less complicated than identifying different human motions. The CSI of no activity and walking will have significant differences in the patterns of the radio frequencies. As no activity will have minimum amplitude compared to the amplitude of the activity taking place. This presents a greater challenge in classifying different human motions. The concept of time windows is a good idea as it can increase the speed of a classification which will help with real-time classifications. This is because the data to be processed in real-time will be much smaller hence increasing processing speeds. This is incredibly useful when making ML classifications especially if multiple classifiers are being used such as ensemble learning.

## 2.3    Vital Signs Monitoring

Vital signs include the heart rate and breathing rate of an individual. Monitoring the breathing rate of an individual can alert caregivers of potential respiratory dysfunction and acidotic states [80]. In a hospital, the vital signs are measured every 8 hours which can result in missing the early signs of vital deteriorating [81]. Constant monitoring of vitals within a home is highly desirable. Heart rate is measured using Beats Per Minute (BPM). The normal heart rate for an adult male is 70 BPM and for an adult female is 75 BPM [82]. Heart rate monitoring can be used to ensure that the human cardiovascular system is in a healthy state [83]. Vital sign monitoring can be used in healthcare systems to monitor health or in emergency recuse situations where sensing vital signs can be used to find survivors[84].

### 2.3.1    Contact-based

Vital Sign Monitoring Vital signs can be monitored using contact-based devices such as watch-like devices that can monitor the vital signs in a medical or fitness context [85]. The contact-based devices implement the use of Micro Electro Mechanical System (MEMS) technologies to be able to detect vital signs [86]. An example of MEMS technology includes the Inertial Measurement Unit (IMU) Sensor. An IMU sensor is made up of accelerometers and gyroscopes which can detect the vibrations of the person who is wearing the device. This can then be used to detect the heartbeat of the individual [87]. The information collected by the sensor can be wirelessly communicated to an interface where information on the vital signs can be viewed [88, 89]. Strain sensors can also be worn by test subjects for detecting the vibrations caused by blood pulses and the small-scale movements caused by the body during breathing [90].

### 2.3.2    Camera Technology for Vital Sign Monitoring

Camera technology can be used as a non-contact method for vital signs by monitoring the subtle changes in skin colour [91]. The pulses of the blood caused by the heart beating can cause very small changes in skin colour. These small colour changes can be detected in the Red Green Blue (RGB) channels of a camera [92]. ML algorithms can be used with the data obtained from the RGB channels to predict the heart rate of an individual [93]. Ghanadian et al. [94] use an RBG video camera to capture a person's face. From the facial video, the heart rate of an individual can be measured. The idea is based on the light absorption of blood cells differing from the skin. This results in the skin colour in the face slightly changing as the blood volume increases within the face. An RBG video camera can pick up these small colour changes. The blood volume increase can indicate the heart rate by giving information on the Blood Volume Pulse (BVP). The method used in this paper looks to use face recognition software and then track the individual's face. Then there is an area of interest in the face where the change of colour will

be detected. The red, blue and green amplitudes are averaged for all pixels in a frame. The paper collected a dataset using 11 adults being videoed for 1 minute. The collected data is then classified using ML. The best results came from the algorithms Random Forest, KNN and K-star. Random Forest had an accuracy score of 91.29%, KNN had an accuracy score of 85.89% and K-star score 87.45%. The paper also employed ensemble learning where the top two algorithms Random Forest and K-star were combined and the accuracy increased to 92.13%. The paper states that combining algorithms is likely to increase the accuracy.

### 2.3.3 Radar Technology for Vital Sign Monitoring

Radar technology can be used to observe the small movements of the chest when a person breathes and there is a pulse [95]. Similar to how the Doppler effect is used to detect large body movements, it can also detect these smaller movements associated with breathing and heart rate [96].

### 2.3.4 RF Technology for Vital Sign Monitoring

Vital sign monitoring can also be monitored with RF signals. Using RF signals to monitor vital signs works similarly to motion detection. Monitoring of vital signs looks is the more minute movements of the human body caused by breathing and heartbeats [97]. Breathing and heart rate monitoring can be implemented in a non-contact way during a person's sleep. This can help with long-term sleeping monitoring as opposed to sleeping in a hospital which is not a familiar environment and comfort can be compromised due to contact-based devices thus affecting results [98]. The monitoring of a person's breathing rate using cost-effective methods to detect respiratory conditions is highly desirable as respiratory diseases account for 17.4% of all deaths according to WHO [99]. RF signals can be used to detect abnormal breathing patterns such as Tachypnea [100], Which is a symptom of COVID-19 [101]. Systems have been developed to allow for real-time monitoring of breathing patterns using RF signals [102]. However, the disadvantage of using RF signals is that they can be vulnerable to other movements within the room. The other movements create noise in the CSI which can then in turn cause false readings [103, 104]. The paper [105] presents the Resbeat system. The system uses 5GHz Wi-Fi to exploit the bimodal CSI for real-time breathing monitoring. The breathing rate is detected by observing the amplitude and phases of the CSI between 3 antennas. The paper uses the Exponentially Weighted Moving Average (EWMA) method to remove the environmental component from the CSI samples. The environment component is seen as the static component which includes reflections from walls and furniture within the room. The dynamic component is seen as the breathing rate where there are changes to the wireless signals due to the cheat moving in and out. The breathing rate is detected by using the most sensitive signals. To find the most sensitive signals the Resbeat system uses a signal selection method that selects the

signals with the lowest energy value. The Resbeat system implements movement detection to detect large-scale movements. Large-scale movements will have large changes in the CSI and will affect breathing monitoring. The movement detection is done by monitoring the average phase difference of the different subcarriers. A counter is used where if the average phase is 0.95 lower or 1.05 higher than the last average the counter is increased. If the counter reaches 10 then a movement has been detected. If a movement is detected then the signal selection process is run again. To detect the breathing rate, peak detection is used. This looks at the peaks in a 13-sample window. If the middle peak in the 13-window sample is equal to the maximum value then the estimated breathing rate can be calculated. This work looks at making calculations based on the data of the CSI. It takes small samples to reduce processing time and allow for real-time breathing monitoring. In practice, it will allow for non-contact methods for monitoring breathing. However, a person will still be required to observe the breathing rate and make medical decisions based on the breathing rate detected. A system can be in place to monitor the breathing rate and alert if the breathing rate falls into a predefined threshold. Zhang et al. [99] developed the WiCare system. The Wicare system is used to detect the subject's breathing rate while the person is moving such as within an office environment. The challenge is that the small chest movements caused by breathing are much smaller than the movements of other body parts such as arms. This can make the body part movement move more prominent in the CSI. The experiments have the subject making small movements such as reading, writing, and using a handheld device. This makes the movement to a minimum and helps with isolating the breathing from other body movements. The system accounts for the environmental component such as walls and furniture by removing the delayed signals. The signals are delayed due to the reflecting on the environment which results in a delay to the receiver compared to signals on a direct path to the receiver. Low-frequency ranges observe the breathing motions. The Wicare system makes use of Dynamic Time Warping (DTW) and curve fitting to be able to select the specific subcarriers that best detected breathing motions from the CSI data where the micro motions are taking place. The CSI data can be collected and ML can be applied to detect if vital signs are within the desired medical requirements. The monitoring of the breathing and heart rate in real-time can allow for subjects to not have to wear devices that may be uncomfortable. The real-time classification with ML can be simplified into binary classification such as expected or unexpected behaviour. This can allow for an alert to be raised if the vital signs are being classified as unexpected behaviour for example an increase in heart rate or a drop in breathing rate. The literature highlights the need to ensure that noise is reduced when monitoring vital signs as the body movement concerned with breathing and heartbeats are so minute any other motion can cloud the small movements. Further research can look at the possibilities of building larger datasets with more samples of breathing and heart rate. This can be used to build ML models that can recognise the small changes in frequencies caused by breathing and heart rate despite the noise due to the high level of samples used in the dataset. Further research can look

into these possibilities and also explore other noise-cancelling methods.

## 2.4 Machine and Deep Learning

ML is the process of computers trying to recognise patterns in data [106]. ML is used in many applications such as self, driving cars and speech recognition, etc [107]. ML comes in a range of different algorithms designed to tackle a range of problems [108]. Algorithms are used to create models using training data. Training data serves as sample data where the algorithms can detect patterns in the training data which can be used to recognise the patterns in future unseen data. From these patterns, ML algorithms can make predictions or decisions based on previous examples of data. An example of this is when sensor information of specific movements is fed to the model, it is expected that ML algorithms will be able to detect patterns of this movement in new previously unseen samples. Some ML algorithms such as deep learning algorithms make use of neural networks which simulate how the human brain works

### 2.4.1 Advantages of Machine Learning

The advantage of using ML is that it is not required to program computers how to recognise these patterns. The ML algorithms find these patterns by learning from the sample data known as training data. This is beneficial in terms of saving time [109] and finding patterns in the data which is difficult for humans to interpret [110].

### 2.4.2 Machine Learning Approaches

ML algorithms can be into three main groups, supervised learning, unsupervised learning, and reinforcement learning. Supervised ML algorithms take labelled training examples to learn the patterns of the data. The algorithms then need to predict or classify the label of the data based on patterns it recognises to differentiate between the different data samples fed in as training data [111]. Unsupervised learning is used when data is not labelled. The unsupervised learning algorithms will then group the data based on patterns recognised in the data. This is known as clustering as data is divided into clusters based on attributes found in the data [112]. Reinforcement learning works on the premise that there is a reward function. The reward function is what should be achieved and the reinforcement learning algorithm will work out how to achieve the reward [113]. Reinforcement learning is used in various applications such as self-driving cars or defeating human opponents at chess [114].

### 2.4.3  Deep Learning

Deep learning is a range of ML techniques that are based on artificial neural networks similar to the human brain [115]. These artificial neural networks are made up of connected neurons similar to the human brain [116]. Deep learning is comprised of an input layer, hidden layers, and an output layer. The input layer is the training data. The term deep learning refers to the number of layers hidden. Deep learning algorithms can have many hidden layers [117]. The purpose of the hidden layers is to multiply the input values with an assigned weight and output the calculated value [118]. As the input is passed through the layers the final output is represented in the output layer. The output layer is then compared to the input layer and weights are recalculated to be more in line with the input data [119]. The weight values are then readjusted which results in small changes in the network's perception of patterns in the data to increase accuracy [120]. The input data is then fed through the network with the updated weights. Backpropagation algorithms are used to adjust the values of the weights based on the results of the previous run [121]. This process is repeated many times until optimal results are obtained. The number of times the data is fed through the neural network is known as epochs [122].

### 2.4.4  Summary

Current real-time monitoring systems make use of contact-based devices. These contact-based devices make use of accelerometers embedded in the device to be able to track human motion. Machine learning techniques are used to recognise the patterns in the accelerometer data associated with specific movements. Contact-based devices can also be used to provide vital sign monitoring. The problem with contact-based devices is that they are intrusive and require contact with the human body. This can be a concern if devices are uncomfortable, need to be charged or users forget to wear the device. Recent literature has looked at implementing non-contact methods to provide real-time monitoring of human movements and vital signs. Non-contact methods include camera and radar technologies. Both systems work by using the information received from the chosen device and using machine learning to recognise when movement occurs or indicators of vital signs. These technologies however have disadvantages such as cameras raising privacy concerns and the introduction of radar technology to the home. There has been substantial work in the use of RF signals to provide human motion and vital sign detection. Current literature looks at using machine learning to detect small and large movements from how these movements affect the signal travels from the transmitter to the receiver. There are gaps in the literature where the concept of RF sensing has not been taken forward to provide a working real-time monitoring system based only on RF signals. The work of this thesis seeks to fill this gap in the literature.

# Chapter 3

# A Review on the State-of-the-Art in Non-Contact Sensing in the Context of COVID-19

COVID-19 disease, caused by SARS-CoV-2, has resulted in a global pandemic recently. With no approved vaccination or treatment, governments around the world have issued guidance to their citizens to remain at home to control the spread of the disease. The goal of controlling the spread of the virus is to prevent strain on hospitals. This chapter focuses on how non-invasive methods can be used to detect COVID-19 and assist healthcare workers in caring for COVID-19 patients. Early detection of the COVID-19 virus can allow for early isolation to prevent further spread. This chapter outlines the advantages and disadvantages and a breakdown of the methods applied in the current state-of-the-art approaches. In addition, the chapter highlights some future research directions, which are required to be explored further to come up with innovative technologies to control the COVID-19 pandemic.

## 3.1   Introduction

Since late 2019, countries around the world have been experiencing a global pandemic through the surfacing and spread of the potentially fatal COVID-19 caused by Severe Acute Respiratory Syndrome Corona Virus 2 (SARS-CoV-2) virus [123]. COVID-19 causes victims to develop a fever and display respiratory difficulties causing coughing or shortness of breath [124, 125, 126]. The National Health Service (NHS) of the United Kingdom is expecting an increased demand for their services as more COVID-19 patients are admitted and staff sick leave increases as staff members contract the disease [127]. Technology is being rapidly introduced in healthcare applications to develop systems that can ease the demand for the health service [6, 7, 128]. Any assistance via healthcare technology will free up valuable clinical resources to focus on other areas of care. This chapter looks at the state-of-the-art non-contact sensing techniques and

how these technologies can be used to assist in the care and detection of people suffering from COVID-19 and how these methods can help to reduce the spread of the disease. Primarily the spreading of the disease from patients to healthcare workers such as doctors, nurses and career staff.

## 3.2 Non-contact Sensing to Detect COVID-19 Symptoms

Non-contact sensing is the ability to detect information without direct contact with a subject. In terms of healthcare, non-contact can be used to monitor the human body without devices physically touching the body. Non-contact techniques are considered highly valuable in dealing with a highly infectious disease such as COVID-19 as contact may contribute to the spread of the disease. This is because healthcare workers will not need to make physical contact with patients to enable the monitoring of the patient. Using contact-based devices can cause risk to healthcare workers as they will need to have physical contact with patients to attach the device. Despite precautions being undertaken such as wearing gloves and face masks, there will be a lower risk if contact with patients can be successfully removed completely. Healthcare sensing technologies aim to collect information from a person which can be processed by AI to provide decision support or directly analysed by a clinician to diagnose a disease or monitor existing conditions. The use of AI can help to relieve pressure on hospital staff while they work hard to manage resources during the global pandemic. Non-contact remote sensing technology can sense such healthcare markers without introducing anything to the body (e.g. contact-based devices). Contact-based devices can be uncomfortable for some which will entice users to remove the device and result in misplacement or damage [129]. The non-contact techniques can assist in the detection of COVID-19 and the care of patients suffering from COVID-19. This will allow for quick diagnosis and allow for healthcare professionals to make clearer judgments on the treatment of the patient and allow for quarantine action to be undertaken. Vital sign monitoring can provide great assistance in the fight against COVID-19 for several reasons. These reasons include the detection of irregular breathing patterns, which is a major symptom of COVID-19 but it can also monitor the health conditions of patients suffering from COVID-19. Although COVID-19 affects the respiratory system [130, 131], it has also been shown to affect the cardiovascular system [132]. These non-contact methods can also monitor heartbeats and therefore provide a monitoring system of the patient's cardiovascular system. It can be concluded that non-contact sensing that monitors these vital signs can be used to aid in the detection and treatment of COVID-19. Examples of Non-contact techniques described in this chapter include computed tomography (CT) scans, X-rays, Camera Technology, Ultrasound Technology, Radar Technology, RF signal sensing, Thermography and Terahertz. Table 3.1 details the advantages and disadvantages of each technique. These methods can be used with AI to help give a diagnosis. Currently testing for COVID-19 is done by doing a swap test. The results of these tests

are currently returned the next day however may be delayed by 72 hours [133]. This chapter will provide a review of the state-of-the-art literature that is using these non-contact methods to be able to assist patients suffering from COVID-19. Table 3.2 provides a summary table of the current literature contained within this review chapter.

Table 3.1: Summary of Non-Invasive Techniques.

| Method | Accuracy | Cost | Timing | Results | Harm | Skill | AI |
|---|---|---|---|---|---|---|---|
| CT [134] | High | High | Med | Fast | Low | High | Yes |
| X-Ray [135, 136] | High | High | Med | Fast | Low | High | Yes |
| Camera [137] | High | Med | Real-Time | Real-Time | None | Med | Yes |
| Ultrasound [138] | High | Med/High | Med | Med | Low | High | Yes |
| Radar [139, 140, 131] | High | High | Real-Time | Real-Time | None | Med | Yes |
| RF [97, 141, 142, 143, 144] | High | Low | Real-Time | Real-Time | None | Low | Yes |
| IR Thermo [145] | High | Med | Fast | Fast | None | High | Yes |
| Terahertz [146, 147] | High | Med | Fast | Fast | None | High | Yes |

Table 3.2: Summary of Current Literature.

| Title of Paper | Key Themes | Authority |
|---|---|---|
| Abnormal respiratory patterns classifier may contribute to large-scale screening of people infected with COVID-19 accurately and unobtrusively 2020 [101] | The paper details that COVID-19 patients display Tachypnea (Rapid breathing). The paper looks at taking Depth images to identify the breathing patterns of volunteers using deep learning | Peer reviewed paper. 24 citations on Google scholar. |

| | | |
|---|---|---|
| Artificial intelligence distinguishes COVID-19 from community acquired pneumonia on chest CT 2020 [148] | CT scan images are used in a COVNet neural network to distinguish between COVID-19, Pneumonia and Non-infected scan images. | Peer-reviewed paper. 157 citations on Google scholar. |
| Automatic detection of coronavirus disease (covid-19) using x-ray images and deep convolutional neural networks 2020 [149] | X-ray scan images are used in a ResNet-50 CNN to distinguish between COVID-19 and Non-infected scan images. | Peer-reviewed paper. 102 citations on Google scholar. |
| Automated detection of COVID-19 cases using deep neural networks with X-ray images 2020 [150] | Xray images are processed using the DarkNet neural network to test binary classification between COVID and Non-infected and multi-class classification between COVID, Pneumonia and Non-infected. | Peer-reviewed paper. 22 citations on Google scholar. |
| Can Radar Remote Life Sensing Technology Help to Combat COVID-19? 2020 [151] | Radar systems have been used to monitor the vital signs of patients in a contactless manner to protect healthcare workers | Paper uploaded on researchgate.net. |
| Combining Visible Light and Infrared Imaging for Efficient Detection of Respiratory Infections such as COVID-19 on Portable Device 2020 [137] | RGB-Terminal camera footage used in a BiGRU neural network model between healthy and ill. | Peer-reviewed paper. |
| Coronavirus (covid-19) classification using ct images by machine learning methods 2020 [152] | CT scan images are used to experiment with various methods of feature extraction and deep learning algorithms to achieve the best results | Peer reviewed paper. 157 citations on Google scholar. 157 citations on Google scholar. |

| | | |
|---|---|---|
| CSAIL device lets doctors monitor COVID-19 patients from a distance 2020 [153] | Radio Frequencies have been used to monitor the vital signs of patients in a contactless manner to protect healthcare workers | Article found on MIT Computer Science & Artificial Intelligence Laboratory website. |
| Covid-19 screening on chest x-ray images using deep learning-based anomaly detection 2020 [154] | X-ray images are used with deep learning to identify if samples are COVID-19 or Pneumonia | Peer reviewed paper. 32 citations on Google scholar. |
| Lung infection quantification of COVID-19 in ct images with deep learning 2020 [155] | CT scan images are used in Deep learning to identify COVID-19. Human in the loop technique is used to focus on increasing accuracy | Peer-reviewed paper. 52 citations on Google scholar. |
| POCOVID-Net: automatic detection of COVID-19 from a new lung ultrasound imaging dataset (POCUS) 2020 [138] | Lung Ultrasound videos of COVID-19, Pneumonia and non-infected patients used deep learning for classification. | Peer-reviewed paper. 2 citations on Google scholar. |

### 3.2.1 CT Scanning

An example of a non-invasive technique to detect COVID-19 is using CT scans [156]. This process involves taking several X-ray images of a person's chest to create a 3D image of the lungs. The images can be reviewed by professionals to look for abnormalities in the lungs. The professionals are trained to review the images and they can tell from the captured image what is normal tissue of the lungs and which part of the lungs looks to be infected. Infection can lead to inflammation of the tissue which will be present in the CT images. This method has been used to look for pneumonia which is an infection of the lungs which can affect the lungs similarly to how COVID-19 affects the lungs of a patient. The activity of COVID-19 in the lungs is more prominent in the later stages of infection, however, ultimately research has shown that CT scans showed a sensitivity of 86 % - 98 % [157]. This technique is non-contact as nothing is directly introduced into the body of the patient. However, if a patient is infected with the COVID-19 virus then the surface of the CT scanning machine is likely to contain droplets of the infection dispensed by the patient. This will therefore need to be cleaned effectively to prevent the spread of the virus to other patients who will be tested using the CT scanner apparatus. It can be noted that cleaning surfaces can be considered safer for healthcare workers than physical contact with

a patient. This is because droplets that are present on surfaces are likely to be static. Whereas infected patients will dispense these droplets from their bodies during breathing and through coughing, which is a symptom of the COVID-19 disease. CT scans can achieve high precision with high image resolution however the technology used to perform CT scans is expensive. CT Scanners are paid for out of hospital budgets and are part of the dedicated equipment used to assist hospital staff in patient diagnosis. Their cost is proportionate to the level of accuracy they can provide within the healthcare industry. The equipment is not portable and it requires skilled professionals for image analysis. The CT scanning machine is a massive piece of equipment. The machine is big enough to scan the entire length of an adult laying down. This also ensures the machine is of a high weight which will further remove the portability of the device. Another disadvantage of CT scanning is that the patient is exposed to radiation [158]. However, radiation levels in CT scans have been found to result in an estimated cancer mortality risk of only 0.08% within a 45-year-old adult [159]. Recently, AI has been used on CT images for diagnosis of COVID-19 [134]. Again AI can allow for support for the skilled professionals analysing the CT images produced by the CT scanners. If AI can assist with the detection and prediction of any disease in the lungs, this can help to ease the workload of the CT scan professionals. The advantages of this can allow for greater care of patients and more opportunity to ensure the appropriate safety prosecutions are being taken to prevent the spread of COVID-19 disease to the hospital staff or other patients who could potentially be classed as high-risk of the COVID-19 disease.

Fei Shan et al. [155] developed a deep learning model which was able to detect COVID-19 and also the level of infection within the lungs. Their model adopted Human-In-The-Loop (HITL) strategy. HITL is when specialists are used for labelling a small amount of training data. Then an initial model is trained. Then this initial model is then used to classify new data. The specialist then corrects any incorrect labels and the dataset can be used to train further models. This task can be iterated numerous times to reduce the tedious task of labelling large amounts of data. The experiment used 249 confirmed cases of COVID-19 for training. The experiment achieved a high result of 91.6 % accuracy. The experiments of the paper used 3 iterations. The first iteration made classifications on the validation data using 36 labelled images as a dataset with an accuracy score of 85.1 %. The labels are then corrected and added to the second iteration. The second iteration used 114 images for training and achieved an accuracy result of 91.0 %. The labels are then corrected and passed to the third iteration The third iteration is used on all 249 training images and achieved an accuracy result of 91.6 %. The improved accuracy greatly reduces the human involvement and time devoted to labelling the full data. Figure 3.1 displays a flow chart of the process of human-in-the-loop.
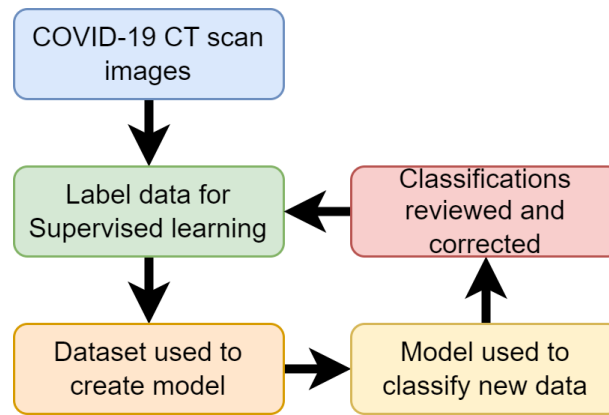
Figure 3.1: Flow Chart of Work for Detection of COVID-19 From CT Scan (Reproduced from [155]).

Li, Lin, et al. [148] used a COVNet - a custom deep learning neural network to predict COVID-19 in CT images. The complete dataset used included 400 COVID-19 CT images, 1396 Pneumonia CT images and 1173 non-infected CT images. The model takes CT images as input and extracts features of COVID-19 and pneumonia evidence found in the CT images. The features are then combined and the neural network can be applied to make predictions on whether the CT images contain COVID-19 or Pneumonia features or if the CT images are of a non-infected person. Results found that the model was able to predict COVID-19 in patients with 90 % sensitivity. The model proved to not only be able to detect infected and non-infected lungs but was also able to differentiate between COVID-19 and Pneumonia with pneumonia having a sensitivity of 87 %. Once the model was trained it was able to classify new samples within 4.51 seconds [148]. Figure 3.2 shows the process followed in this research.
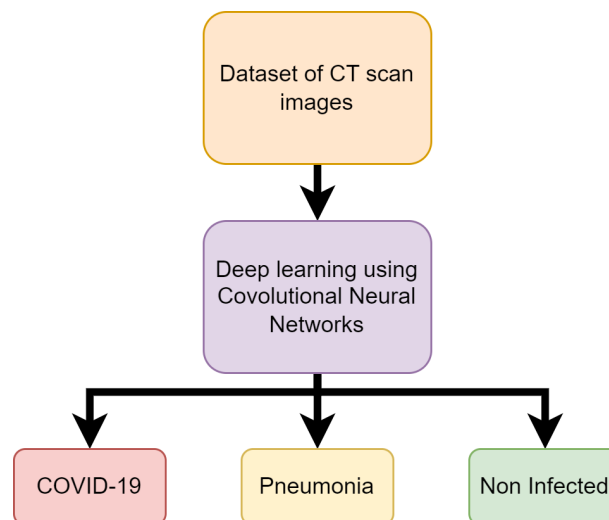


Figure 3.2: Flow Chart of Work for Detection of COVID-19 From CT Scan (Reproduced from [148]).

The research of Barstugan, Mucahid et al. [152] used ML on a dataset of 150 CT images. The dataset contains 53 infected CT images. Patches of the images are taken. Patches in image

processing involve the process of taking images and dividing them into containers of different sizes of pixels. Different-sized patches are used to create 4 different samples of patches. The patch sizes are 16x16, 32x32, 48x48 and 64x64. The images were labelled as infected CT images and non-infected CT images regarding the COVID-19 disease. The research used different methods of feature extraction on the images. These methods include Grey Level Co-occurrence Matrix (GLCM), Local Directional Patterns (LDP), Grey Level Run Length Matrix (GLRLM), Grey Level Size Zone Matrix (GLSZM) and Discrete Wavelet Transform (DWT). The SVM algorithm was then used to classify the extracted features of each of the methods. SVM was experimented on the features using 2-fold, 5-fold and 10-fold cross-validation. Cross-validation is the process of using each fold to work as both training and testing data for the model to make predictions. each fold will take a turn as being the testing data while the others are used as training. This is repeated for however many folds there are so that each fold serves as the testing data at least once. Then the results are compiled together and each sample will have predictions made on it as it served as the testing data through each fold. The best accuracy result achieved out of the various methods of experimentation was 99.64 %. This result was achieved using the Discrete Wavelet Transform feature extraction method with 10-fold cross-validation using the 48x48 patch dimension CT images. A flow chart of the methodology followed in this research is shown in figure 3.3.
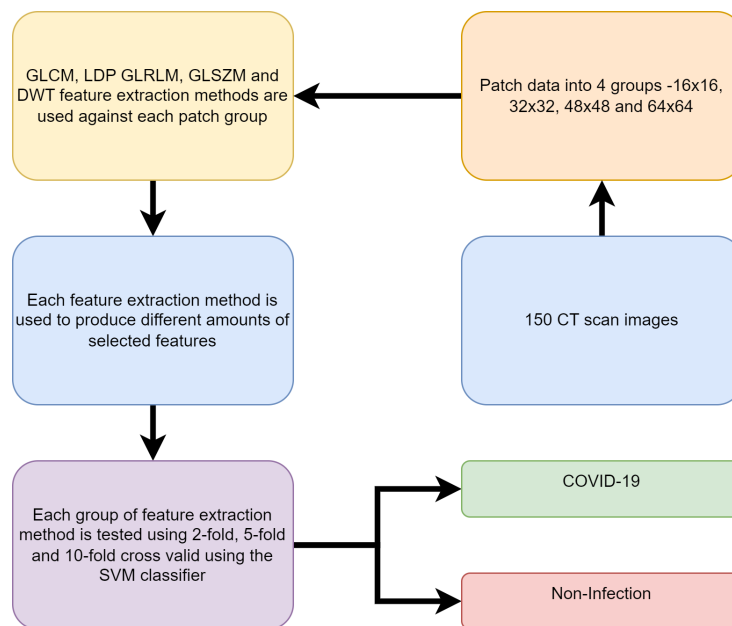
Figure 3.3: Flow Chart of Work for Detection of COVID-19 From CT Scan (Reproduced from [148]).

The above papers have shown through experimentation that CT scanning is capable of displaying the signs of COVID-19 within a person's lungs. The research has also shown how AI can be used to make predictions of CT images and provide assistance in the determination of whether COVID-19 is present in the lungs or not. The studies have also shown that AI can also

determine the level of infection present in COVID-19 patients. The AI has also been able to differentiate between Pneumonia and COVID-19 infections which is a positive as COVID-19 and pneumonia are similar in the way that both diseases attack the lungs. Table 3.3 provides a breakdown of the above research papers on using CT scans for non-contact COVID-19 diagnosis and care of patients.

Table 3.3: Summary of CT Scanning works.

| Citation | Training Data | Algorithms | Results |
|---|---|---|---|
| [155] | 249 CT images of COVID-19 showing different levels of infection. | Custom CNN called "VB-Net" | 91.6 % Accuracy |
| [148] | 400 COVID-19 CT images, 1396 Pneumonia CT images and 1173 non-infected CT images | Custom CNN called "COVNet" | 90 % sensitivity of COVID-19 samples. |
| [152] | 150 CT images including 53 COVID-19 cases. | SVM | 99.64 % Accuracy |

### 3.2.2 X-ray Imaging

X-ray images can provide an analysis of the health of the lungs and are used frequently to diagnose pneumonia [160]. The same strategy is used with X-ray images of the lungs to display the visual indicators of COVID-19 [135, 136]. This is due to the similarities between COVID-19 and pneumonia as diseases that take an effect on the respiratory system. Similar to CT scans, X-ray equipment is also expensive and requires professionals to analyse the X-ray image.

The paper entitled "Automatic detection of coronavirus disease (covid-19) using x-ray images and deep convolutional neural networks" used X-ray images taken of COVID-19 infected patient lungs and patients with lungs that were non-infected with COVID-19 to create a dataset of x-ray images which was then used to predict COVID-19 automatically in patients. The X-ray images are passed into a ResNet-50 CNN which successfully obtained results of 98 % accuracy in differentiating between the COVID-19 infected x-ray images and the non-infected x-ray images [149].

The paper of Zhang, Jianpeng, et al. [154] used Deep learning techniques on a dataset of X-ray images of 70 patients confirmed to have COVID-19. Additional images of patients with Pneumonia are added from a public chest X-ray image dataset. The model is used to identify

differences in x-ray images between patients infected with COVID-19 and patients suffering from pneumonia. The proposed deep learning model was able to achieve a sensitivity of 90 % in detecting COVID-19 and a specificity of 87.84 % in detecting non-COVID-19 cases.

Ozturk, Tulin, et al. [150] also conducted experiments using deep learning to classify x-ray images of patients with a real-time classification of COVID-19. The experiments made use of a custom deep learning model named DarkNet to perform binary classifications between COVID vs. No-Findings and multi-class classifications between COVID vs. No-Findings vs. Pneumonia. The experiments used a publicly available dataset of COVID-19 X-ray images and another publicly available dataset for non-infected and pneumonia X-ray images. The complete dataset included 127 COVID-19 x-ray images and 500 pneumonia x-ray images and 500 non-infected x-ray images. The deep learning process made use of the developed DarkNet neural network. The complete x-ray image dataset was divided between 80 % training data and 20 % testing data. The deep learning was run for 100 epochs using 5-fold cross-validation. Each epoch is an iteration of when the data is passed through the neural network. The neural network will learn about the data being passed through. Repeating epochs can allow the model to fine-tune its biases and weights on what it believes data should be classified as. Then the model can improve its accuracy as it learns what works and does not until it can provide the best results obtained. The results produced an accuracy score of 98 % for binary classification and an accuracy score of 87.02 % for multi-class classification. It is expected that the result will fall as the number of classifications .0..3increase as the AI will need to recognise more features to distinguish between classes rather than differentiate between two data patterns. The complete process followed in this work is detailed in figure 3.4.
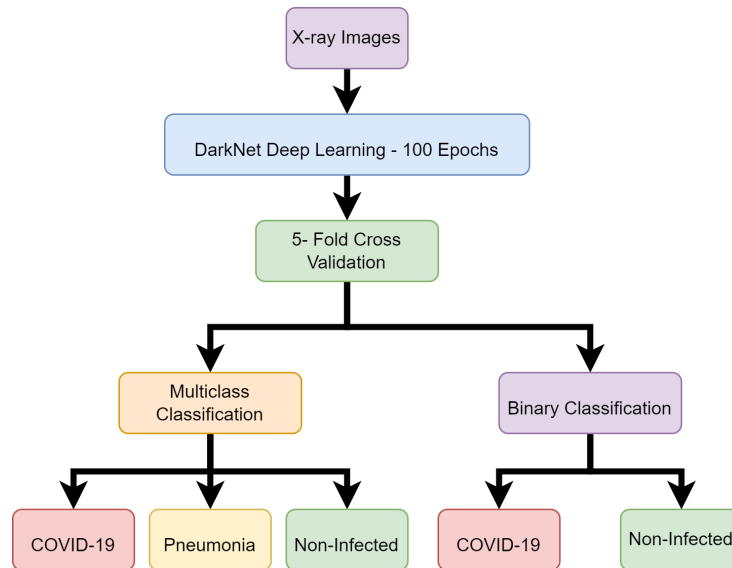


Figure 3.4: Flow Chart of Work for Detection of COVID-19 From X-Ray Image (Reproduced from [150]).

### 3.2.3   Camera Technology

Camera technology can be used to provide non-contact sensing by observing the chest movements of an individual [161]. This can be achieved by capturing video footage of movements of the chest or in the case of depth cameras, they can calculate depth by using two sensors with a known range [162]. The information captured using camera technology can be used to assist in the detection of COVID-19 as one of the symptoms of the disease includes an increase in the breathing rate of patients.

The paper "Combining Visible Light and Infrared Imaging for Efficient Detection of Respiratory Infections such as COVID-19 on Portable Device" used RGB-thermal camera footage for the detection of COVID-19. The footage was used with ML binary classification to detect normal and abnormal breathing from people wearing protective masks. This research is relevant as masks are now commonly worn by people around the world as a preventive measure against COVID-19 disease. The research collected real-world data and applied deep learning to achieve a high result of 83.7 % accuracy which is the highest result found in the literature in regards to breathing detection using RGB-thermal cameras imaging with deep learning models. This research can provide a scanning method which can be used to control the spread of the virus and work with protective masks thus reducing the spread of COVID-19 [137].

Wang, Yunlu, et al. [101] used Microsoft Kinect cameras to take depth images of volunteers breathing. A total of 20 volunteers were asked to sit on a chair and simulate 6 different breathing patterns. The breathing patterns were Eupnea, Bradypnea, Tachypnea, Biots, Cheyne-stokes and Central Apnea. Each of these patterns displays a different breathing rate in the individuals. Patients of COVID-19 display the rapid breathing pattern of Tachypnea. During data collection, a Spirometer was used to ensure the breathing pattern was being simulated correctly by the volunteers. The depth images taken using the camera were used in a deep learning neural network model to classify the abnormal breathing patterns of Tachypnea associated with the COVID-19 disease. The deep learning model used was the BI-AT-GRU algorithm. Gated Recurrent Unit (GRU) is a simplified version of the Long Term Short Memory(LTSM) algorithm. The BI-AT-GRU algorithm results achieved a high accuracy score of 94.5 %. This research shows how depth images can be used to identify the Tachypnea breathing patterns observed in COVID-19 patients in real-time. The process map for this research is shown in figure 3.5. The primary disadvantage of using this method is the cost of thermal and depth cameras and the camera operators. Although the price of these cameras is falling gradually, it remains substantially high [163]. The cost of the equipment is of course less expensive than methods such as CT and X-ray scanning but still more expensive than other methods discussed further in this chapter. The research done with cameras has shown that the devices can be used with AI in the detection of COVID-19 and without contact with the body. This allows for more techniques to be implemented where the diagnosis of COVID-19 can be achieved safely without increasing the risk of spreading the disease.
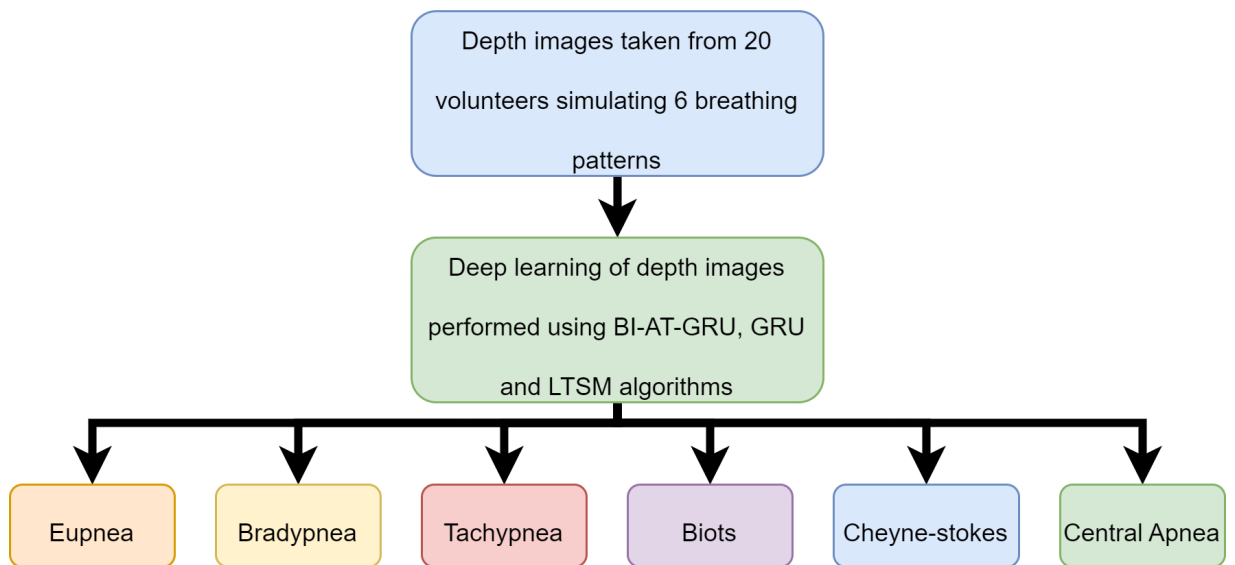
Figure 3.5: Flow Chart of Work for Detection of COVID-19 From Depth Camera Image (Reproduced from [101]).

### 3.2.4 Ultrasound Technology

Ultrasound technology can be applied to detect a respiratory failure of the lungs. An ultrasound machine is a device that uses high-frequency sound waves to image body movements [164]. The sound waves bounce off different parts of the body which create echoes that are detected by the probe and used to create a moving image. Lung ultrasounds have seen great development in recent years [165]. The use of Ultrasound Technology can be used in the detection of COVID-19 in a non-contact method where the risk of healthcare professionals becoming infected by patients can be decreased [166, 167]. Ultrasound technology becomes contactless by using an ultrasound transmitter and receiver. Respiratory movement can then take place between the transmitter and receiver and creates a Doppler effect. This can then be used to create a contactless breathing monitor [168, 169, 170]. Ultrasound technology can be performed using smartphones for the signal and processing of ultrasound images in a portable setting [171]. The disadvantage of ultrasound technology is that patients must prepare themselves before an ultrasound can effectively create an image of the body [172]. This preparation can include not eating for a few hours before.

The work of Born, Jannis, et al. [138] shows that ultrasound technology can be used in deep learning models to distinguish the differences in COVID-19, Pneumonia and no infection within the lungs. The research collects a dataset of lung ultrasound images which contain video recordings of lung ultrasound scans. The dataset includes a total of 64 video recordings with 39 of the recordings of COVID-19 patients, 14 videos of Pneumonia patients and 11 videos of non-infected patients. The paper has developed a Deep learning CNN named POCOVID-Net. The deep learning algorithm was able to achieve an accuracy score of 89 %. These ultrasound

devices can diagnose 4/5 patients per hour. Figure 3.6 shows a simplified flow graph of the experiment undertaken in the paper.
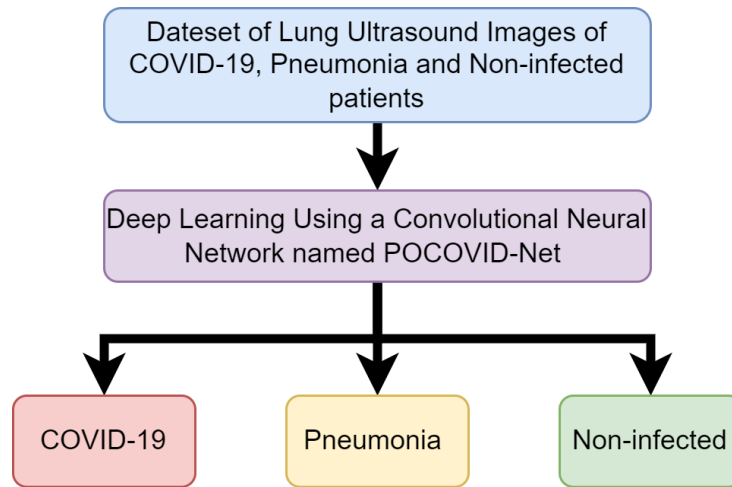


Figure 3.6: Flow Chart of Work for Detection of COVID-19 From Ultrasound Technology (Reproduced from [138]).

### 3.2.5 Radar Technology

Radar Technology can be used to monitor the respiratory system within a home environment and provide a quick response if abnormalities are found which suggest COVID-19 is present. Radar systems use frequency-modulated continuous-wave (FMCW) to observe the Doppler effect when a person moves [46, 173, 174, 175]. This can be used to monitor the fine movements associated with breathing. This is achieved by using the images captured by the Radar systems and then applying AI to classify the images. AI models can be used to give real-time classification on new images [176, 177, 143]. Research done shows that radar technology can achieve 94 % accuracy for the detection of breathing rates and 80 % accuracy for heart rate detection [139, 140, 131]. The Israeli military force has made use of radar systems for monitoring the vital signs of COVID-19 patients. The goal of using this method is to prevent medical staff from becoming infected while caring for patients [151, 47]. Tachypnea is a symptom of COVID-19 and can be detected in a patient by using radar sensing technology [169, 178, 173]. Using radar technology to monitor vital signs can provide non-interference monitoring, however, the disadvantage of radar systems is that it has high power requirements and the technology comes at a high-cost [179].

### 3.2.6 Radio Frequency Signals

The use of RF signal sensing can be used to detect the vital signs of individuals by sensing the minute movements of the chest made while breathing as the heart beats ( [97, 141, 142, 143, 144]). This technique can be used for monitoring the vital signs of patients independent of

their activities [98]. The RF signals detect the movement by observing the CSI which can show amplitudes of the RF signals while movement occurs between an RF transmitter and receiver. [58, 59]. The Emerald system has been developed to monitor COVID-19 patients using RF signals. The system uses RF signals to detect the breathing rate of COVID-19 patients and then uses AI to infer the breathing rate of the patient. This allows doctors treating the patients to be able to monitor the patient from a safe distance. This method prevents the risk of infection to staff and provides the patient comfort as they do not need to wear monitoring devices [153]. RF signals have been used in previous research to detect breathing rates. RF signals can be used to detect abnormal breathing patterns such as Tachypnea[100], Which is a symptom of COVID-19 [101]. Systems have been developed to allow for real-time monitoring of breathing patterns using RF signals [102]. RF signals can be vulnerable to other movements within the room. The other movements create noise in the CSI which can then in turn cause false readings [103, 104].

### 3.2.7 Thermography

Thermography is a widely used non-contact technique within the medical community [180, 181]. It has been used for mass screening of people in other pandemics H1N1 and Ebola so it can be applied in this current pandemic of COVID-19 [145]. Thermography works by using infrared radiation to calculate the temperature of the human body [182]. Abnormal body temperatures are a well-known indication of infection [183]. Symptoms of COVID-19 have been found to include high temperatures over the normal body temperature of 36-37 degrees Celsius [184, 185]. Thermography can also be used to monitor the respiratory systems of patients and provide detection of breathing patterns such as Bradypnea or Tachypnea using AI [186]. Thermography has been recommended as an early detection strategy for COVID-19 amongst large amounts of people in places such as airports [187]. Deep Learning has been applied to thermal images where classifications on new images can be made in under a second [188, 189].

### 3.2.8 Terahertz

Terahertz sensing technology is the process of directing terahertz beams to a person's body to detect the motion of the chest created by a heart beating or lungs inhaling or exhaling breath [146, 147]. Terahertz sensing is a non-contact method which can achieve superior penetration depth [190]. This can be helpful with penetrating a patient's clothes. These terahertz systems can be produced similarly to how the radar imaging takes place except with using terahertz waves and observing the Doppler effect of the Terahertz wave while a patient performs the breathing issue [191]. Terahertz waves refer to electromagnetic frequencies around 0.1 - 10 Terahertz [190, 192]. The use of terahertz can be used in the detection of diseases such as COVID-19 [193]. This will work similarly to the radar system with AI being used to make classifications on the images showing the Doppler effect of terahertz waves. Deep learning can be applied

to these images and give fast classifications of new models once an AI model has been fully trained. Terahertz radiation is considered the first choice in radiation exploitation due to its non-harmful properties to living cells [194]. Terahertz spectroscopy is an example of a powerful tool in medical research and diagnosis used for the analysis of human breath samples and it offers a low-cost [195].

### 3.2.9 Comparison of Contact Methods

The methods discussed in this chapter have looked at non-contact techniques on how COVID-19 can be diagnosed. Due to the nature of the disease, it has been widely acknowledged that reducing contact between people is the best action to reduce the spread. Therefore non-contact technologies for diagnosis are the preferred method. Contact-based devices can also be used for monitoring vital signs [196, 197]. This monitoring of vital signs can therefore be used to detect any displays of COVID-19 symptoms. Popular devices such as AppleWatch, FitBit and Oura ring are highly available and provide monitoring of the heart rate [198]. The Oura ring has been found to show changes in body temperature associated with COVID-19 and has led to several studies being conducted into the use of Oura rings in the early detection of COVID-19 [199, 200]. These technologies are known as personal health trackers and in terms of COVID-19 detection, these devices will be better for self-diagnosis. If these devices can inform users that they are displaying COVID-19 symptoms then the user can take action. Non-Contact methods will serve healthcare workers better as they can assist patients whilst still reducing contact with the patient and thus reducing the risk of infection.

### 3.2.10 Future Directions

This section will detail some of the future directions which may be suitable for expanding on the research presented in this chapter. The research has highlighted how the detection of COVID-19 is possible using various techniques. This section will now discuss how this research can be taken further to work within real-life scenarios.

- One of the biggest challenges with CT scanning as a means to diagnose COVID-19 is the lack of portability. This means that although the method is non-contact, its use still requires individuals to travel to a location where the machine is available. As the CT images can provide high resolution, AI can be used for the detection of COVID-19. Therefore future directions of this method should look to creating highly accurate models that can eventually lead to the automation of COVID-19 detection. This can allow for faster diagnosis. This can allow for more patients to be tested and increase the availability of staff operating and analysing CT scans.

- X-rays similar to CT scans are not portable. Like CT scans professionals are required to

operate these machines and analyse the X-ray images. The research presented in this chapter has shown that AI can be used to make predictions if COVID-19 is present in the lungs. This can be usefully similar to CT scans where AI can be applied to make predictions and speed up the process. The more data collected, the more advanced the model will become. Perhaps initially the predictions will need to be confirmed by humans but eventually, the checks can become less frequent. Since the research above has displayed the ability of AI to distinguish between not just COVID-19 and non-infected but also pneumonia at high accuracy, then AI has proved to be capable of accurate classifications.

- Thermal and Depth cameras can detect the irregular breathing patterns that are associated with COVID-19 symptoms. The issue here is that even though the camera can detect irregular breathing patterns it is unable to categorically define COVID-19 as the cause of individuals displaying irregular breathing patterns. In a real-life situation, the camera method may be better suited to monitoring vulnerable people who are considered high risk from COVID-19. Then once the monitoring system has identified the irregular breathing patterns an alarm can be raised with a career or family member. Then appropriate action can be taken for greater accuracy such as diagnosis with CT or X-ray scanning.

- Ultrasound technology can take moving images of the lungs and detect COVID-19. This can also be made portable by using mobile devices. AI can be applied to recognise if COVID-19 or pneumonia is present in the lungs. This research can be further applied to develop applications on a mobile that device can capture an ultrasound of the lungs and then be compared to an AI model to predict if COVID-19 is present. Although not all phones may not have the necessary hardware to achieve this, the non-contact method can allow others to be able to use the devices for diagnosis at a safe distance.

- Radar technology can identify the breathing patterns of individuals. Much like camera technology, the identification of breathing patterns can raise a cause for concern but it cannot isolate COVID-19 as the sole cause. Radar technology can again be used to monitor individuals but due to the high costs, it is more likely to be used as a monitoring system within a hospital and not a home environment.

- Any future directions should consider the use of RF signals as a means to detect the breathing patterns which indicate COVID-19 symptoms. The RF systems can be implemented inexpensively using existing Wi-Fi technology present within many homes. This allows for the monitoring of individuals without the costs incurred in implementing radar or camera technologies highlighted in this chapter.

- Thermography has been shown in previous research to be able to detect the body temperatures of large amounts of people in previous pandemics. Therefore it can be implemented in mass screening during the current COVID-19 pandemic. With the use of thermography

being able to detect respiratory issues it is clear that these systems can also be implemented for COVID-19 detection.

- Terahertz can provide deeper penetration and detect smaller movements such as chest movements while breathing. This can therefore be used in the early detection of COVID-19. The earlier the disease is detected the sooner isolation can begin and insure that further spread is reduced.

## 3.3 Summary

The works listed in this chapter have shown that the COVID-19 virus can be detected using contactless techniques. Techniques such as CT scans and X-ray imaging provide high accuracy and high image resolution but the cost of the equipment is high and not portable. Thermal and depth camera technology has been used to detect breathing patterns which are associated with COVID-19 symptoms. However, these cameras are expensive and need to be operated by a professional. Radar technology is also able to detect breathing patterns but carries the disadvantages of high operating expenses and capital expenditures. RF signals provide low cost and high accuracy as compared with other non-invasive technologies. The technologies can work on AI which can allow for skilled professionals to be available to assist in other areas of healthcare during the pandemic. The non-contact methods also protect healthcare workers from contracting the disease. The future direction of non-contact detection should look at the use of RF systems as the cost is cheap and it is easier to implement within a home environment in comparison to other methods. This gives the advantage of allowing the users to remain within isolation.

# Chapter 4

# Investigation of Machine Learning Techniques in the Context of Contactless Healthcare Monitoring using Available Radar Spectrograms

## 4.1 Introduction

The growing numbers of elderly people present numerous challenges within the healthcare industry. These new challenges demand new methods which can be implemented in a cost-effective manner [201]. Assistive technology can serve to improve the care of elderly people. The healthcare industry is looking to technology to support growing needs as demonstrated in [6, 7, 128]. Advances in sensor technology are currently being used to support the elderly population [202] and can be used to detect large-scale body movements such as walking, sitting down on a chair, standing up from a chair, picking up objects, fall events and so on.

The WHO has reported that 42 % of people over 70 years old experience falls at least once a year [203] and can be caused by various hazards such as slippery floors and low lighting conditions and the damage can be greater due to elderly people's bodies being fragile [204]. The risk of falling also increases with age. Falls in elderly people can cause more serious injuries than in younger people [205]. Conditions such as arthritis and visual impairment can increase the chance that an elderly person will fall [206]. Arthritis is a condition that causes pain in the joints [207]. This pain when moving could potentially result in elderly people falling as they struggle to move. Visual impairment can cause the elderly to struggle to see hazards and thus trip and fall. Conditions such as Nocturia, which causes older people to wake up during the night with a need to go to the toilet can pose a greater risk of falling as they try to manoeuvre around the home when tired and under poor lighting [205]. Falling can risk serious injury which can result in hospital visits or permanent disabilities [208]. This can lead to the victims of falls

no longer being able to live independently for fear of further injury. Moreover, fall events are the second leading cause of accidental death [209].

In this context, various sensing technologies such as contact-based accelerometer devices, vibration sensing, visual sensing, and radar-based sensing [210] has been used to monitor the daily routine activities of elderly people. Contact-based devices use accelerometers to be able to detect the movement of the person wearing the device as it considers several factors, as elderly people may not wear the devices if they find them uncomfortable [211]. Additionally, elderly people may suffer from conditions that inhibit memory. They may forget to wear the device at times, and they will no longer be able to sense the movements of that person. Vibration, visual sensing, and radar-based sensing work without having any devices introduced to the body. These methods are classified as non-invasive sensing methods. Vibration sensing works using a microphone to record the vibrations on the floor as a fall occurs [212]. Visual sensing can be achieved by leveraging camera-based technology. Cameras can be used to record elderly people and frames can be analysed using ML techniques to assess if a fall has occurred. It also allows caregivers to view the situation and decide if further care is required [213]. Cameras may not be ideal as some elderly people will not wish to be under constant surveillance. radar-based sensing work by exploiting the Doppler signatures created on the radar when a fall occurs [214]. This chapter aims to implement different ML and data processing techniques to work to improve the existing results of an available dataset containing radar micro-Doppler spectrograms of human activities. The research detailed in this study focus on the effectiveness of radar-based sensing in detecting ADLs. ML algorithms are applied to a dataset to predict if these activities can be classified using AI. The ML algorithms used are Random Forest, KNN, SVM, LSTM, Bi-directional Long Short-Term Memory (BiLSTM) and CNN.

## 4.2   Methodology

This section discusses the proposed methodology for fall detection in elderly people. This chapter makes use of radar micro-Doppler spectrograms of human activities. This data is taken from the paper [47] and is publicly available, where the data was collected for 99 elderly people at nine different locations namely the University of Glasgow, North Glasgow Elderly care home and Age UK West Cumbria. The dataset can be found at `http://researchdata.gla.ac.uk/848/`. The dataset consists of six motions walking, sitting down, standing up, picking up an object, drinking water and falling. The dataset of the radar spectrograms is in the format of 227 by 227 pixel PNG image files. There is a total of 1,633 spectrograms in the dataset. Table 4.1 shows the breakdown of how many spectrograms are present for each motion.
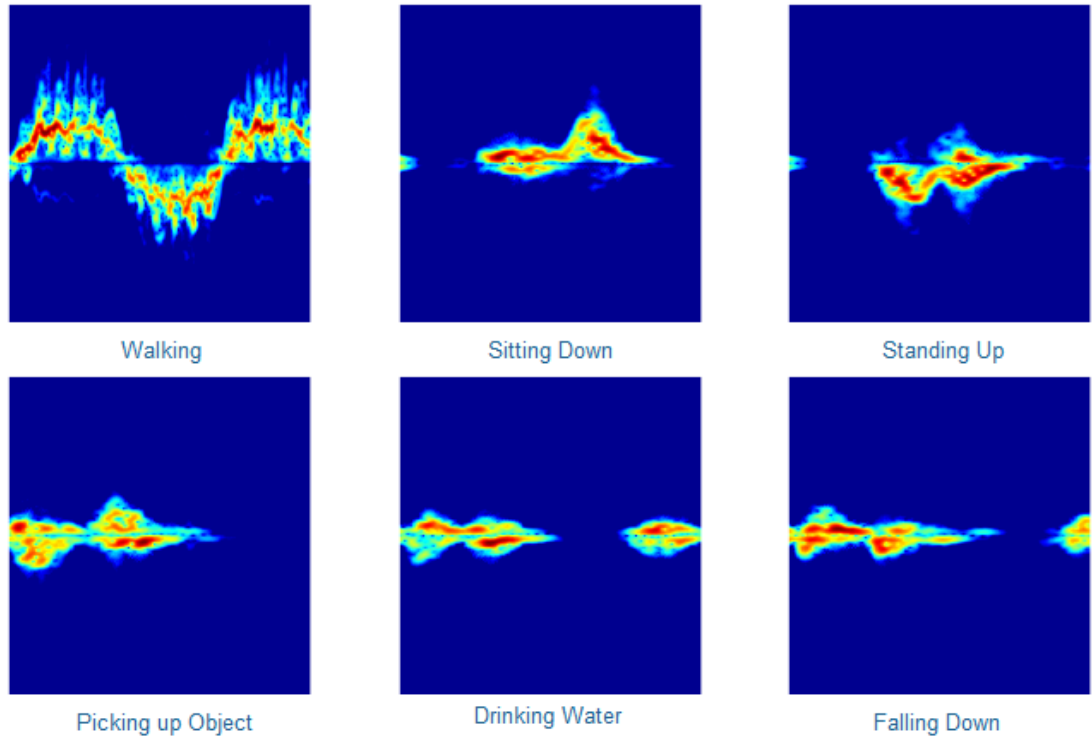
Figure 4.1: Raw Spectrograms Examples of Each Activity [47].

Table 4.1: Number of Spectrograms per Motion in Dataset.

| Algorithm | Number of Samples |
|---|---|
| Walking | 286 |
| Sitting Down | 289 |
| Standing Up | 287 |
| Picking up an object | 287 |
| Drinking Water | 286 |
| Falling | 198 |
| Total | 1633 |

Figure 4.1 shows Spectrogram examples of each activity. The Skimage Python package is used to convert the image files into data based on pixel information and store this data into Python arrays [215]. The image data array is in the shape of 227,227,3. This represents the 227-pixel width and 227-pixel height of the PNG file. The 3 represents the RGB values of the pixels. The images are then converted into Grey-scale which removes the colour and changes the array shape to 227,277,1. This array of data is saved in CSV format for ML processing. The conversion to Grey-scale is used to reduce the dimensions. The RGB channels have thus been converted to a single intensity value [216]. Grey-scale images have been shown to have

improved classification accuracy over coloured images [217] and this method has been used in various related works involving radar image classification [49, 218]. The experiments conducted in this study used four different data processing methods. Namely raw Grey-scale pixel data on original images, PCA Grey-scale pixel data on original images, raw Grey-scale pixel data on Augmented images and PCA Grey-scale pixel data on Augmented images. Using these four data processing techniques produce 4 different datasets that can then have ML applied, and results analysed.

### 4.2.1 Original Dataset

**Raw Images**

The first method uses the raw Grey-scale pixel data only. A dataset is compiled from all the Grey-scale pixel information from the images in the dataset.

**Principal Component Analysis**

The second method then applies PCA to the Raw Grey-scale pixel data. PCA is a technique used to further reduce dimensions [219]. PCA finds common components of the data which can summarise the variation of the data [220]. PCA is applied in this chapter by using Sklearn. Sklearn provides a function that can fit and transform the image data using PCA. PCA is configured to use all components of the data.

### 4.2.2 Augmented Dataset

**Raw Images**

The third method uses data augmentation of the raw Grey-scale pixel data.Data augmentation is the process of increasing the training data by transforming an existing sample [221]. The original and transformed samples can then be part of the same dataset and thus the training data has increased. The transformed samples must keep intact the variance that defines the original samples label within the dataset. Data augmentation in this chapter has tripled the size of the dataset. The data augmentations contain the original Grey-scale images, blurred Grey-scale images and horizontally flipped Grey-scale images. Using blurred and flipped images increases the dataset but these occurrences are unlikely to happen in real-life systems. The reason this is done in this work is that it allows for more data to be produced and still maintains some of the original features of the data without causing duplicates in the dataset. Figure 4.2 shows the process followed when creating the data augmentation dataset.

**Principal Component Analysis**

The fourth and final method uses data augmentation and PCA combined. This takes the complete augmented dataset and then applies PCA to the increased dataset. This allows for more PCA images to be used for training than with using PCA on the original dataset

### 4.2.3 Dataset Preperation

The datasets are divided into 90 % for training data and then the remaining 10 % is used for testing data. This is achieved by using the train_test_split function included in the Sklearn Python package. The function's parameters are used to define the percentage of testing data and the rest is used as training data. The data is shuffled but the random seed parameter is always set the same to ensure all algorithms use the same samples as testing and training data. This allows for the results to reflect the model generalisation of the algorithms due to the specific training data remaining consistent and ensuring that the testing samples are the same unseen samples as every experiment conducted.
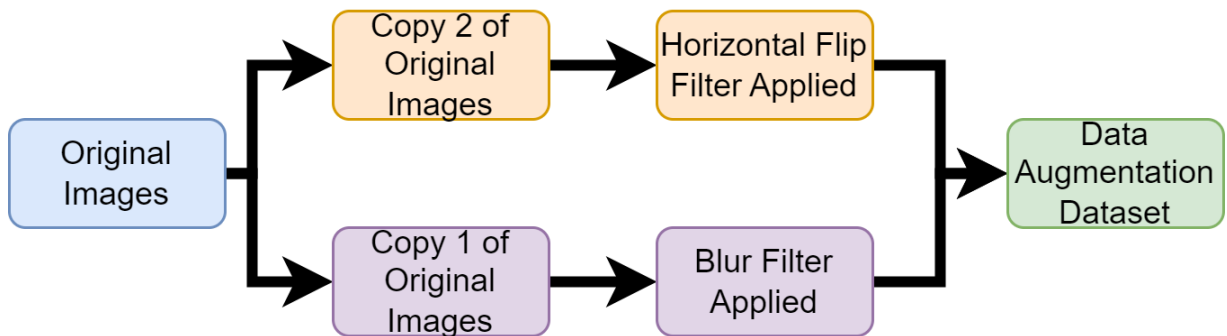


Figure 4.2: Flow Graph of How Data Augmentation Dataset Was Created.

### 4.2.4 Machine Learning

This chapter has used different ML algorithms used in related works such as Random Forest [54], KNN [55], SVM [47], LTSM, BiLTSM and CNN [50]. The Scikit Python package is used to implement Random Forest, KNN and SVM. Scikit is widely used by industry and research within the field of data science [222]. To implement the neural network algorithms LTSM, BiLTSM and CNN, the Tensorflow Python package is used. Tensorflow is used for this research as it is open source and can be used with a Graphic Processing Unit (GPU) [223]. The use of a GPU allows for neural network processes to run faster than if the processes were to be run on a CPU.

The Random Forest algorithm is a collection of decision trees. Each decision tree will decide on which classification to assign to new data based on key features learnt in the training phase. The classification each tree reaches is considered a vote. The final classification decided by the

Random Forest algorithm is the ensemble classification of the combined decision trees. [224]. In these experiments, the Random Forest algorithm is configured to use 200 trees in the forest of decision trees. This number of trees resulted in the best results with initial experimentation.

The KNN algorithm simply looks to compare the training data to the new unseen data [225]. The features of the training data are assigned K values. The features of the new data are then assigned to a K value that best matches the features of the training data [226]. The parameters used for KNN in this chapter are set to use 10 neighbours.

SVM aims to create boundaries between each classification. these boundaries are known as hyperplanes. The hyperplane is positioned as far as possible from the closest data points of the classes present in the data. These points are known as the support vectors. [227]. The hyperplanes are used to divide the support vectors into different categories. The training data features are used to place the hyperplanes. Then the features of the new data are used to place the new data between the hyperplanes and provide classification. [228]. The SVM parameters have the gamma set to auto and make use of the RBF kernel for these experiments.

Table 4.2: Parameters set for ML Algorithms

| ML Algorithm | Parameters Set |
|---|---|
| Random Forest | Number of Estimates = 200 |
| K nearest Neighbours | Number of Neighbors = 10 |
| Support Vector Machine | Gamma = auto |
|  | Kernal = rbf |
|  | Regularization parameter (C) = 6.7 |

Table 4.2 shows the parameters set for the machine learning algorithms for this experimentation. These parameters were selected as they gave the best performance for each algorithm when hyper tuning the parameters.

The LSTM Deep Learning algorithm is an extension of Recurring Neural Networks(RNN). Recurring Neural Networks is a type of neural network which models the dynamic behaviour of sequences of data between nodes of the neural network. LSTM expands on this concept by adding 3 different gates to the nodes. One gate is used to decide if the current state should be forgotten. Another gate is used to control if the input should be read or not and the final gate decides if the state should be added to the node output. These gates allow LSTM to decide if the sequence of data is relevant to the output of the node. [229]. In this experiment, LSTM was used with 50 nodes also known as units. The learning rate was set to 1e-6 using Rectified Linear Unit (ReLU) activation and ran for 200 epochs. Figure 4.3 shows a visual representation of LSTM works.
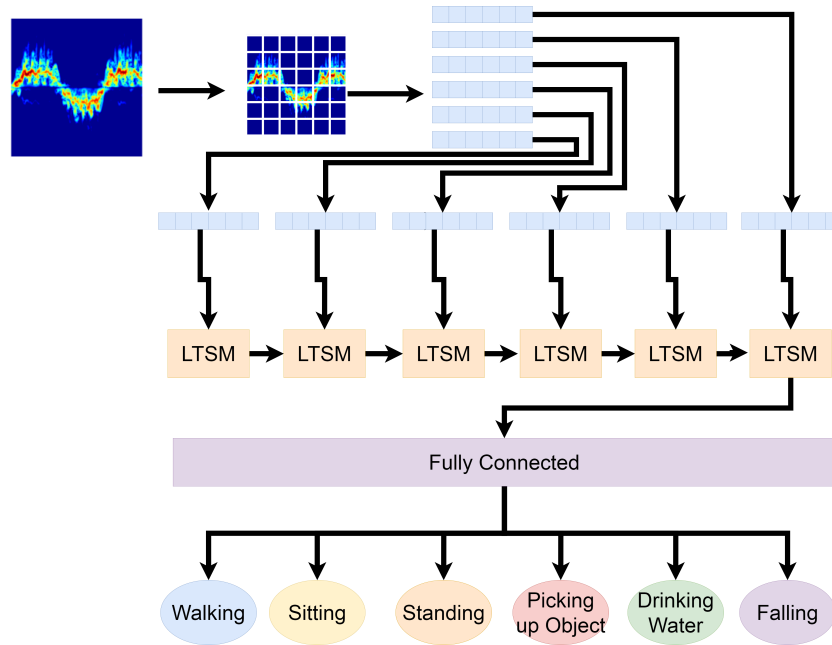
Figure 4.3: Visual Representation of How LSTM Works.

The Bi-directional Long Short-Term algorithm is an extension of the LSTM Deep Learning algorithm. Where LSTM only makes use of the past behaviours of data sequences, The Bi-directional Long Short-Term Algorithm can look at data in two directions. The two directions look at past and future data in a sequence. This is achieved by using two LSTM networks. One LSTM network the forward LSTM network can review past data sequences and the backward LSTM network can review future data sequences [230]. The BiLSTM was configured to use the same parameters as the LSTM setup. Figure 4.4 shows a visual representation of BiLSTM works.
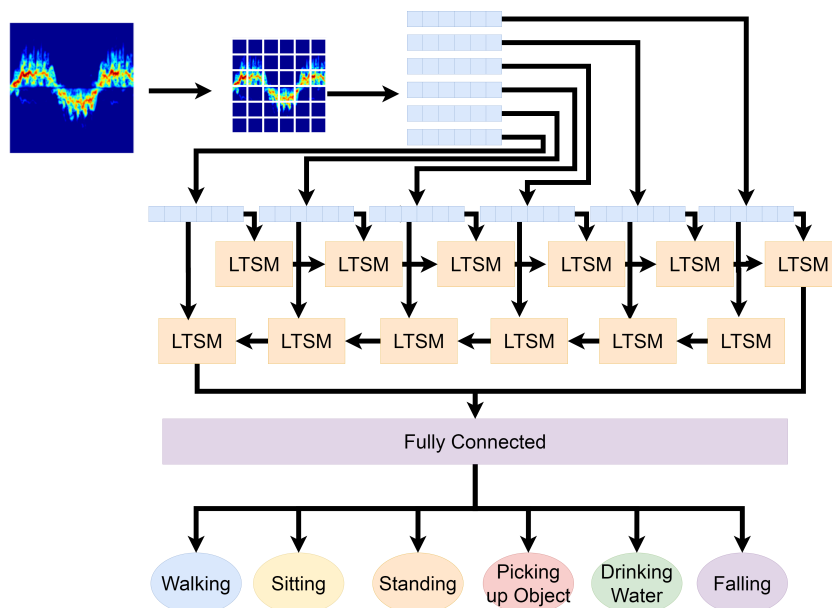


Figure 4.4: Visual Representation of How BiLSTM Works.

The CNN algorithm is an emerging technology which is a powerful solution for image classification problems which were initially thought to require human intelligence [231, 232]. The CNN algorithm is made up of densely connected layers that take the activations of all the previous layers as input. The layers produce feature maps from this input which are known as growth rates [233]. The Convolution Neural Network architecture used in this chapter consists of multiple Convolutions and Pooling layers followed by multiple connected layers and finally a SoftMax layer for creating the output classes. The Convolution and Pooling layers are used to capture the features of the images. The weight and bias of the features are parameters of the CNN which are configured automatically during the training process [234]. Figure 4.5 displays the CNN model used in this experiment.
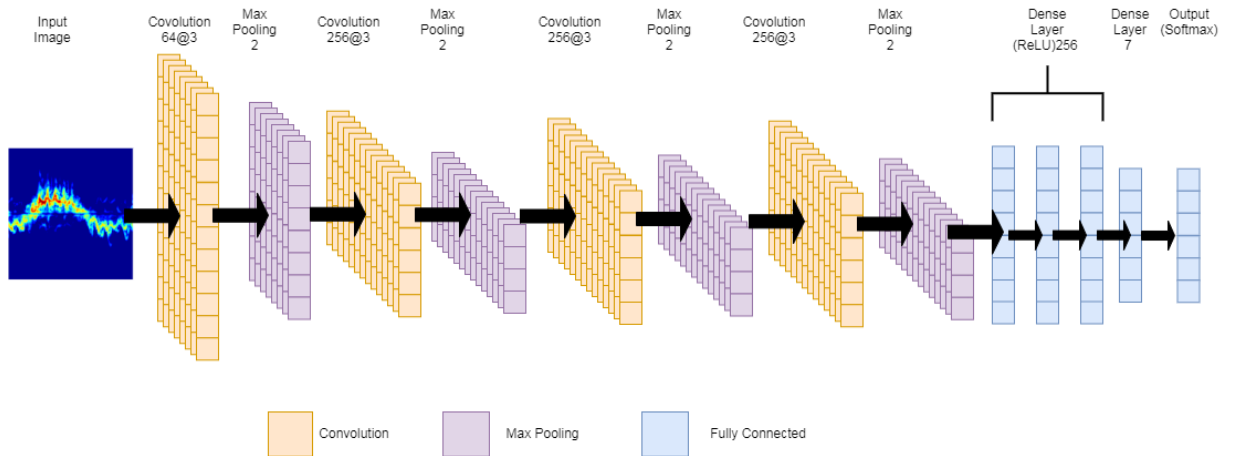


Figure 4.5: Visual Representation of CNN Model Used in Experiment.

## 4.3 Results and Discussion

This section presents the weighted average results of each of the classifications carried out in each experiment. Each experiment presents the weighted average accuracy in bar chart format and then the weighted average accuracy, precision, recall and F1-score in table format.

### 4.3.1 Original Dataset

**Raw Images**

The accuracy results of each ML algorithm using just the Raw Images are visually displayed in bar chart format in Figure 4.6.

The results of the ML algorithms show KNN has superior performance using the raw image data. KNN has an accuracy of 90.85 %. KNN performs the best out of all the algorithms and can therefore classify the majority of the images correctly. These results show that the ML algorithms applied to the image data can identify the differences in the image data with KNN

being able to distinguish the differences at a higher rate than the other algorithms. The other algorithms were still able to recognise differences in the images. CNN was the second-best performer with 85.97 % accuracy. SVM is the weakest performer out of all algorithms but still achieved 71.34 % accuracy.

Table 4.3 shows the accuracy and the average precision, recall and F1-score of the ML algorithms using the raw images.
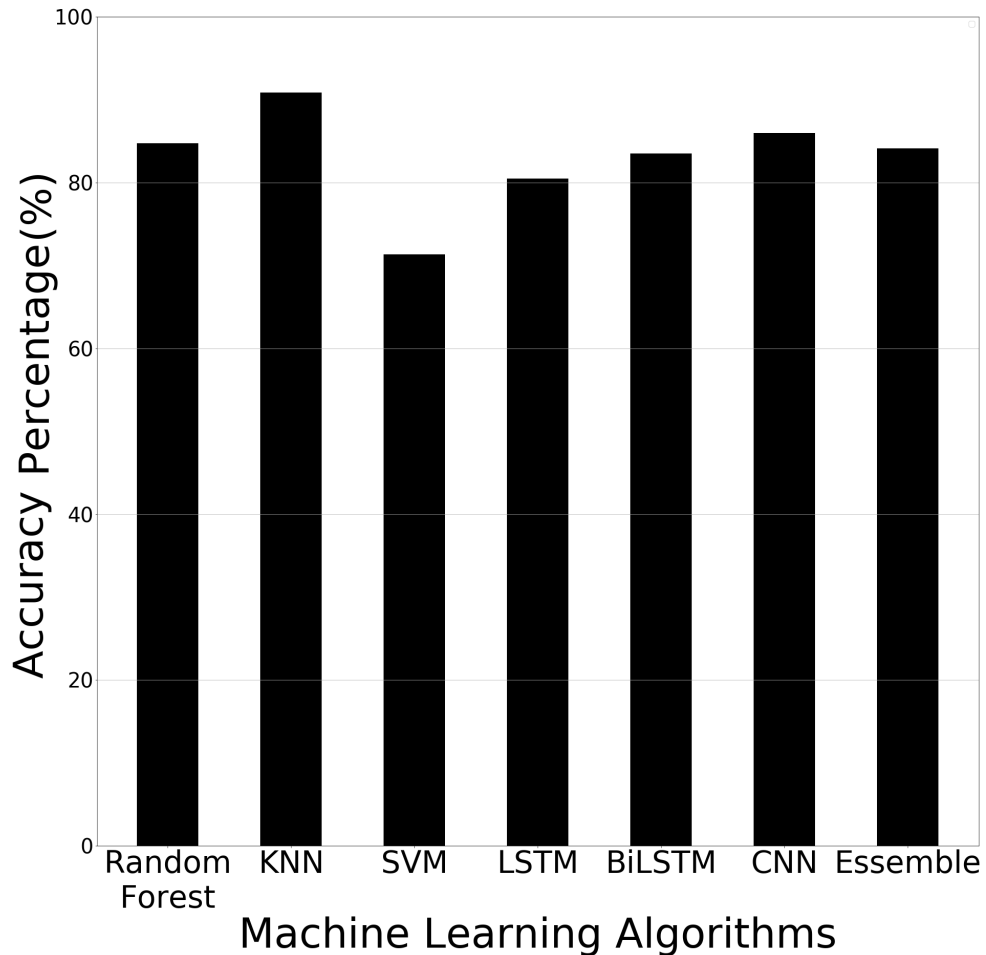


Figure 4.6: Machine Learning Results Using Raw Image Data.

Table 4.3: Machine Learning Results Using Raw Image Data.

| Algorithm | Accuracy | Precision | Recall | F1-score |
|---|---|---|---|---|
| Random Forest | 84.75 % | 0.86 | 0.85 | 0.85 |
| KNN | 90.85 % | 0.91 | 0.91 | 0.91 |
| SVM | 71.34 % | 0.74 | 0.71 | 0.71 |
| LSTM | 80.48 % | 0.83 | 0.80 | 0.80 |
| BiLSTM | 83.53 % | 0.87 | 0.84 | 0.84 |
| CNN | 85.97 % | 0.86 | 0.86 | 0.86 |

**Principal Component Analysis**

The accuracy results of each ML algorithm using PCA are visually displayed in bar chart format in Figure 4.7.

The results of the PCA displayed a drop in comparison to using the raw image data.  KNN has maintained its status as being the highest performer in the ML algorithms but it has dropped by 13.42 % in accuracy from 90.85 % using raw data to 77.43 % using PCA. SVM had the smallest drop in performance compared to the other algorithms when using PCA with a drop of 1.22 % from 71.34 % down to 70.12 %.  These results show that using PCA decreases the accuracy compared to the results of using raw data.  The Deep Learning algorithms are still ultimately able to differentiate between human motions using PCA despite the drop in accuracy.

Table 4.3 shows the Accuracy and the Average Precision, Recall and F1-score of the ML algorithms PCA with the image data.
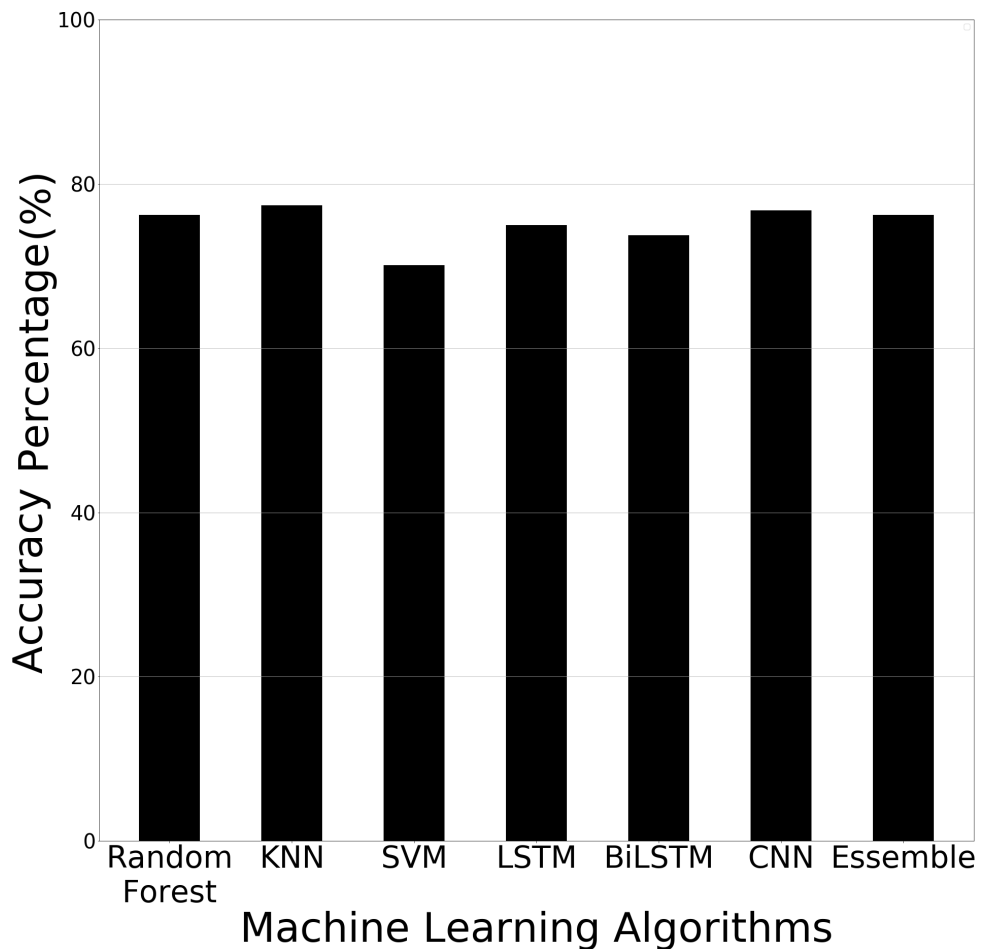


Figure 4.7: Machine Learning Results Using Raw Image Data With PCA.

Table 4.4: Machine Learning Results Using Raw Image Data With PCA.

| Algorithm | Accuracy | Precision | Recall | F1-score |
|---|---|---|---|---|
| Random Forest + PCA | 76.21 % | 0.78 | 0.76 | 0.76 |
| KNN + PCA | 77.43 % | 0.78 | 0.77 | 0.77 |
| SVM + PCA | 70.12 % | 0.71 | 0.70 | 0.70 |
| LSTM + PCA | 75.00 % | 0.76 | 0.75 | 0.75 |
| BiLSTM + PCA | 73.78 % | 0.74 | 0.74 | 0.74 |
| CNN + PCA | 76.82 % | 0.78 | 0.77 | 0.77 |

## 4.3.2 Augmented Dataset

**Raw Images**

The accuracy results of the ML algorithms using data augmentation are visually displayed in bar chart format in Figure 4.8.
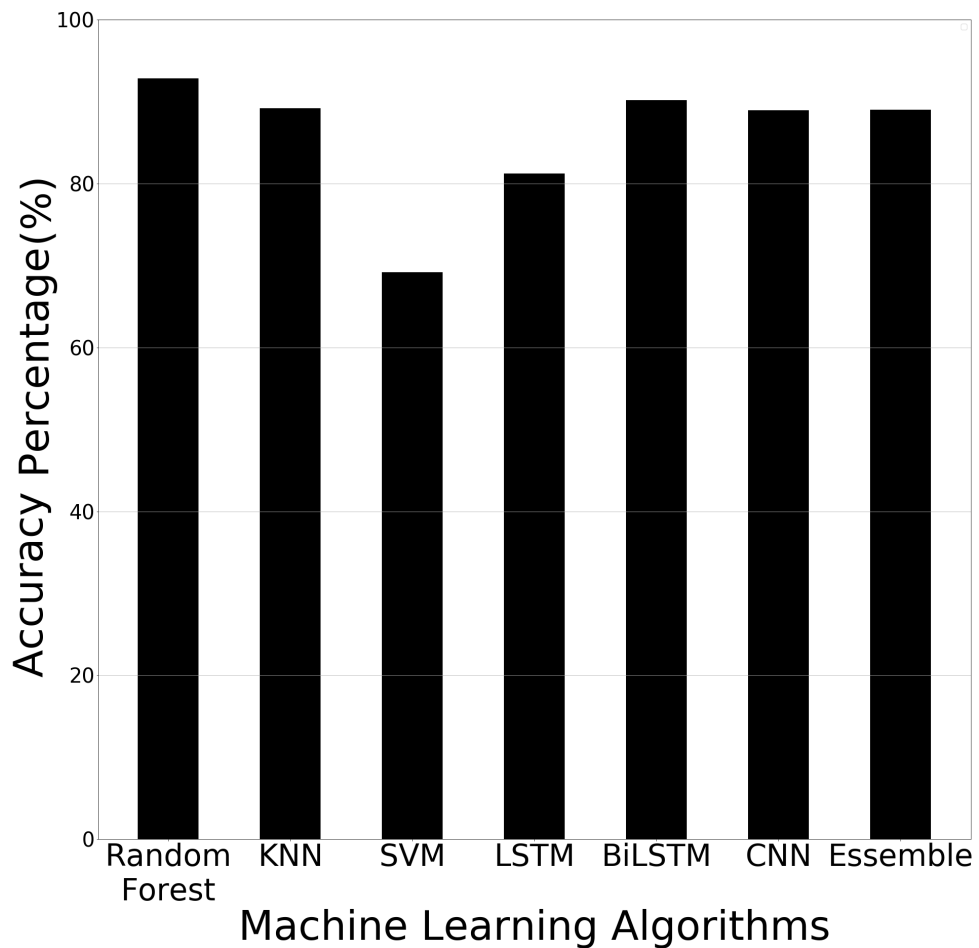


Figure 4.8: Machine Learning Results Using Data Augmentation.

The results of using Data Augmentation have shown that Random Forest has increased in

accuracy with the benefits of having more training data in comparison to only using raw images with no data augmentation. The accuracy of Random Forest has increased by 8.1 % from 84.75 % to 92.85 %. KNN and SVM have decreased their accuracy scores with the added training data. The accuracy of KNN has dropped by 1.67 % from 90.85 % to 89.18 %. The drop in accuracy with SVM is 2.16 % from 71.34 % down to 69.18 %. SVM remains the lowest performer out of all the ML algorithms. SVM and KNN are both known to not be suited to large datasets. This would explain why they both had a decrease in accuracy with the augmented data. Whereas Random Forest has now outperformed KNN. The BiLSTM algorithm result increased accuracy by 6.67 % from 83.53 % to 90.20 % making it the second-best performing algorithm. The CNN algorithm has an accuracy of 88.97 % when using the Data Augmentation dataset. It had an accuracy increase of 3.00 % compared to using the raw image dataset. The LSTM did improve slightly when using the data augmentation dataset with an increase of 0.74 % from 80.48 % to 81.22 %. Table 4.5 shows the accuracy and the average precision, recall and F1-score of the ML algorithms using data augmentation techniques.

Table 4.5: Machine Learning Results Using Data Augmentation.

| Algorithm | Accuracy | Precision | Recall | F1-score |
|---|---|---|---|---|
| Random Forest | 92.85 % | 0.93 | 0.93 | 0.93 |
| KNN | 89.18 % | 0.89 | 0.89 | 0.89 |
| SVM | 69.18 % | 0.70 | 0.69 | 0.69 |
| LSTM | 81.22 % | 0.83 | 0.81 | 0.81 |
| BiLSTM | 90.20 % | 0.90 | 0.90 | 0.90 |
| CNN | 88.97 % | 0.91 | 0.89 | 0.89 |

**Principal Component Analysis**

The accuracy results of the ML algorithms using data augmentation with PCA are displayed in Figure 4.9 The ML results using PCA, and data augmentation have shown that KNN, SVM, LTSM and CNN have improved when using PCA and data augmentation in comparison to just using data augmentation. KNN results increased from 89.18 % to 91.63 % compared to using only data augmentation techniques. SVM increased from 69.18 % to 74.28 % compared to using only data augmentation techniques. LSTM increased the accuracy result from 81.22 % up to 87.14 % and CNN increased accuracy from 88.97 % up to 95.30 %. The result from CNN is the highest achieved result through all experiments undertaken throughout this chapter.

When the KNN, SVM, LTSM and CNN algorithms were applied to the PCA dataset without data augmentation, the results decreased in performance. These results show that for KNN, SVM, LTSM and CNN, the additional training data helps to improve the performance. The Random Forest and BiLTSM algorithms showed a decrease in performance using PCA and data augmentation in comparison to only using data augmentation. The accuracy only fell by 2.24
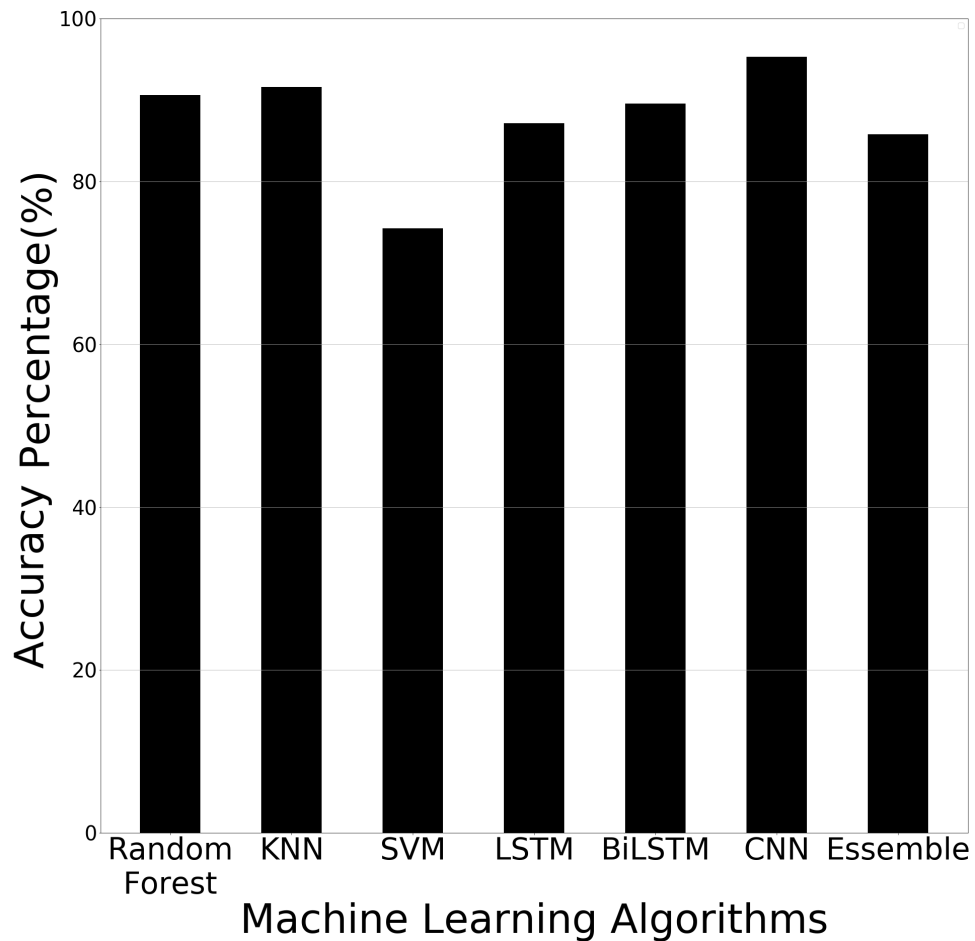
Figure 4.9: Machine Learning Results Using Data Augmentation With PCA.

% from 92.85 % down to 90.61 % for Random Forest and BiLTSM fell from 90.20 % to 89.59 %. This drop is significantly less severe than the drop observed in the results of Random Forest and CNN when using raw images to then using the raw images with PCA. Where Random Forrest dropped accuracy by 8.54 % and BiLTSM dropped accuracy by 9.75 %. This shows that PCA performs better in most of all ML algorithms when the training data is increased with the exception being the Random Forest and CNN algorithms.

Table 4.6: Machine Learning Results Using Data Augmentation With PCA.

| Algorithm | Accuracy | Precision | Recall | F1-score |
|---|---|---|---|---|
| Random Forest + PCA | 90.61 % | 0.91 | 0.91 | 0.91 |
| KNN + PCA | 91.63 % | 0.92 | 0.92 | 0.92 |
| SVM + PCA | 74.28 % | 0.75 | 0.74 | 0.74 |
| LSTM + PCA | 87.14 % | 0.88 | 0.87 | 0.87 |
| BiLSTM + PCA | 89.59 % | 0.90 | 0.90 | 0.90 |
| CNN + PCA | 95.30 % | 0.95 | 0.95 | 0.95 |

### 4.3.3 Ablation Studies
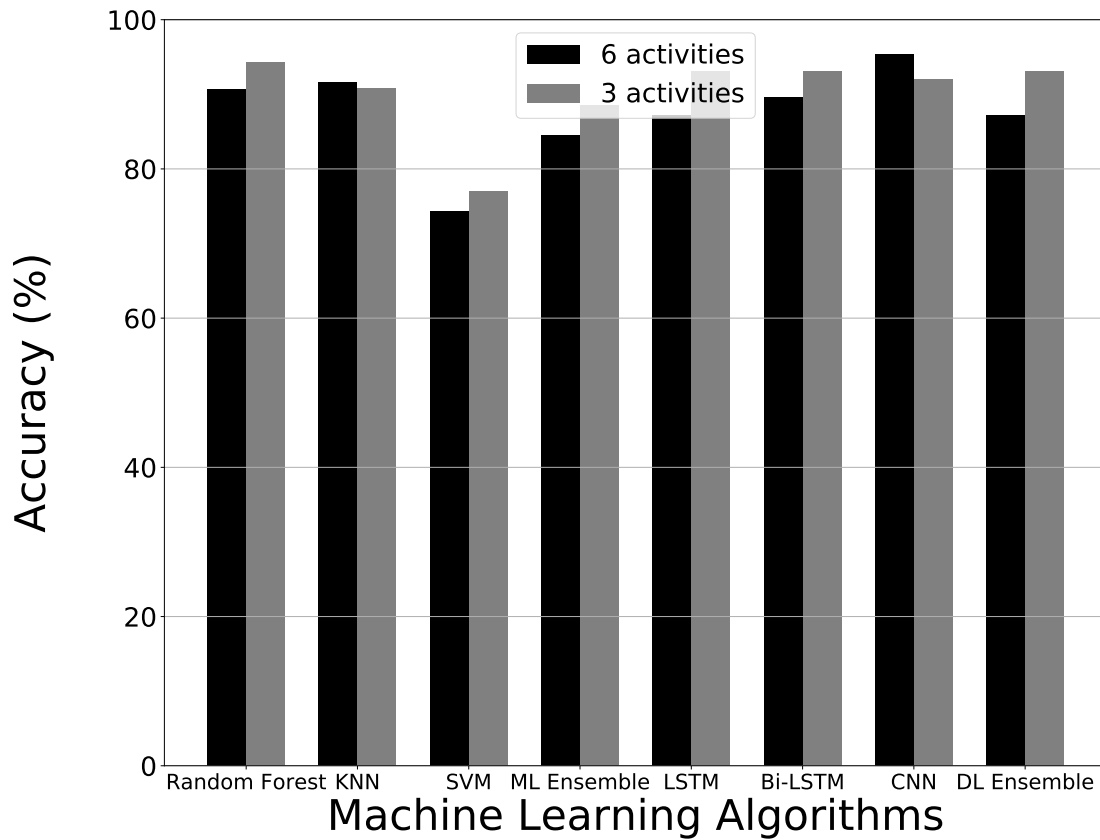


Figure 4.10: Ablation Studies Results Using Data Augmentation Paired With PCA.

This section details ablation. Ablation is the process of removing activities within the dataset and an analysis of how the reduced number of classifications has compared to results achieved using the complete dataset. For this section, the best-performing dataset using data augmentation and PCA has been reduced from 6 activities to 3. The 3 activities used are walking, sitting and standing. Figure 4.10 shows the accuracy of the comparison of each algorithm between 3 and 6 activities. Most algorithms achieved higher results while using fewer classifications however KNN and CNN algorithms performed worse with 3 activities. The difference with KNN is negligible and the difference in performance with CNN is likely due to the reduced amount of training data. In experiments using 6 activities, it was observed that CNN performs better with more training data.

## 4.4 Comparison to State-Of-The-Art Approaches

The results of the proposed approach can be directly compared to the results of [47] as this work used the same dataset used in the experiments of this chapter. [47] used SVM and KNN algorithms and these algorithms achieved an accuracy score of 78.25 % and 77.15 % respectively. SVM in the results presented in this chapter achieved the highest result of 74.28 % which was lower than the work done in [47]. However, in this work, KNN achieved its highest result of 91.63 % when using data augmentation paired with PCA. The data processing techniques used in this chapter have allowed for the KNN algorithm to improve the accuracy results by nearly 15 %. The highest results achieved in this chapter by using the CNN algorithm paired with PCA and data augmentation of the original dataset achieved an accuracy score of 95.30 %. This result shows that by applying PCA and data augmentation to the data of [47], the results have increased from 78.25 % in [47] to 95.30 %. Therefore it can be stated that by implementing data processing techniques and more complex algorithms, we can increase the accuracy of identifying different human activities.

## 4.5 Summary

This chapter presented results obtained when Machine and Deep Learning techniques were applied to a radar dataset that was previously generated containing radar micro-Doppler spectrogram for various human activities. The research work has found that using PCA paired with Augmentation of the available data, achieved the best results of 95.30 % using the Deep Learning algorithm namely CNN. These results have outperformed the state-of-the-art approaches. The results also highlighted how PCA can help to increase accuracy when the training data is expanded using Data Augmentation. Without Data Augmentation, it was found that PCA harmed the results. Although the highest ML result was obtained using Random Forest without PCA, the rest of the ML algorithms displayed higher results when PCA was used with Data Augmentation. The results of this chapter have shown that AI can identify the different ADLs that are detected by radar sensing by performing image classification on the acquired micro-Doppler signature. Future work of this research can seek to implement systems that make use of the data processing and Deep Learning techniques presented in the findings of this chapter to improve the lives of elderly people.

# Chapter 5

# Introduction to Machine Learning Assisted RF Sensing

This chapter demonstrates how human motions can be detected in quasi-real-time scenarios using Contactless RF sensing. Patterns in the wireless signals present particular human body motions as each movement induces a unique change in the wireless medium. These changes can be used to identify particular body motions. This work produces a dataset that contains patterns of radio wave signals obtained using software-defined radios (SDRs) to establish if a subject is standing up or sitting down as a test case. The dataset was used to create an ML model, which was used in a developed application to provide a quasi-real-time classification of standing or sitting state. The ML model was able to achieve 96.70 % accuracy using the Random Forest algorithm using 10-fold cross-validation. A benchmark dataset of contact-based devices was compared to the proposed dataset and results showed the proposed dataset to have similar accuracy of nearly 90 %. The ML models developed in this chapter are tested for two activities but the developed system is designed and applicable for detecting and differentiating x number of activities.

## 5.1   Introduction

This research will explore the use of a USRP device to build a dataset of CSI of human activities and then use ML for binary classification of a human either sitting down or standing up. USRPs will be used because they offer a simple framework for experimentation rather than setting up complex systems for functionality testing [235, 12]. USRPs are widely used in research applications because of their ability to transfer and receive frequencies in several bands [236]. URSPs provide flexibility as they can be tuned to a wide range of frequencies [237]. This work will use 64 subcarriers. OFDM is used for 64 points of Fast Fourier Transformer (FFT) producing 64 frequency carriers (subcarriers) [238]. Lower frequencies can detect the smaller movements while higher frequencies can detect larger movements [99]. Using USRPs allow for a range of

frequencies to be used in the experimentation which will allow a greater detection of movements overall. This chapter aims to research the ability to use RF signals to be able to classify human motion in a real-time application. This chapter reports two major contributions to the state of the art. The first contribution is presenting a simple set-up of how an ML model can provide a real-time classification of human motion using data retrieved from a URSP. The second contribution is providing a comparison between the newly acquired dataset and an existing contact-based device human motion dataset. This chapter is organised into the following sections. Section 2 will detail some of the related work. Section 3 will detail the methods employed to collect the data. Section 4 will describe the methods of ML used and section 5 will display the results and discuss said results as well as compare the results to a benchmark dataset collected from contact-based devices.

## 5.2   Collection of Data
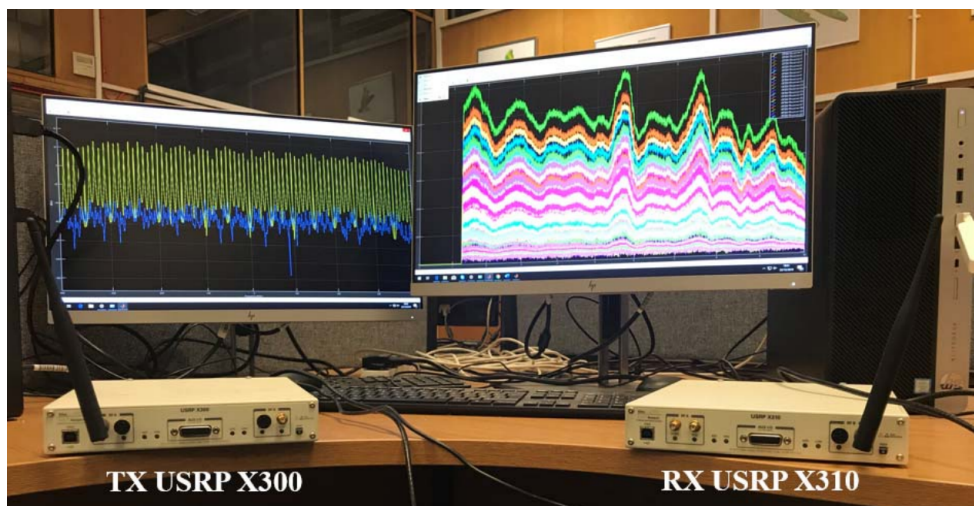


Figure 5.1: USRP Devices Used in This Chapter.

In this section, the methods of how the data is collected are discussed. The work of this chapter makes use of USRP devices to send packets between antennas[239]. Two USRP devices used are the X310/X300 models from National Instruments (NI), each equipped with extended bandwidth daughterboard slots covering DC– 6 GHz with up to 120 MHz of baseband bandwidth. The X300 model was used as the transmitter with the X310 model performing as the receiver. The devices were connected to two PCs through 1G Ethernet cable connections. The USRP's were equipped with two VERT2450 Omni-directional antennas. The simulation was designed using MATLAB/Simulink program linked to the USRP devices. The experiment was undertaken in an office environment and USRP devices were kept at 4 metres within line of sight of each other, to achieve the best performance. Figure 5.1 shows the two USRP devices used in this experiment. Experiments were performed with set parameters. Table 5.1 lists the parameters of the software

configuration of the USRP devices.

Table 5.1: Software Configuration Parameters Selection.

| Parameters | Values |
|---|---|
| Input data (Signal) | round(0.75*rand(104,1)) |
| Sample time | 1/80e4 |
| Modulation type | QPSK |
| Bit per symbol M | 2 bits |
| OFDM Subcarrier | 64 subcarriers |
| Pilot subcarrier | 4 |
| Null subcarrier | 12 |
| Cycle prefix M | NFFT-data subcarrier |
| Samples per frame | Used subcarrier log2 (M) |

The USRP devices used in the study have a frequency range from 1 GHz to 10 GHz. The centre frequency for the USRPs was set as 5.32 GHz. The gain of USRP devices was set to be 70 for the transmitter and 50 for the receiver. The hardware parameter values of the USRP are summarised in table 5.2.

Ethical approvals of participants have been acquired through the University of Glasgow ethics review committee. The participants were asked to perform standing-up and sitting-down motions. Participants completed the task multiple times to be able to collect many samples of CSI to allow for error and allow the cleanest samples to be taken forward. The test was performed in a 7 by 8 meters office space containing furniture such as tables, chairs, draws, etc. The human motions are then carried out between the antennas and the CSI is then recorded while this human motion is carried out. As the radio signal propagation is affected by the movement of the human; the CSI will differentiate as different human movements take place. The goal is that the CSI will display specific patterns which can be associated with specific human movements. In this chapter, the CSI for multiple subjects sitting down on a chair and then standing from a chair is collected. As there are many variations in the way the signals propagate and human movement will never be the same, the movement should follow the same patterns in the CSI data. Some samples can be considered good samples where interference is set to a minimum and some samples may be affected by ambient movement or atmosphere factors. Multiple samples of the movements are captured to provide an adequate representation of the overall patterns associated with specific movements despite variations in signal propagation caused by differences in posture and timing between samples. The final dataset contains 30 samples each of sitting and standing. Which is enough samples to display the general pattern of each activity.

Figures 5.2 and 5.3 display the CSI of the 64 subcarriers of the USRP. Each colour represents a subcarrier and the amplitude of the subcarrier is shown along the Y-axis and time is shown along the X-axis while an activity is taking place. Figure 5.2 shows the pattern followed in a good sample of sitting down and Figure 5.3 shows the pattern followed in a good sample of standing up.

Table 5.2: Hardware Configuration Parameters Selection.

| Parameters | Values |
|---|---|
| Platform | USRP X300/X310 |
| TX IP address | 192.168.11.1 |
| RX IP address | 192.168.10.1 |
| Channel mapping | 1 TX, 2 RX |
| Centre frequency | 5.32 GHz |
| Clock source | Internal |
| Master clock rate | 120 MHz |
| Gain (dB) | TX 70, RX 50 |
| Sample time | 1/80e4 |
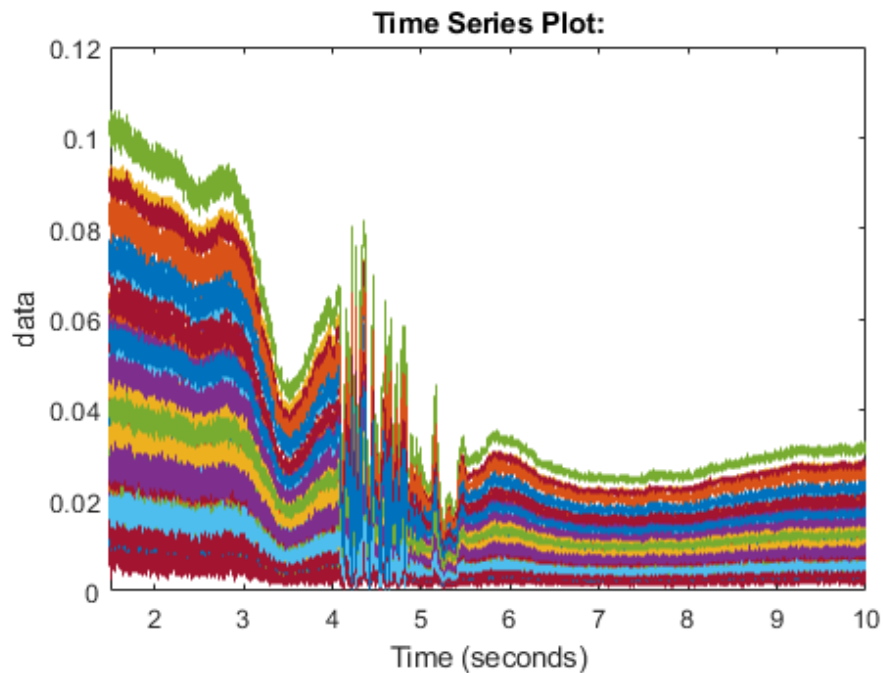


Figure 5.2: CSI for the Human Motion of Sitting Down.
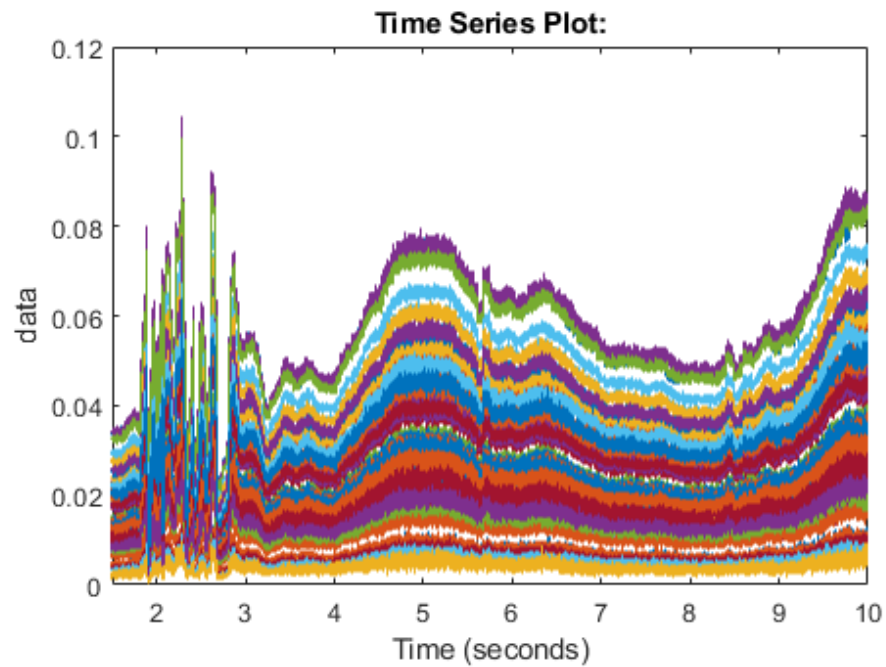
Figure 5.3: CSI for the Human Motion of Standing Up.

The USRPs are configured to transmit data from one antenna to the other for 10 seconds. As the signals propagate in different ways each time a sample is taken then the number of packets received has slight variations. However, this has little effect as the aim is to detect patterns in the radio waves as a certain human motion is carried out during the transmission of packets. Figure 5.4 details the process used in this experimentation.
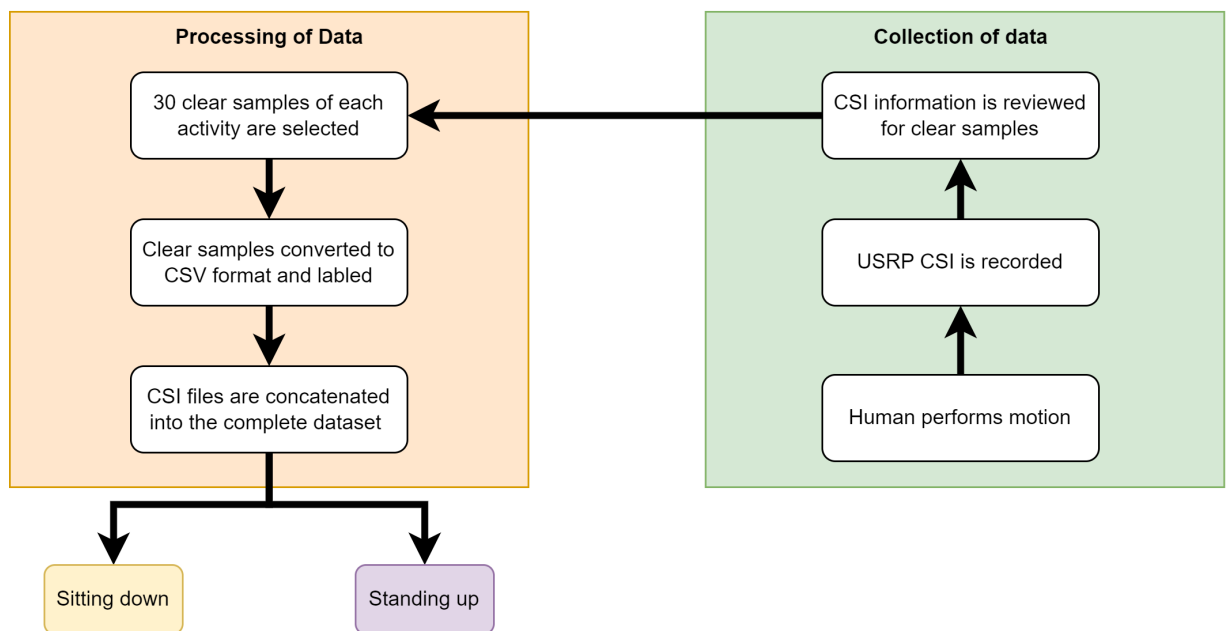


Figure 5.4: Experiment Flow Chart.

## 5.3 Machine Learning Process

The dataset performance has been measured using a range of ML algorithms using the Python SciKit library. Scikit is an ML package that is widely used in the data science field [222]. The Samples are converted into CSV format so that they can be processed using the SciKit library. The Python library Pandas is used to process the CSV files. Pandas imports the CSV files as dataframes within Python which the SciKit library then processes [240]. The labels are added as the first column on the dataframes as the data is of varying lengths throughout the samples. Then the dataframe of each sample is combined to make the full dataset, the varying lengths result in Not a Number (NAN) values being part of the dataset. To resolve this issue SciKit provides a function called simpleimputer. This is used to replace all NAN values with a 0. Therefore the shorter samples of the dataset will contain 0 values tailing the row on the CSV file. This is not perceived to be a problem as the different lengths are minor and the pattern of the RF signals is still apparent. This is part of the variance between different samples. Then a dataset is produced including all samples similar to the work done in chapter 4. The main difference is that the previous chapter's data was pixel information, Now the data is a time series of amplitude values of the RF signals. The dataset is then divided into two variables, one for the labels and one for the data itself. Then the four ML algorithms are declared. The four algorithms used to test this dataset are Random Forest, KNN, SVM, and Neural Networks. The ensemble classifier takes each algorithm's prediction as a vote and then whichever prediction has the most votes will be the prediction declared by the ensemble classifier.

The Random Forest algorithm is a collection of decision trees. Each tree predicts the output by analysing features found in the training phase. This prediction is considered a vote. The majority of votes is the final Random Forest prediction [224].

The KNN algorithm is known for its simplicity. The algorithm works by comparing the testing data to the training data [225]. The features of the training data are assigned a K sample then the testing data is assigned to the K sample that nearest matches the new data [226].

The SVM algorithm works by constructing hyperplanes and uses these hyperplanes to separate the input data into different categories. The training data is used to train the hyperplanes based on features of the training data [228].

The Neural Network model is inspired by the human brain [241]. A Neural Network consists of an input layer, hidden layer and output layer which are all interconnected. The aim is to transform a set of inputs to the desired outputs by using weights associated with the neurons in the hidden layer [242]. The Neural Network passes training input, and output is observed. If the output is incorrect then the hidden layer is adjusted until the correct output is achieved. Then the testing data can be passed through the model as the input data and the output is the prediction [243].

Two experiments are done using each algorithm on the dataset. The first experiment makes use of 10-fold cross-validation. 10-fold cross-validation is used to test ML models where the

data is divided into training and testing data. 10-fold refers to the number of groups. Each group takes a turn as the test data and the rest of the groups are used as training data. This ensures that there is variance in the test data. The results of the 10 runs are then averaged to give the final results [244]. The second experiment uses the train test split method where the dataset is split 70/30. 70 % of the dataset is used to train the algorithm and 30 % of the dataset is used for testing. The results of this chapter will use the performance metrics of accuracy, precision, recall and F1-score. These performance metrics are calculated by looking at four classification values. The classification values are True Positive (TP), True Negative (TN), False Positive (FP) and False Negative (FN). The equations for how the performance metrics are calculated are shown in equations 5.1, 5.2, 5.3 and 5.4.

The accuracy displays the total number of correct classifications versus the total classifications made.

$$Accuracy = \frac{TP+TN}{TP+TN+FP+FN}[245] \tag{5.1}$$

The precision metric is used to measure one of the classifications against how precise it is in comparison to all classifications. The results are presented as an average between both sitting and standing.

$$Precision = \frac{TP}{TP+FP}[245] \tag{5.2}$$

The recall is used to show the ratio of the correct classification to all classifications for that label. This is run for both sitting and standing and presented as an average.

$$Recall = \frac{TP}{TP+FN}[245] \tag{5.3}$$

The F1-score is used to provide an average between the precision and recall Metrics.

$$F1 - score = 2X\frac{Precision * Recall}{Precision + Recall}[245] \tag{5.4}$$

## 5.4   Results and Discussion

This section presents the output of the ML algorithms after they have completed 10-fold cross-validation and train test split using the Python variables containing the data and comparing the prediction of the data to the actual labels of the data. The performance metrics used to compare the algorithms include the accuracy score as well as precision, recall and F1-score. A confusion matrix is also provided to show how each sample has been classified.

## 5.4.1 Cross-Validation

Table 5.3: Cross-Validation Results.

| Algorithm | Accuracy | Precision | Recall | F1-Score |
|---|---|---|---|---|
| Random Forest | 92.47 % | 0.93 | 0.92 | 0.92 |
| KNN | 88.17 % | 0.89 | 0.88 | 0.88 |
| SVM | 84.68 % | 0.86 | 0.85 | 0.85 |
| Neural Network model | 90.05 % | 0.90 | 0.90 | 0.90 |
| Ensemble Classifier | 92.18 % | 0.92 | 0.92 | 0.92 |

In table 5.3 it can be seen that the best accuracy is from Random Forest followed by the Neural Network. Although both KNN and SVM still have high accuracy. When the algorithms are compiled together in the ensemble classifier the accuracy is 92.18 %. The accuracy is calculated as an average of the 10 sets of testing data used in each of the 10-fold cross-validation processes. The dataset is made up of 30 samples each of sitting and standing which each contain 64 sub-carriers. So the total number of rows contained in the dataset is 3840 subcarriers. The confusion matrix is a table used to describe how an algorithm has performed. The confusion matrix shows exactly how many samples were classified in which category. The X-axis represents the actual classification and the Y-axis on the confusion matrix represents the prediction of the algorithm.



Figure 5.5: Confusion Matrix for Random Forest.

The Random Forest algorithm was the best performer out of all the algorithms. It can be seen in Figure 5.5 how the 3840 samples have been classified. 1821 sitting samples were correctly classified as sitting. This is represented in the top left square where the X axis matches the Y axis. Then 99 sitting samples were incorrectly classified as standing. This is where the X-axis

and Y-axis mismatch. The majority of sitting samples were correctly classified so this shows good results. The classification of standing samples was slightly less accurate but still had good results. This can be attributed to the variance of noise between collected training samples. 190 samples were classified incorrectly as sitting, which is higher than the 99 sitting samples incorrectly classified as standing. This leaves the remaining 1730 standing samples as being correctly classified.
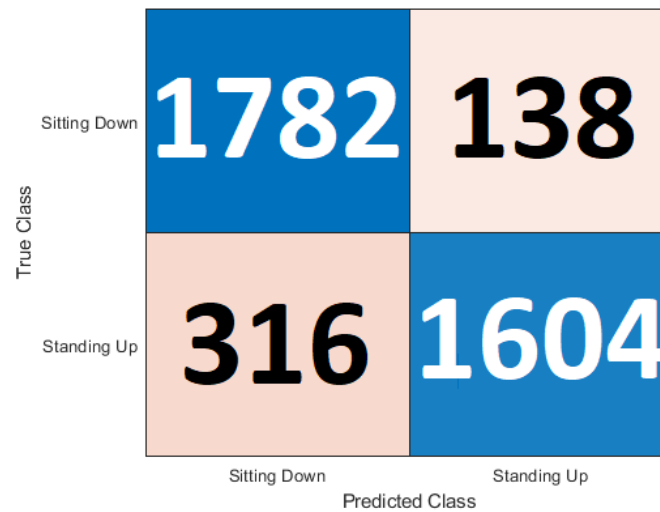


Figure 5.6: Confusion Matrix for KNN.

The KNN algorithm had an accuracy score of 88.17 %, which is only around 4 % less than Random Forest. In the confusion matrix shown in Figure 5.6 it can be observed how much the classifications differ in the 4 % difference in accuracy. It appears that both algorithms had better classification results with sitting over standing. KNN had 138 sitting classified incorrectly classified as standing but had 316 standing classified incorrectly classified as sitting. However, the majority of subcarriers were classified correctly.

Figure 5.7: Confusion Matrix for SVM.

SVM was the lowest-scoring algorithm in this experiment but with an accuracy score of 84.68 %, the majority of samples were classified correctly. Unlike Random Forest and KNN, SVM showed better performance with the standing-up samples. Only 111 of the standing sub-carriers were wrongly classified as sitting down. 477 sitting-down samples were classified incorrectly as standing. As shown in Figure 5.7. This is likely due to the standing-up samples being dominant in the training data as SVM is sensitive to high-class imbalance.



Figure 5.8: Confusion Matrix for Neural Networks.

The Neural Network classifier had the second-best accuracy score of 90.05 %. Like Random Forest and KNN, it had better performance with sitting-down samples. The confusion matrix shown in Figure 5.8 shows only 132 sitting samples were incorrectly classified compared to the 250 standing samples classified incorrectly.

Figure 5.9: Confusion Matrix for Ensemble Classification.

The confusion matrix for the ensemble classification is shown in Figure 5.9. The ensemble has the best performance with the sitting-down samples with only 75 of the samples being classified as incorrect. The ensemble classifier was let down by the standing-up samples as it incorrectly classified 225 samples. It can be seen that the ensemble technique worked well with the sitting-down samples but was not so good with the standing-up samples. The SVM algorithm had the lowest error rate for standing-up samples.

### 5.4.2 Train Test Split

Table 5.4: Train Test Split Results.

| Algorithm | Accuracy | Precision | Recall | F1-Score |
|---|---|---|---|---|
| Random Forest | 96.70 % | 0.97 | 0.97 | 0.972 |
| KNN | 90.71 % | 0.91 | 0.91 | 0.91 |
| SVM | 81.77 % | 0.87 | 0.82 | 0.82 |
| Neural network model | 93.40 % | 0.94 | 0.93 | 0.93 |
| Ensemble Classifier | 93.83 % | 0.94 | 0.94 | 0.94 |

Train Test Split is used to split the data between training and testing data. It allows for explicitly setting how much of the dataset should be reserved for testing. The algorithms use the training data to attempt to learn patterns in the data. The algorithms then perform predictions on the reserved test data. These predictions are then compared to the labels of the test data. This comparison is how the results are calculated. In table 5.4 it can be seen that the best accuracy is still Random Forest followed by the Neural Network. Although both KNN and SVM still have high accuracy. When the algorithms are compiled together in the ensemble classifier the

accuracy is 93.83 %. The accuracy is calculated by comparing the 30 % test data predictions to the actual labels of the data. The full dataset is made up of 30 samples each of sitting and standing which each contain 64 subcarriers. So the total number of rows contained in the dataset is 3840 subcarriers. 1152 subcarriers is the number of the 30 % test samples used in the train test split method rather than the whole dataset used for testing data at some point. The percentage of testing data influences the amount of training data available. The more training data the more opportunity the algorithms have to learn. 30 % is selected to have a large portion of testing data but still have the majority of the data as training data. In the testing data, there are 512 standing-up samples and 640 sitting-down samples. The confusion matrix in this experiment shows only the 1152 samples, the total number of tested samples.



Figure 5.10: Confusion Matrix for Random Forest.

The Random Forest algorithm was the best performer out of all the algorithms. It can be seen in Figure 5.10 how the 1152 samples have been classified. 606 sitting samples were correctly classified as sitting. This is represented in the top left square where the X axis matches the Y axis. Then 34 sitting samples were incorrectly classified as standing. This is where the X-axis and Y-axis mismatch. The majority of sitting samples were correctly classified which is a positive result. The classification of standing samples was more accurate than sitting in contrast to the cross-validation results. Only 4 samples were classified incorrectly as sitting this leaves the remaining 508 standing samples as being correctly classified.

Figure 5.11: Confusion Matrix for KNN.

The KNN algorithm had an accuracy score of 90.71 %, which is an improvement over the cross-validation experiment. In the confusion matrix shown in Figure 5.11, KNN just like Random Forest performed better with the standing-up samples rather than the sitting-down samples. KNN had 69 sitting subcarriers incorrectly classified as standing but had only 38 standing classifiers incorrectly classified as sitting. However, the majority of subcarriers were classified correctly.



Figure 5.12: Confusion Matrix for SVM.

SVM was the lowest-scoring algorithm in this experiment but with an accuracy score of 81.77 %, the majority of samples were classified correctly. Like Random Forest and KNN, SVM showed better performance with the standing-up samples. Only 1 of the standing subcarriers was wrongly classified as sitting down however 209 sitting down samples were classified incorrectly

as standing, as shown in Figure 5.12.



Figure 5.13: Confusion Matrix for Neural Networks.

The Neural Network classifier had the second-best accuracy score of 93.40 %. Like the other algorithms, it had better performance with standing-up samples. The confusion matrix shown in Figure 5.13 shows 76 sitting samples were incorrectly classified compared to the 0 standing samples classified incorrectly.
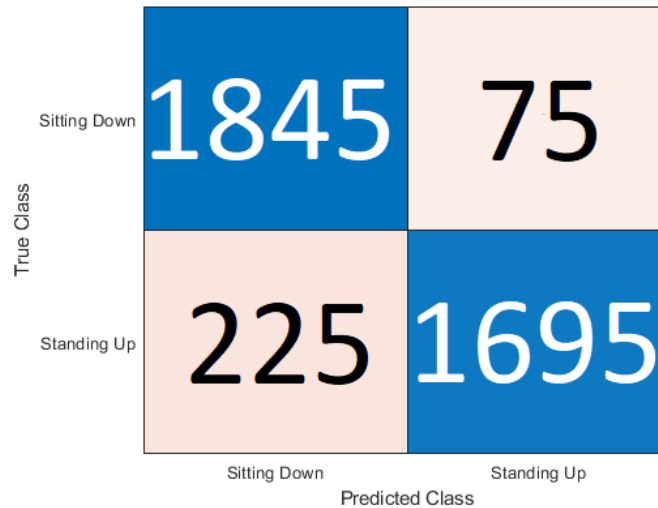


Figure 5.14: Confusion Matrix for Ensemble Classification.

The confusion matrix for the ensemble classification is shown in Figure 5.14. The ensemble method shows better performance with the standing samples as expected as all the algorithms performed better with the standing samples. The ensemble method gave a good average number for the incorrect sitting samples preventing it from going too high, making use of the voting system.

### 5.4.3 Comparison of Cross-Validation and Train Test Split

The difference in accuracy can be seen in Figure 5.15. The train test split shows better classification results with the standing-up samples. This is because there are more standing-up samples within the 70 % training set. This shows that more training on a sample gives better results. All of the algorithms have higher accuracy except for SVM with the train test split. Cross-validation however gives a better representation of the algorithm performance since all of the data takes a turn of training and testing so every possible combination is tested.
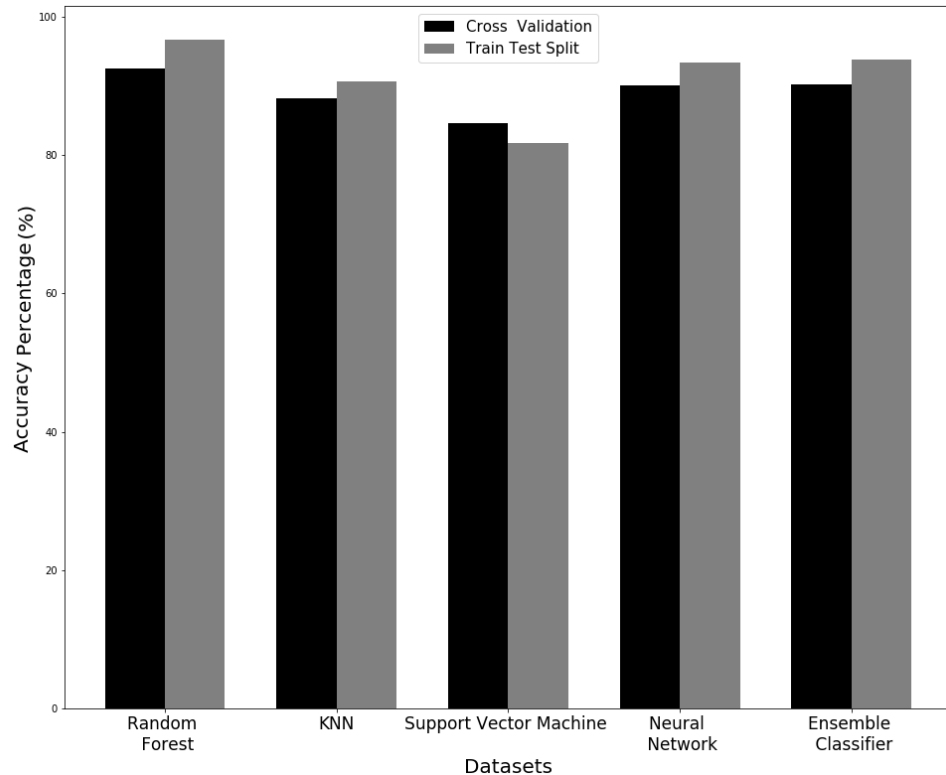


Figure 5.15: Comparison of Cross-Validation and Train Test Split.

### 5.4.4 Real-Time classification

For Real-Time classification of data, the dataset needs to be used to create a model. As Random Forest provided the highest accuracy results in experiments using cross-validation and train test split, it was chosen to create the model. As it has shown to perform well with this time series data. Instead of dividing the dataset into 10 groups for cross-fold validation, the whole dataset was used for training. This allows models to be trained on all available data. The SciKit Python package allows for models to be saved and recalled later by using the Joblib package. Flask was used to create a web interface that could action Python scripts.

The application works when the user presses the "Run Classification" button. The button then actions a Python script within the Flask app. The Python script works by connecting to the Matlab session that records the CSI from the USRP. The Matlab session will need to be shared

and then Python can connect and access the variables stored on Matlab. When an experiment is run on the USRP the CSI is stored in a time series called CSI in Matlab. The Python script first activates a Matlab script which then extracts the raw CSI data from the time series. Once the raw data is stored on a variable in Matlab the Python script can access the variable and apply the previously saved model to make classifications on the new data obtained from the USRP devices. As this process takes place, the interface will display "Loading..." as the output. To test the real-time application additional samples of sitting down and standing up were taken. Six of each group were taken to give a total of 12 samples. These 12 samples were completely unseen when training the model as they were not contained in the dataset. The trained model was able to correctly classify all of these samples. As seen in Figure 5.16, the classification is displayed as the output after the script has run. This web application has proved to be able to access the Matlab variable that contains the CSI obtained from the USRP and make classifications using a previously stored model. The real-time web application can be extended to make any amount of classifications as it is based on the model used to make the classifications of newly received data. Figure 5.17 details the process undertaken by the real-time application web interface.
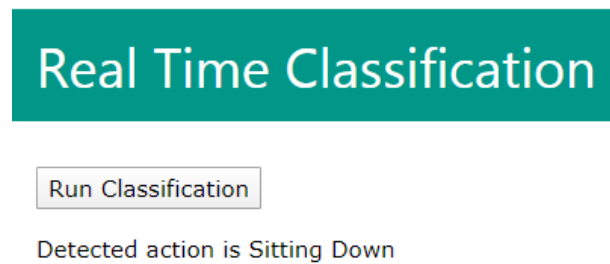


Figure 5.16: Flask Web Interface Displaying Classification Result.
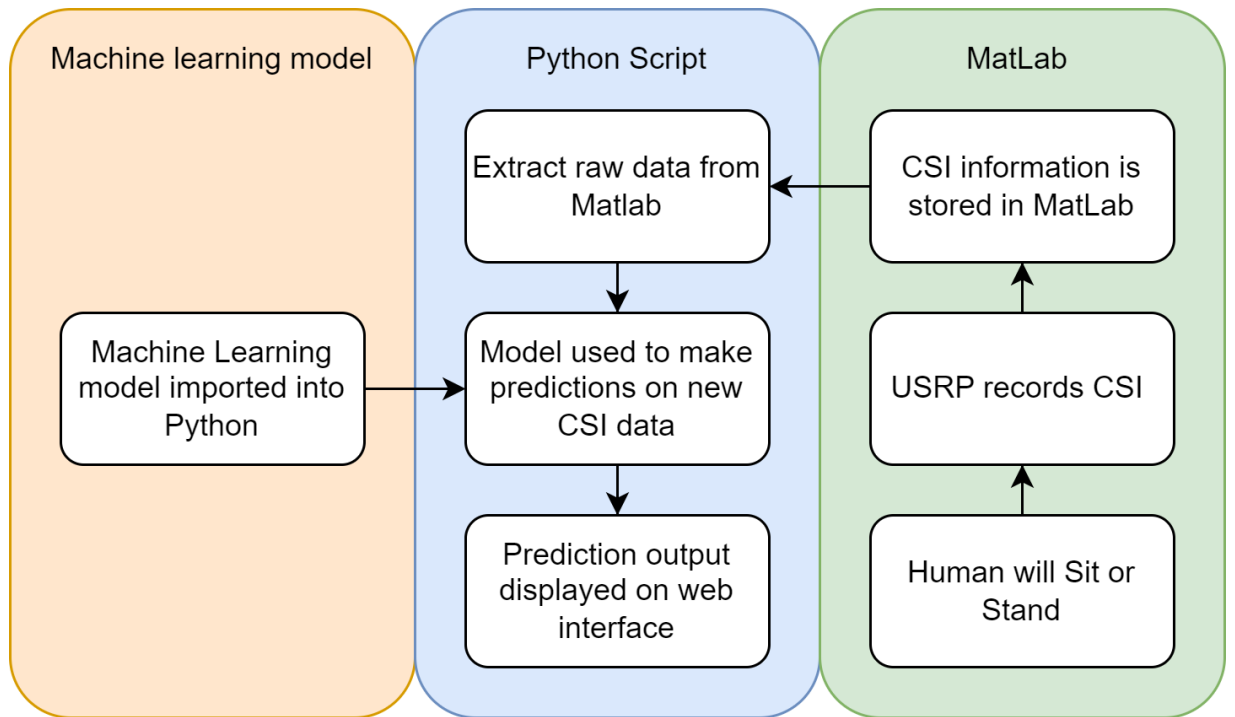
Figure 5.17: Flask Web Interface Process.

### 5.4.5 Benchmark Dataset

As the ML results for the dataset were of high accuracy, it evidences that CSI is a viable method for human motion detection. For a comparison of how effective CSI can be to identify human motion, the machine-learning results of this dataset have been compared to that of another dataset. [246] have published a dataset detecting a range of human motions using smartphones that are equipped with accelerometers. The ML process used with the USRP dataset created in this research has been applied to this benchmark training dataset. Using this contact-based dataset can show that the algorithms are able to detect patterns associated with specific movements with accelerometer data and CSI data. It also validates the use of CSI as an effective method to detect human movements.

Table 5.5: Comparison of Results With Cross-Validation.

| Algorithm | USRP Dataset Accuracy | Benchmark Dataset Accuracy |
|---|---|---|
| Random Forest | 92.47 % | 91.20 % |
| KNN | 88.17 % | 77.06 % |
| SVM | 84.68 % | 85.90 % |
| Neural network model | 90.05 % | 89.21 % |
| Ensemble Classifier | 92.18 % | 92.40 % |

Table 5.6: Comparison of Results With Train Test Split.

| Algorithm | USRP Dataset Accuracy | Benchmark Dataset Accuracy |
|---|---|---|
| Random Forest | 96.70 % | 96.49 % |
| KNN | 90.71 % | 92.48 % |
| SVM | 81.77 % | 86.21 % |
| Neural network model | 93.40 % | 96.11 % |
| Ensemble Classifier | 93.83 % | 97.74 % |
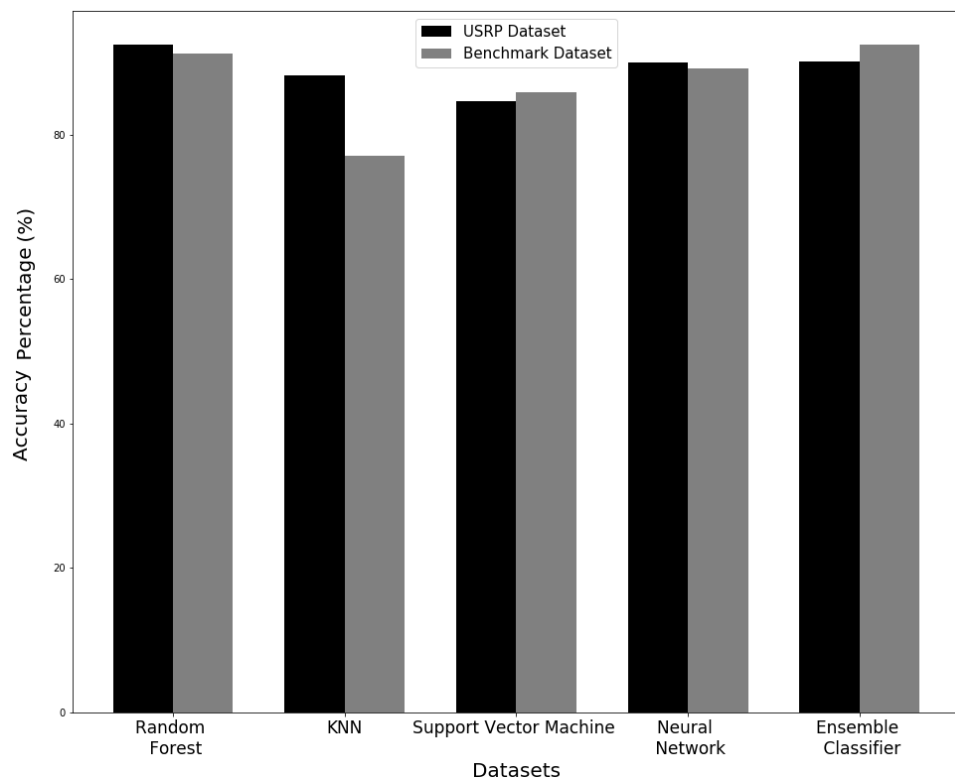


Figure 5.18: Comparison of Results With Cross-Validation.
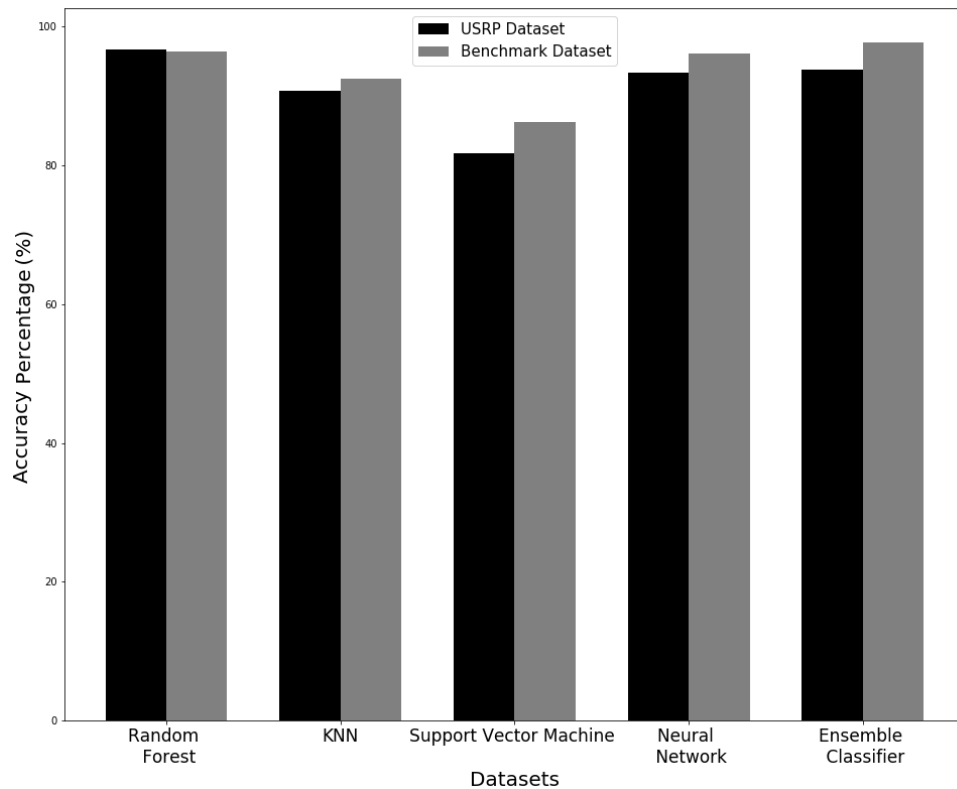
Figure 5.19: Comparison of Results With Train Test Split.

The results show that the USRP dataset can provide similar results to the benchmark dataset which is using contact-based devices. The Random Forest algorithm displays similar results. The accuracy values are shown in tables 5.5 and 5.6 for cross-validation and train test split experiments respectively. Figures 5.18 and 5.19 give a visual representation of the differences between the two datasets for cross-validation and train test split experiments respectively. The Random Forest was the best performer in both sets of data with both cross-validation and train-test split methods. KNN performed much better using the USRP dataset with cross-validation but was lower with the train-test split. SVM had similar performance within the two datasets. The Neural Network algorithm also had a small difference between datasets with a slight increase with the cross-validated USRP dataset but a larger difference in favour of the benchmark dataset when using train test split. The ensemble classifier performed better with the benchmark dataset in both methods but by only a small difference when using the cross-validation method. The results of the cross-validation experiment showed that the majority of the algorithms performed better on the USRP dataset. This is likely due to the USRP data containing raw data and the benchmark dataset containing features of the contact-based sensors. Such findings demonstrate that the USRP device is capable of producing similar results and even higher precision scores compared to a dataset obtained using contact-based devices. The primary reason that the datasets collected using USRP devices outperform the contact-based devices datasets is that USRP operates on multiple subcarriers operating on different frequencies thus providing more

data. An intricate change in wireless medium is picked up by the multiple carrier USRP model, whereas the contact-based devices such as accelerometer and magnetometer as not sensitive enough against body motion. That is why, due to high sensitivity against body motion, the USRP works better in detecting body movements.

## 5.5   Summary

This chapter has proposed an algorithm and dataset which can be used in the detection of human motion. The dataset includes observations of the CSI from USRPs as human activities take place between the antennas. The dataset is designed for binary classification between sitting down and standing up human motion. The performance of ML shows good results with the Random Forest algorithm producing a high accuracy result of 92.47 %. The high accuracy in the results shows that there is a significant difference between the CSI of standing up and sitting down for a machine algorithm to be able to establish the difference. The web application was able to successfully classify samples of data that were absent during the training phase directly from the Matlab session which contained the CSI directly from the USRP. The use of USRP data to detect human motion was also compared to a benchmark dataset where human motion was detected using contact-based devices. The same ML techniques were applied to the benchmark dataset and the results show good accuracy with the benchmark dataset.

# Chapter 6

# An Implementation of Real-time Activity Sensing Using RF signals to Identify Movement, No Activity and Empty Space

The elderly population is growing, and the healthcare system is experiencing a strain on services provided to the elderly. The recent COVID-19 pandemic has increased this strain and has resulted in an increased risk of exposure during visits to elderly homes. Increasing the desire to provide technological solutions to counteract this. Currently, there is a lack of reliable real-time non-invasive sensing systems. This chapter makes use of RF sensing, where signal propagation observed in CSI reports ADLs in real-time. Real-time data has been collected for three classifications, "movement", "empty room", and "no activity". A filter is applied to reduce the noise in the CSI data. Then the mean value, max value, min value, kurtosis, skew, and standard deviation features are extracted from the CSI data. An ML model provides classifications for the real-time monitoring system allowing the detection of abnormalities in the expected ADLs of the elderly. The timing measurement of classifications gives insight into the real-time capabilities of the system. The Random Forest algorithm is chosen to create the ML model based on accuracy and timing capabilities. The model was able to achieve an accuracy of 100 % on new unseen testing data with an average classification time of 7.31 milliseconds.

This chapter looks to introduce the use of RF sensing for a working monitoring system. This is an improvement on Chapter 5 by making classifications on streaming CSI that is constantly being fed to the AI model.

The contributions in this chapter can be summarised in the following points:

1. Evaluation of ML algorithms in the context of real-time RF sensing.

2. The development of a monitoring system that makes use of RF signals to accurately sense if a person is present in a room and performing movements within the monitored room.

3.  The development of a dashboard that displays the current classification from the real-time
    system.
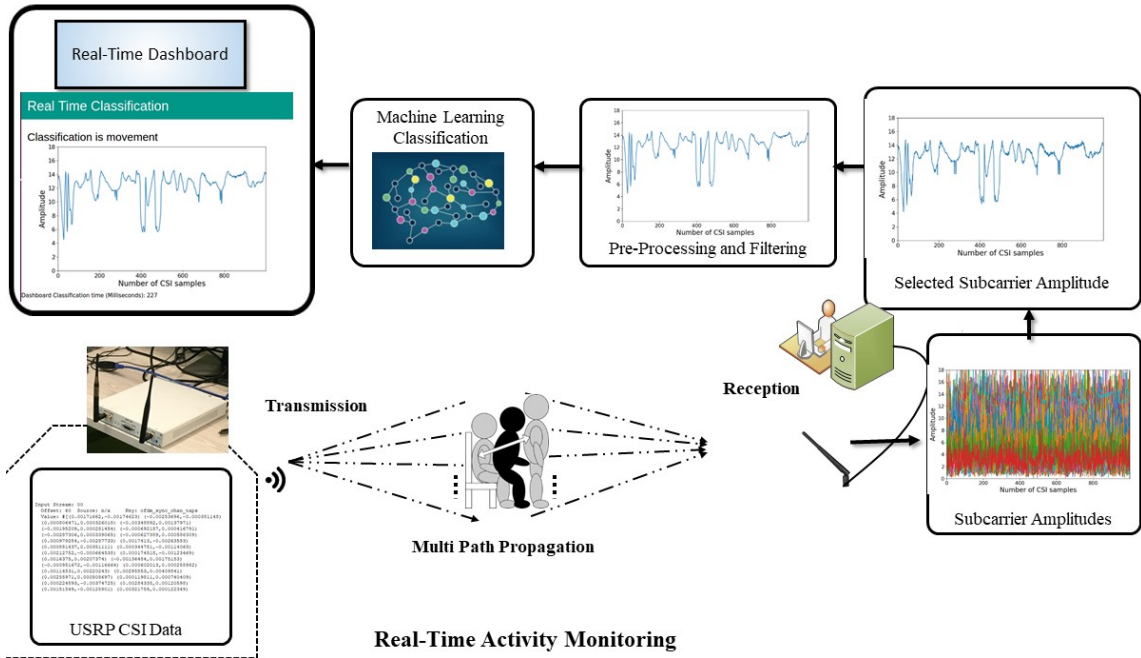


Figure 6.1: Process of Real-Time Activity Monitoring.
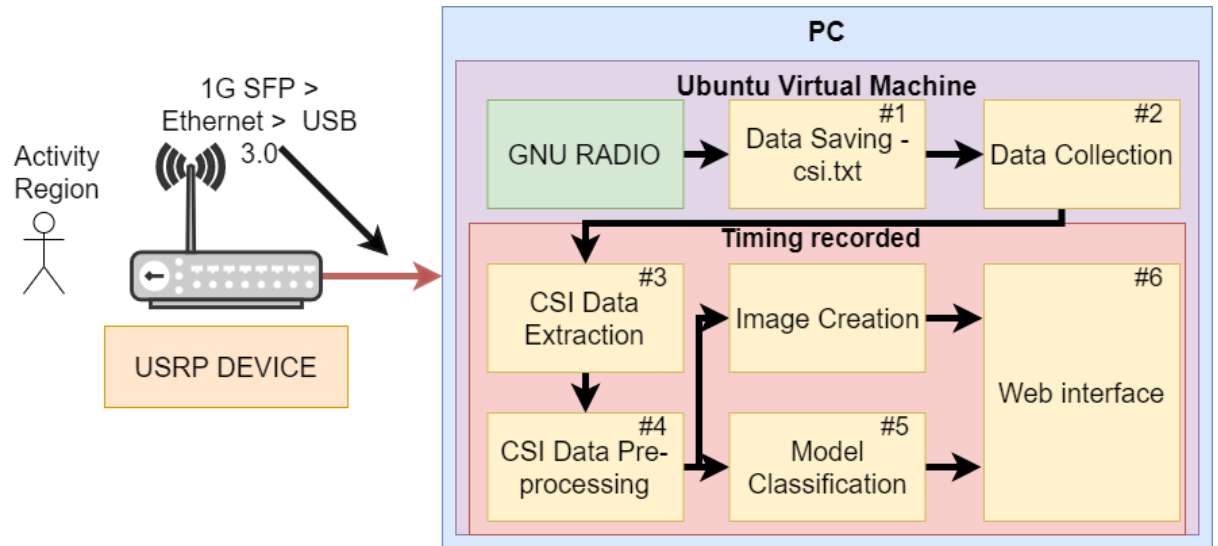


Figure 6.2: Full System Diagram

## 6.1   Methodology

This section details the hardware setup, software configuration, data pre-processing, and dash-
board design.  Figure 6.1 displays the process of real-time activity monitoring with the human

movement taking place between the transmitter and receiver. The amplitude CSI of a selected subcarrier is processed for ML classification and output. Figure 6.2 details the system architecture and data flow including data collection, data preprocessing, classification and output display on the web interface.

### 6.1.1   Hardware Setup

This work makes use of an X300 USRP. As seen in Figure 6.3, the person performs activities in front of the USRP and the CSI is transferred to the computer using 1 Gigabyte Ethernet. Table 6.1 lists the parameters used to configure the USRP device for communication.



Figure 6.3: Experimental setup of USRP Placement With Chair.

### 6.1.2   Software Configuration

This chapter makes use of open-source, GNU Radio software running in an Ubuntu virtual environment. GNU Radio is used to create a Python script using the parameters in Table 6.1. The Python script defines the USRP operation. The output of this script contains the CSI. The Raw output is piped to a buffer. A second Python script is used to read the buffer and extract the CSI.

Table 6.1: Parameters Set for USRP OFDM Communication.

| Parameter | Value |
| --- | --- |
| Number of Subcarriers | 64 |
| Pilot Carriers | 12, 26, 40, 54 |
| Sample Rate | 400 kHz |
| Centre Frequency | 2.4 GHz |
| Bandwidth | 20 MHz |

## 6.1.3 Data Collection

The training data is collected from a real-time stream. Three phases of data collection are completed for each of the three classifications. The three classifications used in this model are an "empty room", "no activity" and "movement". Figure 6.3 is used for the initial demonstration of a real-time sensing system using RF signals. For real-life scenarios, multiple devices can be used as a transmitter and receiver and placed 2 metres apart. This can allow for a larger monitoring area. The CSI is collected and saved in CSV format. 300 CSV files for each classification are collected. The data collected for movement consisted of a person performing sitting and standing simultaneously while the USRP transmits and receives RF signals until 300 CSVs of the movement action are collected. For "no activity" the person remains still sitting for 150 samples and a further 150 samples of standing still are collected. The reason for this is to allow the real-time model to account for any differences between sitting still and standing still to remain as "no activity". For the "empty room" samples, participants leave the room while CSI data is collected. Steps 1, 2 and 3 in Figure 6.2 show the steps taken in the data collection stage. The extracted data is then saved in CSV format for the training stage.

## 6.1.4 Proposed Real-Time Activity Monitoring System

**Subcarrier selection**

The CSI of a single subcarrier from the 64 captured subcarriers is selected to reduce processing times and ensure real-time application. Additionally, subcarrier selection removes redundant CSI subcarriers and duplicate information, which can result in overfitting during ML processes [247]. Overfitting is when too much data is passed through the algorithm, and it causes the algorithm to memorise the training data rather than recognise patterns of the data. The selection of the subcarrier is decided in two steps; firstly by looking at the pilot subcarriers which show the variations caused by the human movement as they are used to carry the pilot symbols in the Channel Estimation process [248]. Subcarrier number 40 shows to have the most variation. This is calculated by taking the standard deviation of each of the pilot subcarriers. standard deviation is selected as the metric to show this as it provides a measure of variation amongst the group of pilot subcarriers. subcarrier 40 was shown to have the highest standard deviation value in all

collected movement samples.

**Pre-processing of Selected Sub Carrier**

The next step is to filter the data and then once a filter is taken, the features can be extracted. A Butterworth low-pass filter with an order of 1 and a cut-off frequency of 0.5 is applied to the data to remove high-frequency noise from the signal. high-frequency noise is not the result of human activity as human activity is detected at low frequencies [249]. Figure 6.4 shows a comparison of a movement sample before and after the pre-processing.



(a) Non-Filtered.  (b) Filtered.
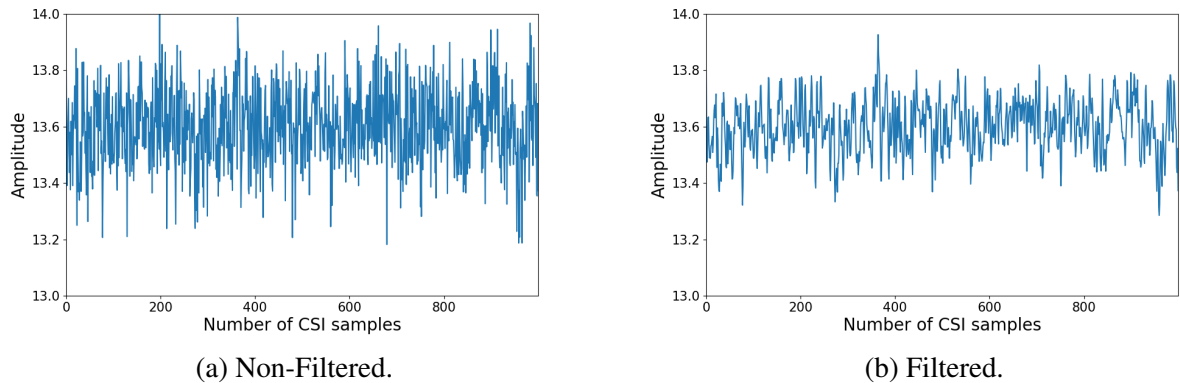
Figure 6.4: Non-Filtered vs Filtered CSI Data.

The last step is to take the features of the filtered 1000 CSI data points. Six features are taken to summarise all the CSI amplitude data of subcarrier 40. The six features used are mean, max, min, kurtosis, skew, and standard deviation [250]. These features describe the wave of the signal including the peaks and size of peaks. Mean is used to show the mean of each value. CSI samples with peaks caused by movements will show a higher mean than samples with fewer peaks in amplitude. Similar to the min and max values, where lower movement samples will have a lower max value and may display lower min values. Kurtosis and skew will also vary on the shape of the peaks observed in the CSI samples. Standard deviation will take note of the variance of the samples. These features provide an effective way of highlighting the differences between the 3 classifications. During the training phase, this process is carried out for each sample and the appropriate label is added. In the real-time process, the CSI data is processed and then fed via the AI model to give the prediction of the model.

**Machine Learning**

A selection of ML algorithms is tested against the data. The selected algorithms are selected based on the related work using these algorithms with CSI data and algorithms used in the work of Chapter 5. These algorithms are Random Forest [128, 251], Bagged Trees [252], KNN and SVM [253, 254].

**Real-time Classification**

This chapter aims to provide users with the detection of movement as it happens. A real-time system is defined as a system in which input data is processed within milliseconds so that it is available virtually immediately [255].

In this experiment, the sensing data is the CSI and it is constantly being collected from received RF signals. The system works by using a window size of 1000 CSI data points. During the time of classifying the CSI window, another 1000 CSI data points are collected. 1000 CSI data points are equal to approximately 2.5 seconds due to the 400 kHz sample rate used in the RF communication. The real-time system must classify the data before the new data is received. Therefore the system must perform classification within the 2.5 seconds time frame as the next CSI window will be complete by the end of this time frame. Within this time frame, raw samples are passed to code which will carry out all pre-processing of the data and then pass the pre-processed data to the ML model. The entire process is recorded by taking timestamps before and after classification is provided. The time of classification is taken on a virtual machine with an i7 9700 3.00GHz CPU and 12GB of RAM.

To evaluate the timing performance, 20 samples from each classification are removed from the training data. The remaining 240 samples are used to train a model and that model is used on the new testing samples and the time and accuracy are recorded. Additionally, a real-time comparison is made between the different algorithms using full CSI data and features to justify a choice in algorithm and between complete CSI data and the extracted features of the CSI data.

**Dashboard Design**

The Dashboard is created using the Flask Python package. Flask is a micro framework that uses Python to create web pages. The web page is designed with simplicity in mind. The reason for a simplistic design is to refrain from distractions as this system is designed with alerts in mind. The web page is comprised of a title banner, a heading declaring the classification of the data, and a visual image of the current CSI to which the classification relates. Additionally, for this chapter, the web page displays the total time of the classification at the bottom of the web page. This is used to calculate the total time between stages 3, 4, 5 and 6 shown in Figure 6.2. Python is used to take a timestamp at the start of stage 3 and JavaScript is used on the web page in stage 6 to take the end timestamp and duration can be calculated by using these two timestamps.

## 6.2   Results

### 6.2.1   Comparison of Machine Learning Algorithms

Figure 6.5 displays the accuracy of each of the algorithms when using 10-fold cross-validation. Table 6.2 shows the results achieved after all data has been tested during each of the 10 folds

of the k-fold cross-validation method including the Accuracy, Precision, Recall and F1 score which are common indicators of how ML algorithms perform.
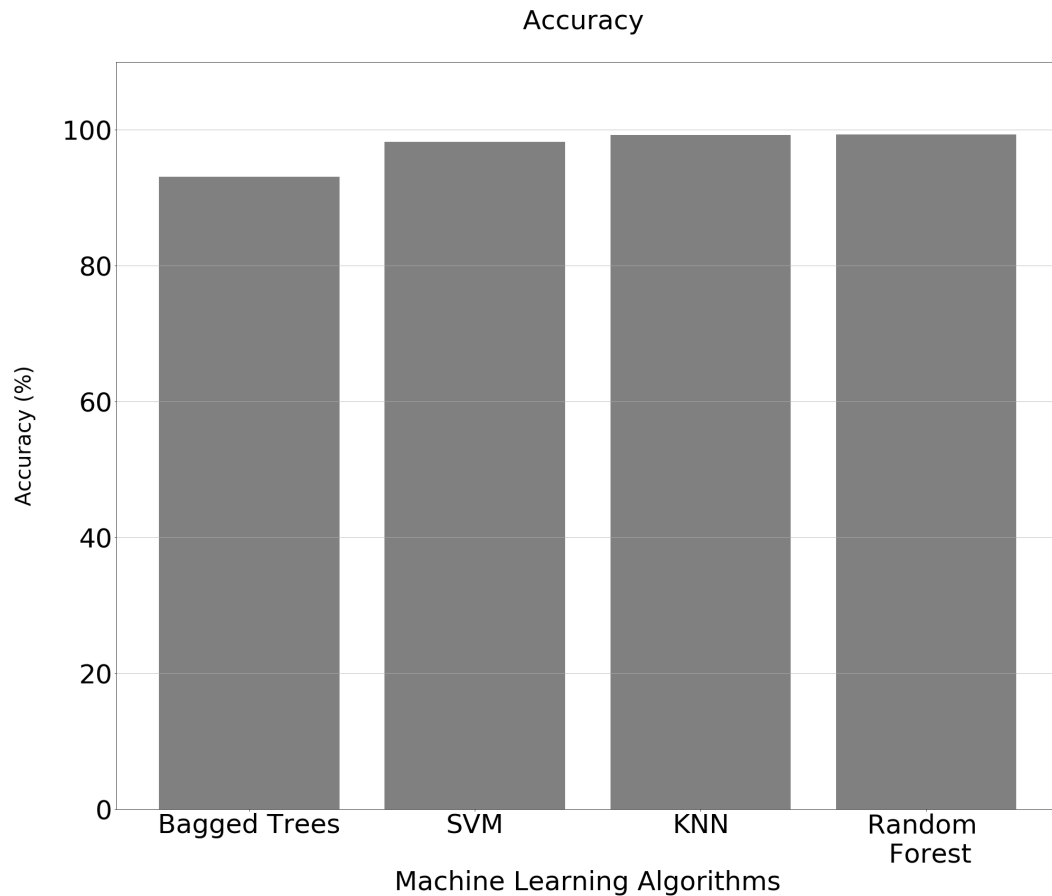


Figure 6.5: Accuracy Comparison of Selected Algorithms.

The results show that Random Forest performed the best with an accuracy of 99.33 %. KNN had an accuracy result of 99.11 % and SVM had an accuracy score of 98.22 %. Bagged trees showed the lowest accuracy score of 93.11 %. All the algorithms however were able to achieve an accuracy score of over 90 %. This, therefore, indicates that the data of the three classifications are distinctive. Figure 6.6 shows the confusion matrix of the best-performing Random Forest algorithm. The figure shows how all 300 samples were classified in each of the 10-folds during cross-validation testing. The 10-fold cross-validation testing method splits the data into 10 groups, with each group taking a turn as the testing data and the remaining 9 groups used as training data. Once all 10 groups have been used as testing data once, then the classification results for all samples can be presented.

The Random Forest confusion matrix shows all the movement samples were correctly classified. 299 out of 300 samples were correctly classified as "no activity" samples. The "empty room" correctly classified 295 samples. As expected, most of the algorithm results have been

Table 6.2: Results From Comparison of Machine Learning Algorithms.

| Algorithm | Accuracy (%) | Classification | Precision | Recall | F1 Score |
|---|---|---|---|---|---|
| Random Forest | 99.33 | Empty | 0.99 | 0.99 | 0.99 |
| | | Movement | 1 | 1 | 1 |
| | | No Activity | 0.99 | 0.99 | 0.99 |
| Bagged Trees | 93.11 | Empty | 0.86 | 0.95 | 0.90 |
| | | Movement | 1 | 1 | 1 |
| | | No Activity | 0.94 | 0.85 | 0.89 |
| KNN | 99.11 | Empty | 0.99 | 0.99 | 0.99 |
| | | Movement | 1 | 1 | 1 |
| | | No Activity | 0.99 | 0.99 | 0.99 |
| SVM | 98.22 | Empty | 0.99 | 0.96 | 0.97 |
| | | Movement | 0.97 | 1 | 0.99 |
| | | No Activity | 0.98 | 0.99 | 0.99 |

able to establish the movement. The difficulty lies with differentiating between "empty room" and "no activity" as this is where most of the errors in the classification occur. The algorithms have classified most of the samples correctly for all three classifications. hence the high accuracy score achieved. For the implementation of a real system, some inference can be implemented which will work on the assumption that a movement must take place before a room can be empty. This can eliminate the small error rate in classifying between "empty room" and "no activity".

**CSI data vs Feature selection**

The above results are achieved by using features from the CSI data described in Section 6.1.4. To justify the use of features in this chapter a comparison is made between the processed CSI data and extracted features. Figure 6.7 shows the comparison of accuracy between using the CSI data vs the Features.

The algorithms perform better when using the features of the CSI data except for SVM. Random Forest had the highest accuracy out of all results 99.11 % when using features. The Bagged Trees and KNN had significantly better results using extracted features. This improved accuracy is used as justification in this chapter to use features in the real-time system.

## 6.2.2 Evaluation of Real-time Classification

Due to the real-time nature of the proposed system, the section will evaluate the real-time aspect of this work. To evaluate real-time classification the data is split into 80 % training data and 20 % testing data. Models are trained with the training data and then used to classify and record the time of the testing data. The results are displayed in the below table 6.3. Table 6.3 presents the results of the average classification time and accuracy of 20 % testing samples of the data with

## Random Forest

| | Empty | Movement | No Activity |
|---|---|---|---|
| Empty | 295 | 1 | 4 |
| Movement | 0 | 300 | 0 |
| No Activity | 1 | 0 | 299 |

Figure 6.6: Confusion Matrix's of the Random Forest Algorithm.

full data vs feature extraction.

The results show that all algorithms can classify the data in milliseconds which would therefore be considered real-time classification. The results of the full features show the Random Forest algorithm as being the most accurate at 100 % and the fastest time at 7.31 milliseconds. The Bagged Trees algorithm has the lowest accuracy of 50 % and took the longest time of 940.13 milliseconds. KNN had an average time of 215.77 milliseconds and an accuracy of 85 %. The SVM algorithm had the second-best accuracy of 96.67 % with an average time of 49.30 milliseconds.

When the features were reduced Random Forest, KNN and SVM all had the same accuracy of 95 % with SVM performing the fastest at 8.47 milliseconds, KNN at 10.86 milliseconds and Random Forest at 12.63 milliseconds. The Bagged Tree algorithm was still the lowest-performing algorithm with an accuracy score of 91.67 % and an average time of 17.81 seconds.

The results show that the Bagged Trees, KNN and SVM show improvement in timing when the features are reduced. The best time in all of the results is the Random Forest algorithm when using full features. This suggests that Random Forest classification time is not affected by the size of the data and the additional time is due to the extra steps of producing the features of the full CSI data. To prove this the classification time is recalculated by not including the pre-processing steps and purely the classification time. The results showed that with full features the Random Forest was able to obtain an average classification time of 6.42 milliseconds and with the features, it was 6.48 milliseconds. This is a negligible difference of 0.02 milliseconds.
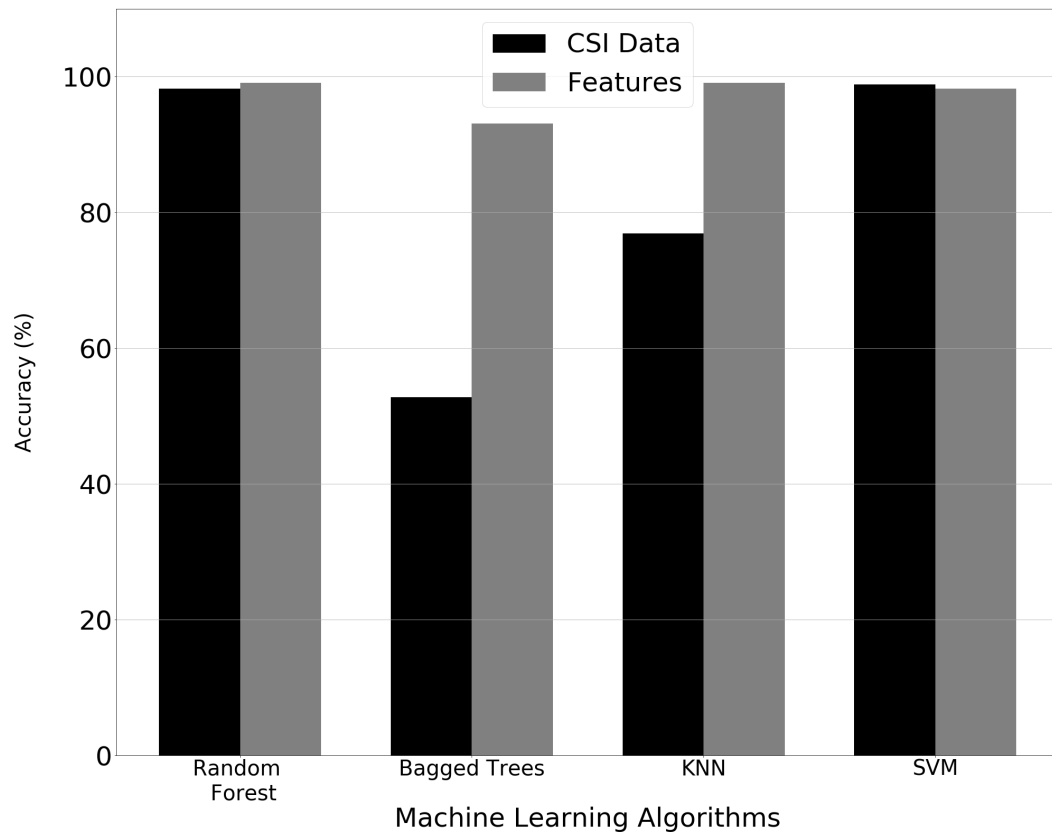
Figure 6.7: Accuracy Comparison of CSI Data vs Features.

From these results, the authors have chosen Random Forest with features as the algorithm to create the AI model for the real-time system. This is justified by the fast classification time paired with the highest accuracy using a 10-fold cross-validation shown in Table 6.2. All algorithms can perform real-time classification, but Random Forest had the highest accuracy when using the 10-fold cross-validation Therefore has been selected as the algorithm for the real-time model.

Table 6.3: Results From Comparison of Machine Learning Algorithms.

| Algorithm | Average Runtime Cost (Milliseconds) | Average Features Runtime Cost (Milliseconds) | CSI Accuracy | Extracted Features Accuracy |
|---|---|---|---|---|
| Random Forest | 7.31 | 12.63 | 100.00% | 95.00% |
| Bagged Trees | 940.13 | 17.81 | 50.00% | 91.67% |
| KNN | 215.77 | 10.86 | 85.00% | 95.00% |
| SVM | 49.30 | 8.47 | 96.67% | 95.00% |

### 6.2.3   Classification of Unseen Data

## New Unseen Data

| | Empty | Movement | No Activity |
|---|---|---|---|
| Empty | 100 | 0 | 0 |
| Movement | 0 | 100 | 0 |
| No Activity | 0 | 0 | 100 |

Figure 6.8: Model Classification of New Unseen Data.

As presented in the previous section, Random Forest with reduced features is best suited to the proposed system. New unseen data is collected to test how the trained model can classify new unseen data using the selected methods. This will indicate how the model will classify new incoming data during the operation of the real-time system. A total of 100 additional samples are collected and compiled into a new testing dataset. All the Data collected and tested in previous

sections is used in the creation of an AI model which is applied to each sample and results are recorded. Figure 6.8 shows the confusion matrix and it shows that all new unseen testing samples were correctly classified. This provides sufficient evidence that the model will be able to classify the 3 classifications during the real-time operation of the monitoring system.

## 6.2.4 Dashboard
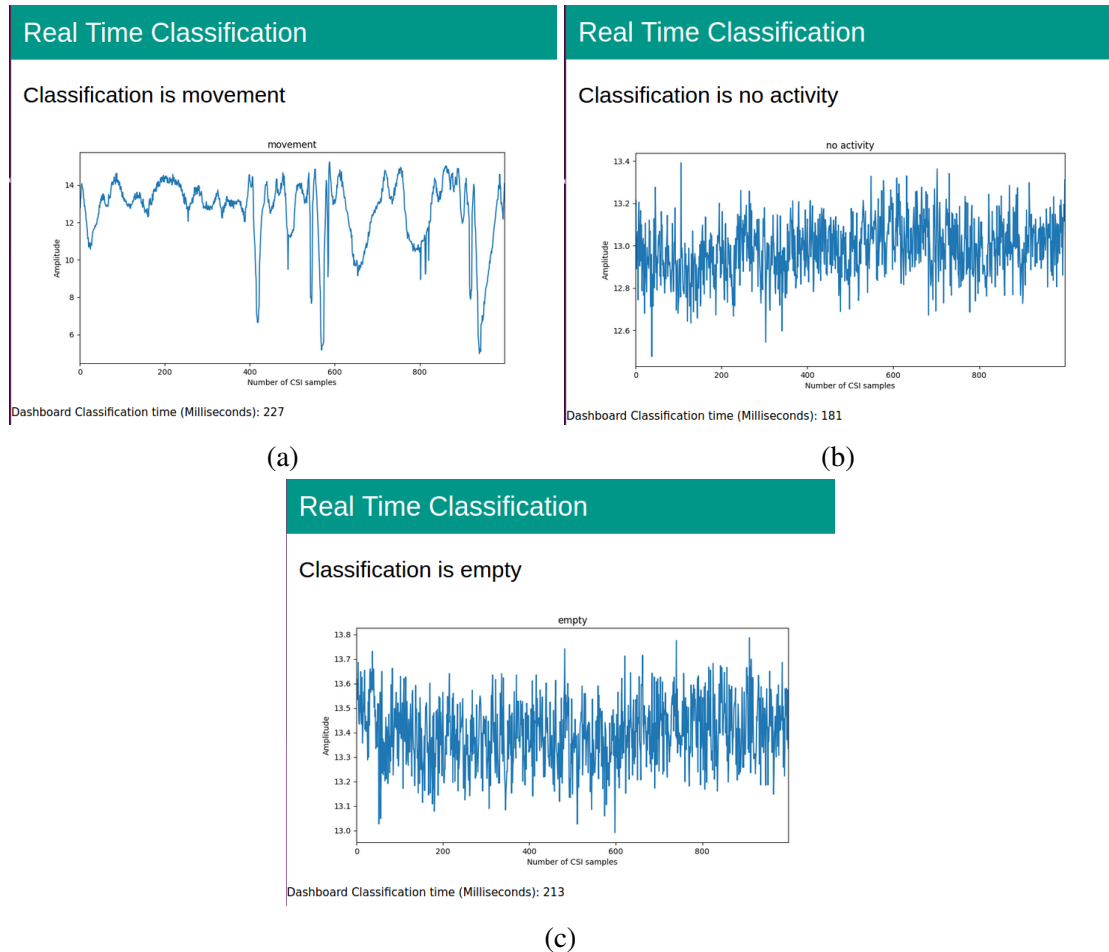


Figure 6.9: Dashboard Output for All (a) Movement, (b) No Activity and (c) Empty Classifications.

The Dashboard is used to provide visualisation of the classification produced from the AI model. The result of the AI must be presented, and it is not expected that family members or care staff read from terminal outputs. The result of the AI model is passed to the dashboard Python code as a variable. Then the dashboard loads the web page based on the contents of the variable. Rules can also be set to create alerts if any activity is detected which is not considered regular and then raise an alert. These alerts can be used to provide reactive assistance. The dashboard displays the detected classification and a visual representation of the CSI. Figure 6.9 shows all of the classes outputted on the dashboard with images and time for classification. It can be seen

how the amplitude is affected in the movement sample. The difference between "empty room" and "no activity" is less clear to visualise but it can be noted that the "empty room" sample has a slightly higher amplitude than the "no activity". This is the reason why most errors in classification were caused by the "empty room" and "no activity" classes as shown in Figure 6.6.

Due to the current system's constraint of range from the use of a single USRP shown in Figure 6.3, as soon as the person leaves the small monitoring area, the system will then trigger the empty classification. The timing recording is done by taking a UNIX timestamp from Python when the web page is first loaded then the processes of the web app take place and then when the web page is displayed on the browser, JavaScript is applied to take a new UNIX timestamp which is then subtracted from the first timestamp and thus providing a time for how long the entire process took. This time is displayed on the bottom of the web page shown in Figure 6.9. The time is still in milliseconds but much larger than the times shown for Random Forest model classification in Section 6.2.2. This extra time is due to the extra functions of the web page such as creating the CSI image displayed on the web page additionally time is taken for retrieving the data before data processing and model classification can take place. However, the time is still in milliseconds and clearly in line with the definition of real-time. It is worth considering that more complex web pages may result in higher latency and will thus affect the real-time functionality of the web page. It is also worth considering the processing power of web servers that will host the dashboard.

## 6.3   Summary

In this chapter, a novel real-time sensing system is presented. The system makes use of AI to identify the movement or presence of a person in a room using Wi-Fi. The use of Wi-Fi ensures a non-contact method of movement detection where a contact-based device is not required. A USRP device is set up to use Wi-Fi between a transmitting antenna and a receiving antenna. The Wi-Fi signals are then transmitted through the atmosphere and when a person is present or moves the Wi-Fi signal is disrupted. These disruptions are present in the CSI. Every 1000 CSI data points received at the receiver side is then processed and passed to AI models to make a classification on whether the disruption indicates an empty area, the presence of a person or movement. 300 training samples are collected for each classification and the accuracy and computational time of four ML algorithms are compared. The results are presented, and the justification is given for the choice of algorithm to create an AI model. The AI model which achieved 100 % accuracy on new unseen testing data is used in a dashboard to create a real-time monitoring system. Future work will seek to create an alert system where irregularities in movements can be flagged up. This will create a more effective monitoring system that will not require constant monitoring of a dashboard.

# Chapter 7

# Novel Contactless Sensing Technique for Real-time Detection of Human Sitting and Standing Activity

This chapter expands on the real-time contactless RF sensing monitoring system proposed in the previous chapter. This chapter introduces features of the monitoring system that can accurately classify specific movements from streaming CSI data. The work proposed in this chapter can accurately detect if a person is sitting or standing from a desk. This is achieved by implementing a novel algorithm that analyses incoming CSI windows to detect if a movement began and ended in the CSI window. If the movement did begin and end, then the CSI window containing this movement is passed to a trained AI model which can classify if the movement that occurred in the CSI window is standing or sitting. This classification is then output in real-time.

## 7.1 Introduction

In-home healthcare monitoring technologies are vital to allow vulnerable people to live independently within their own homes [7]. The work of this chapter looks at the use of RF signals to provide real-time contactless monitoring. AI algorithms have been implemented in recently published work to learn and detect RF signal amplitude changes caused by movements [73, 128, 256]. RF signal motion detection works by observing the changes in signal propagation while human movement takes place. This chapter makes use of a USRP X300 device to create a communication link between a transmitter and receiver from which CSI amplitude data can be mined. Previous work has been able to classify different activities from the recognition of CSI amplitude patterns in non-real-time applications [257]. Non-real-time experiments provide proof of concept that RF signals can be used to detect specific activities with the help of machine learning. One of the key challenges is being able to detect specific activities in real-time from streaming data. In real-life scenarios, monitoring systems are run constantly and report when

movements occur [258]. Chapter 6 was able to achieve the detection of movements in real-time but was unable to identify what movement took place. This uses novel techniques to detect movements in overlapping windows of incoming CSI and then uses AI to classify if a person is performing sitting or standing motions in real-time.

## 7.2 Methodology

The system works by using a single USRP device placed on a desk with two antennas attached. The USRP has software configured to allow the transmission of OFDM signals between the antennas. The software outputs CSI which describes the signal propagation during transmission. The USRP is configured to simulate Wi-Fi communication at a frequency of 2.4GHz. The goal of the system is to detect if a person sits or stands from the desk. Training data is collected from a real-time stream of CSI during which time a person sits and stands from the desk. The amplitude of this CSI stream is extracted and then sliced into smaller overlapping windows of 80 %. The windows are overlapped to ensure that the complete movement action is included in the entire sample. Large variations of amplitude values are indicative of movements occurring. Windows that include no movement or partial movement are dismissed. Partial movement is defined as movements occurring at the start or end of the windows. This suggests that the entire movement is in the next overlapping window. Windows that include the entire movement cycle are labelled appropriately as "Sitting" or "Standing" and stored for training data. Figure 7.1 shows the effect of the CSI amplitude stream when a person stands and sits.
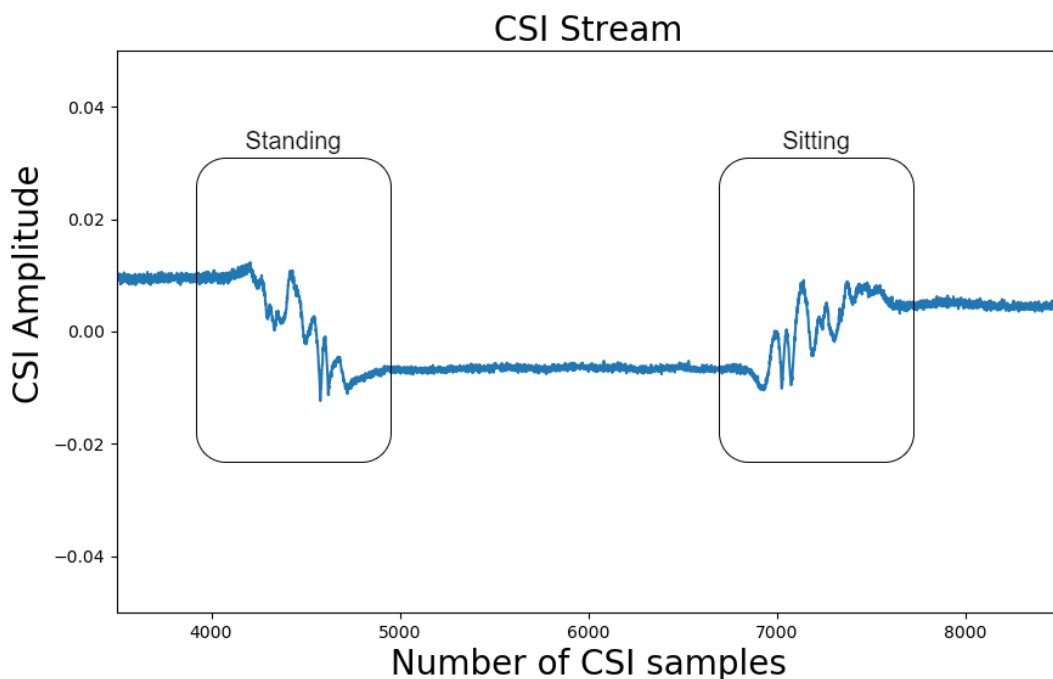


Figure 7.1: CSI Stream Showing the Standing and Sitting Variations.

The training data is then constructed into a dataset that can be passed to an ML algorithm. The Random Forest ML algorithm is selected [128]. In total there are over 300 samples each collected for both sitting and standing. Data processing is used to apply a low pass filter to the data and then features are extracted. The features extracted are the mean, maximum, minimum, kurtosis, skew, standard deviation, and the difference between the maximum and minimum values. The dataset contains the label of the action sitting or standing and then the values of the extracted features.

## 7.3 Results and Discussion
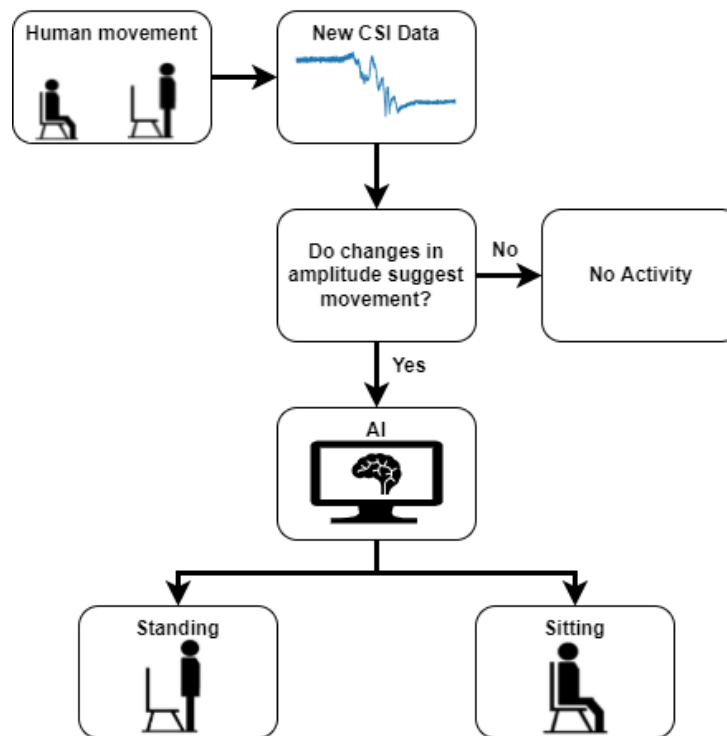


Figure 7.2: Flowchart of the Real-Time System.

The dataset is used with the Random Forest ML algorithm using 10-fold cross-validation which produced an accuracy of 94.63 % as shown in Figure 7.3. An AI model is then created using the Random Forest classifier and is carried forward for real-time application. Software is set up to run the USRP communication and save the output similar to the collection of training data. The amplitude of the new data is extracted from the software output and movement samples are filtered out. If no movement is detected then the system will output "No activity". If movement is detected then the data will be passed to the AI model which will establish if the activity is sitting or standing. The system will then output the value of "Sitting" or "Standing" depending on the prediction of the AI model. The system is tested and can perform real-time classifications. The system is additionally tested in multiple office environments and the system was still able

to perform correct classifications in real-time. This is because the action of sitting or standing still produces similar propagation patterns in the CSI of the RF signals. Figure 7.2 presents a flow chart of the real-time system. New CSI data is passed into the system and if an activity is detected then the AI model is used to differentiate between sitting and standing movements. Future work will seek to implement activity detection for greater distances by making use of multiple devices to serve as a separate transmitter node and receiver node that can be placed further apart.

```
Random Forest
Confusion Matrix
[[315    9]
 [ 24 267]]
              precision    recall  f1-score   support

     Sitting       0.93      0.97      0.95       324
    Standing       0.97      0.92      0.94       291

   micro avg       0.95      0.95      0.95       615
   macro avg       0.95      0.94      0.95       615
weighted avg       0.95      0.95      0.95       615

Random Forest Accuracy 94.6341463414634 %
```

Figure 7.3: Results of Random Forest Algorithm Using 10-Fold Cross-Validation.

## 7.4 Summary

This chapter has presented a real-time system that can classify sitting and standing movements in real-time using contactless sensing. The system can determine if a person is sitting or standing by analysing the signal propagation of RF signals. A real-time data stream is collected while a person sits and stands from a chair and the movement samples are extracted from the stream. The movement samples are then stored as sitting and standing samples. these samples are then compiled and features extracted to create a dataset which is used to create an AI model which is used in the real-time system. The real-time system was able to identify if the person is sitting or standing within multiple environments. Future work will seek to extend the number of actions detected and allow for real-time classifications within larger areas such as an entire room.

# Chapter 8

# Implementation of Contactless Real-time RF Sensing Prototype with Secure Cloud Storage and Alert System

This chapter focuses on implementing the ideas of chapter 7 into a prototype monitoring system that includes features such as cloud storage and an alert system. The real-time system is set up to store incoming CSI data on the cloud. As this data is sensitive monitoring data, encryption is implemented to ensure privacy. The experimental setup of this chapter also expands the monitoring area by placing the transmitter and receiver antennas at opposite sides of a room, where all movements in the room have an effect on a signal that is travelling across the entire room. A dashboard is used to collect the CSI from the cloud and performs decryption of the data. The data is filtered to detect movements. Movements are then passed to the trained model and the detected movements are displayed. The automated notification system is designed to email a family member or caregiver if no movements are detected within an hour during daytime monitoring hours. The system makes use of two AI models. The first differentiates between sitting and standing with an accuracy of 90.75 %. The second differentiates between walking and no activity with an accuracy of 99.83 %. These models are then able to provide accurate classification of new incoming data when testing the real-time system. The proposed system can capture movements from received RF signals and apply ML to the movements to identify sitting, standing, or walking classifications in real-time. Trained models are used to recognise new data incoming in real-time and output the classification to a designed dashboard.

## 8.1   Introduction

This chapter proposes a system that can monitor a single person within a bedroom environment with the implementation of cloud storage with encryption and an alert system when no movements are detected during times when some movement is to be expected.
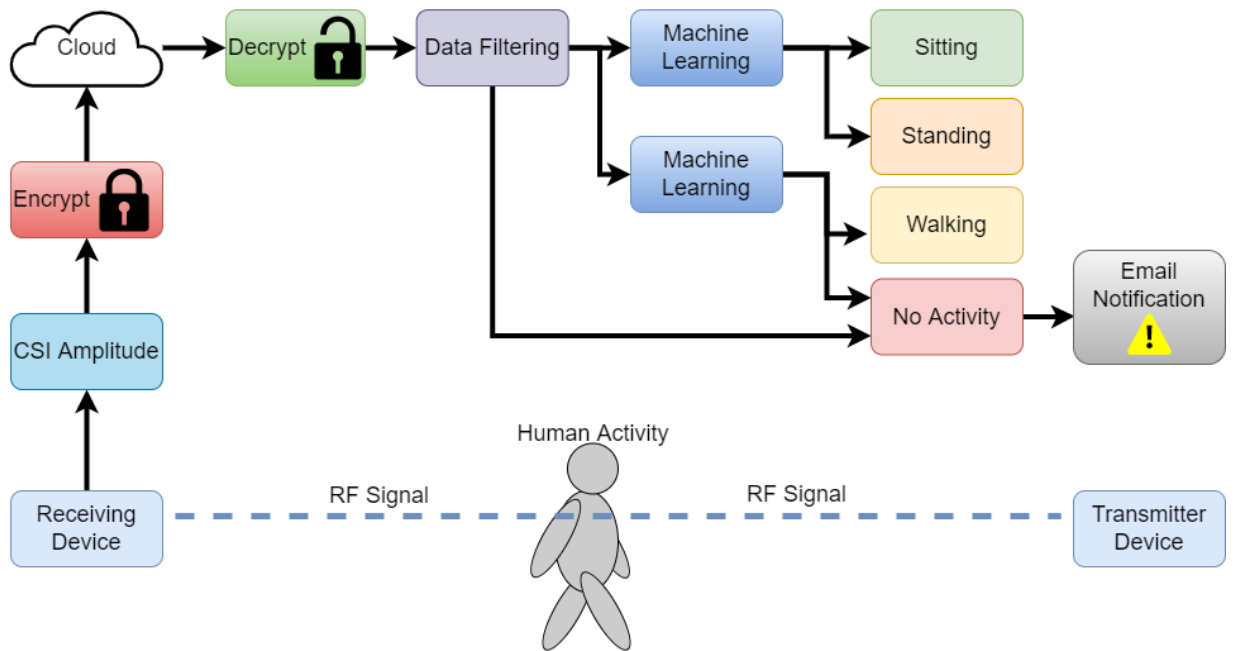
Figure 8.1: Complete Process of Proposed System.

The proposed system can be viewed by caregivers or family members using a web-based dashboard.  The dashboard displays the output of the ML techniques, the CSI amplitude data, and a graphical representation of the detected movement.  The dashboard gives information to family and/or caregivers about the patient's activities [259].  This works by making use of cloud computing.  The local CSI amplitude data is stored on the cloud and the webserver of the dashboard downloads and performs ML techniques on the data [260].  The output is then displayed on the dashboard. The dashboard is designed to be simplistic to allow for quick and clear indications of the detected movements.  This will allow for the optimal human-machine interaction between the users of the system such as family members and/or caregivers and the real-time system [261].

As an activity monitoring system is related to the movement of the person within the home, there are privacy concerns associated with this data leaving the local system. If malicious agents could access the data, then they would have information that can be related to the movements of a person. This information can be considered sensitive as relates to an individual. exposure of this data can cause risk to the security and/or health information of an individual.  As this sensitive data will be leaving the local system, the proposed system makes use of encryption to secure the data.  As the system focuses on human activities in a healthcare environment, data leaving the local system is encrypted. This is to mitigate the risk of any data leaks on the cloud. This will protect the vulnerable person in the case of a data leak as the data cannot be read. This protects sensitive information related to the person's health and their activity around the home. This ensures privacy in the monitoring system with only authorised users able to view system output [262].  Encryption is achieved by using the Rivest-Shamir-Adleman (RSA) encryption

algorithm, where public and private keys are utilised. The public key is used to encrypt the data and the dashboard contains the private key. which is used to decrypt the data retrieved from the cloud. This algorithm is common in cloud security [263, 264, 265] because the public key can be present on local systems to encrypt the data for storage on the cloud and the private key can be stored securely on the server side to decrypt the sensitive data.

The final stage of the system provides a notification system when no activity is detected within the last hour. This works by logging all of the classifications the system has outputted and observing the outputs every hour. If the last hour has shown only no activity outputs, then an automated email is sent out to a caregiver or family member to inform them that there have been no movements detected. The notification system is designed to only be active during the daytime when movement is expected. The notification system will not be active during nights when movement is not expected.

This chapter makes the following contributions to research in the field of real-time human activity detection using RF signals:

1. Introduction of a new walking classification within the contactless RF monitoring system.

2. Implementation of two separate devices, one for transmitting and another for receiving at opposing corners of the room so that an entire room can be monitored for movements.

3. The use of encryption to protect the data leaving the local contactless Wi-Fi monitoring system.

4. An automated email service that can provide notifications of no detected movements using a contactless Wi-Fi monitoring system.

## 8.2   Methods

This section will describe the steps taken to construct the proposed real-time system. Figure 8.1 shows the complete process of the proposed system. The human movement takes place between the transmitter device and the receiver device. The amplitude of the signal is observed at the receiver device. This amplitude information is then encrypted and uploaded to the cloud. A monitoring dashboard then downloads the encrypted CSI from the cloud and performs decryption. The CSI amplitude is then analysed for indications of movements. If no movements are detected in the CSI amplitude data the system outputs no activity. If movement is present the data is passed to an AI model for detection of sitting or standing or if the movement is walking based on the properties observed in the CSI amplitude data. The AI models can then differentiate between sitting and standing or walking and no activity. If there are no activity classifications continuously for a specified duration of time, an email notification is sent out to inform family members and/or caregivers of this concern.

### 8.2.1   Experimental Setup

The system makes use of two USRP X300 devices to transmit and receive RF signals. Each device is connected to separate PCs via Ethernet connections and virtually connected to Linux virtual machines. The virtual machines are using the Ubuntu 16.04 Linux operating system with 12GB Ram and an i7-9700 3.00GHz processor. The USRP devices are positioned at opposing corners of a single room as shown in Figure 8.2 with one device serving as the transmitter and the other as the receiver. The aim is to detect human movement between the transmitter and receiver devices.
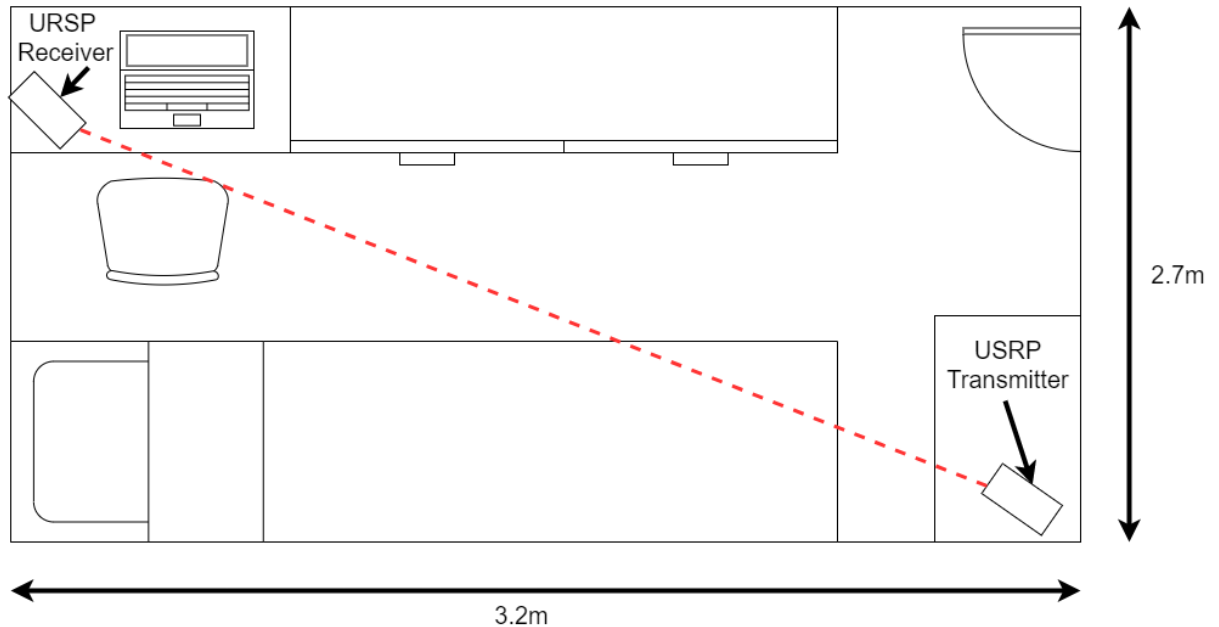


Figure 8.2: Room Setup of Monitoring System with USRP Devices Shown.

RF wireless communication link between the USRP devices is set up using the GNU Radio software toolkit. GNU Radio is an open-source package designed to create signal processing blocks that define the software to be used on USRP devices. The signals are designed to simulate Wi-Fi communication by using the 2.4 GHz centre frequency used in Wi-Fi [266]. During the transmission, CSI is collected at the receiver side and stored in a file buffer. CSI refers to channel properties of the communication link and is used to describe the signal propagation between transmitter and receiver. This signal propagation is observed in this system whilst human movement occurs within the monitored room.

### 8.2.2   Data Collection

The experimental setup detailed in the previous section is used to collect CSI data for training AI models, which are used to classify new unseen data in the finalised system. Collected CSI data during the communication is stored in a file buffer. The first stages are to collect training data

for the classifications reported in this chapter. The classifications are sitting, standing, walking, and no activity. The file buffer contains a series of CSI complex numbers collected throughout the RF communication. The CSI data stored in the file buffer contains 64 subcarriers. The system uses the amplitude of a single subcarrier to reduce the computational time by reducing the overhead of processing all 64 subcarriers. This is essential for the real-time nature of the system. The amplitude values of the signal propagation are captured by calculating the absolute value of the CSI complex numbers. The amplitude values are then normalised by taking the average amplitude value of the subcarrier and then subtracting this value from each value of the subcarrier individually. This ensures that the amplitude variations are set to a common scale. The complete normalised amplitude subcarrier is fed into a Python script which takes a window of 1500 CSI samples and moves the start and end position of the file buffer in increments of 300 samples. This creates an overlapping effect across the stream of 80 %. As the file buffer is fed through the Python script each CSI window can either be captured and stored in CSV format for training data or processed for the application of ML in the real-time system. When the finalised system works in real-time, the data is collected in real-time. The system will process the CSI data as it is received during transmission. Figure 8.3 shows an example snippet of a CSI amplitude stream with 4 overlapping CSI windows. It can be seen that windows move 300 samples from the start and end of the previous window with the initial window capturing the first 1500 samples.
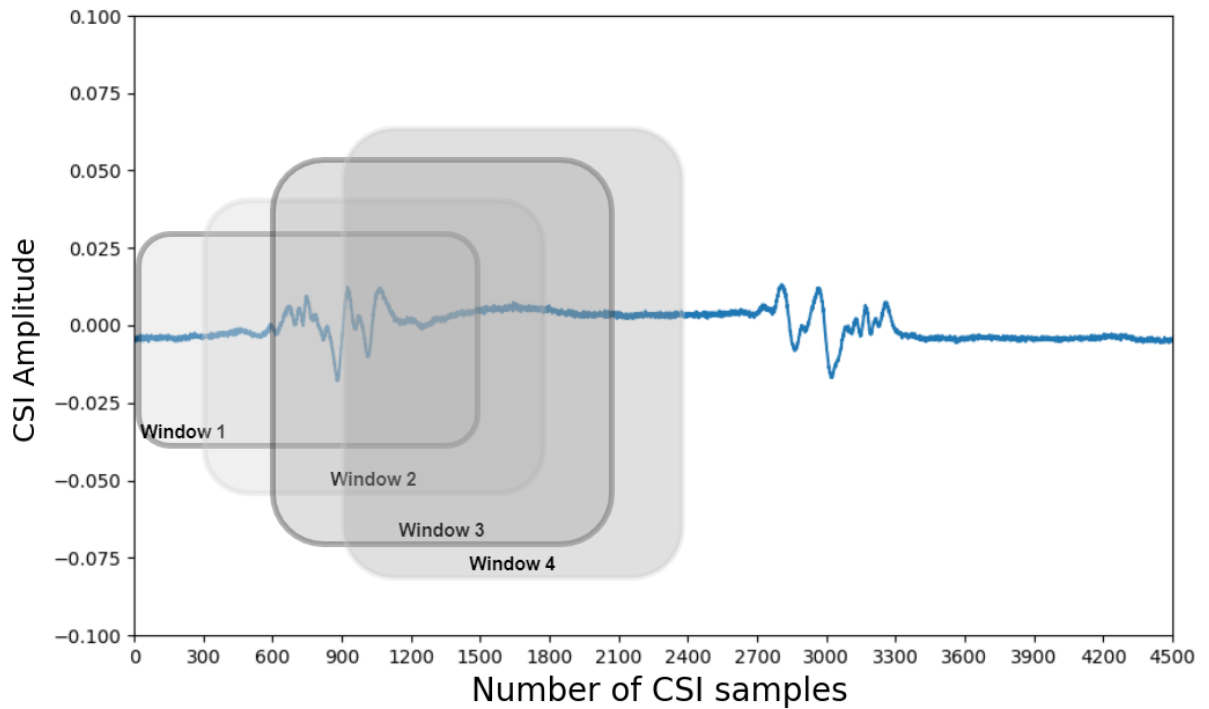


Figure 8.3: Example of CSI Windows Overlapping Across a Snippet of a CSI Amplitude Stream.

The complete system makes use of two AI models which implement the Random Forest

algorithm. Previous work has shown Random Forest to perform well with data of this nature [128, 267]. The first AI model is used to classify walking vs no activity and The second model is used to classify between sitting and standing. The reason two AI models are used in this system is because of the nature of the data for different classifications. Sitting and standing are short activities that need to start and end in the CSI window. Therefore windows that contain these movements are passed to the sitting vs standing model. The walking movement has a longer duration than sitting or standing and there is a vast difference between walking and no activity therefore no data filtering is required to extract the walking movements from no activity. Data filtering techniques described in the next section, are used to process the data based on properties of amplitude variation. If the CSI window amplitude variations indicate longer duration movements such as walking it is passed to the walking vs no activity AI model and if CSI window amplitude variations indicate shorter movement durations such as sitting or standing, the window is passed to the sitting and standing AI model.

**Data Filtering**
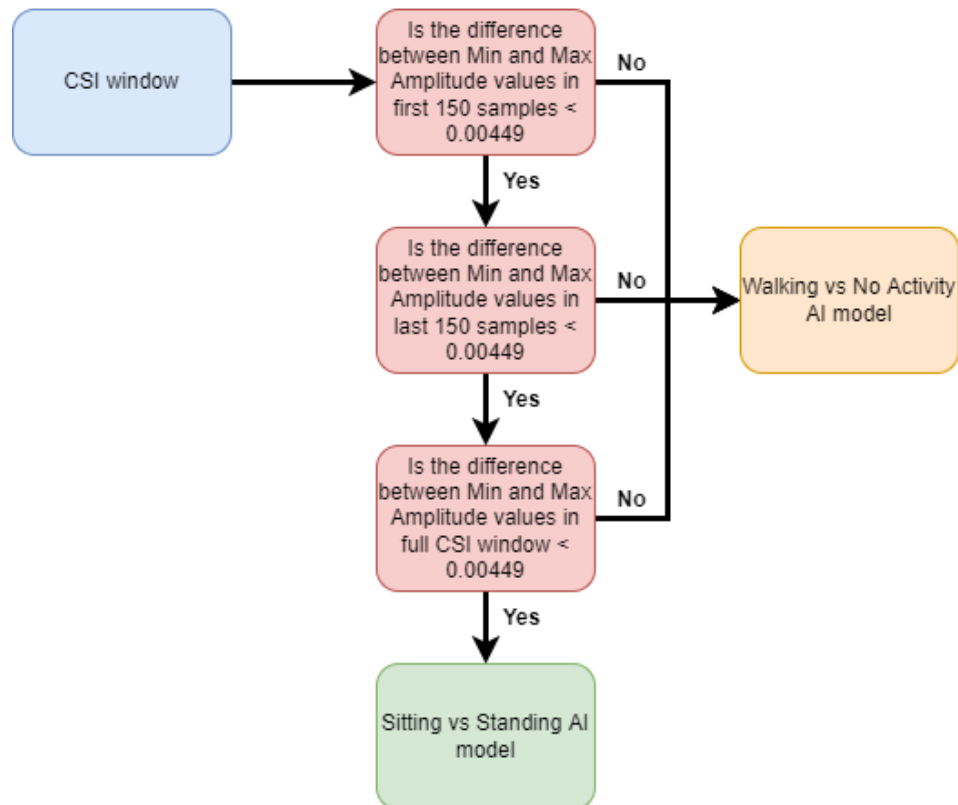


Figure 8.4: Flow Diagram of Python Rules Followed to Filter Data.

Data filtering is achieved by applying rules in Python to make decisions on which AI model the CSI windows should be directed to. These rules are based on the amplitude values observed

at various sections of the CSI window. Figure 8.4 shows a flow chart of the rules followed to filter the data. The rules observe the difference between the minimum and maximum amplitude values of the CSI window.

When there is no human movement during the transmission of the RF signals, the amplitude displays minimum variation. Analysis of all collected data has shown that if the difference between the maximum amplitude value and minimum amplitude value is below 0.00449 then there is no activity taking place. An example is shown in Figure 8.5, which shows the CSI amplitude while no activity is taking place with a difference of approximately 0.0026 between the maximum amplitude value and the minimum amplitude value. This indicates minimum variation as no human movement has taken place in this CSI window.
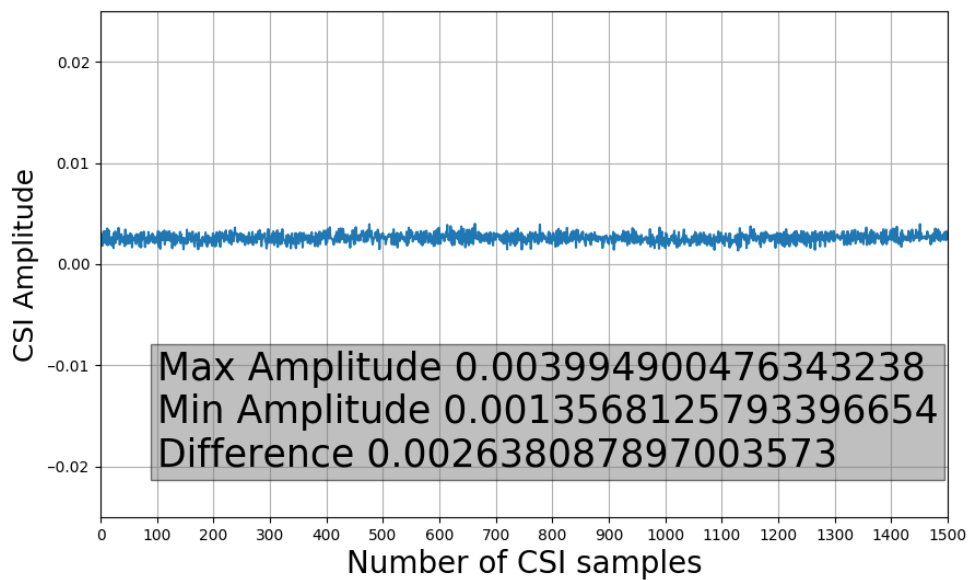


Figure 8.5: CSI Amplitude of No Activity.

For data to be passed to the sitting or standing AI model it must match the 3 rules shown in Figure 8.4. The first rule observes the difference in minimum and maximum values in the first 150 samples of the CSI window. 150 samples are selected as it is half of the overlapping metric of 300. If the values do not exceed 0.00449, then this indicates there is no activity currently occurring at the start of the CSI window. This is essential because if an activity is currently taking place when the CSI window begins, then the initial information of the activity is missing in this current CSI window and this will affect the accuracy of the AI model. Figure 8.6 shows an example where an activity is taking place during the first 150 samples of the CSI window and thus not acceptable to pass to the sitting vs standing AI model as the start of the action is missing in the shown CSI window.
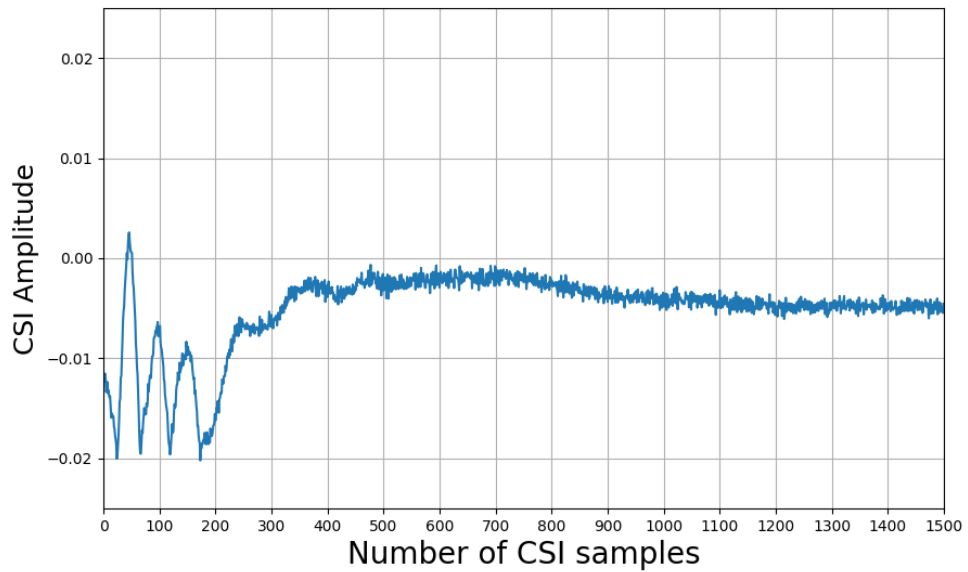
Figure 8.6: Start of CSI Window Showing Partial Movement.
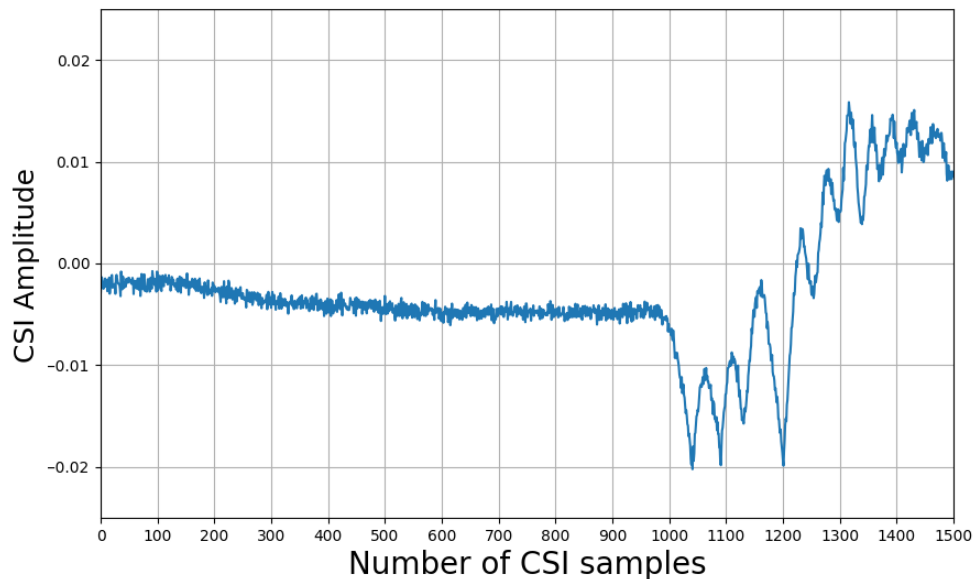


Figure 8.7: End of CSI Window Showing Partial Movement.

The second rule is similar to the first rule except it looks at the last 150 samples in the CSI window. This ensures that the end of the activity is not missing from the current CSI window and thus the CSI window does not contain the complete sitting or standing action. Figure 8.7 shows an example of a CSI window where the last 150 samples contain partial activity. For the CSI window to be passed to the sitting or standing AI model, the start and end of the sitting or standing action must take place within the CSI window. The first two rules will ensure that there is no partial movement taking place between the start and endpoints of the sample. If there is any partial movement then the window is dismissed. Figure 8.9 shows a CSI window that will

be passed to the AI model as the start and endpoints are considered flat and the start and end of the human movement can be observed in the CSI window.
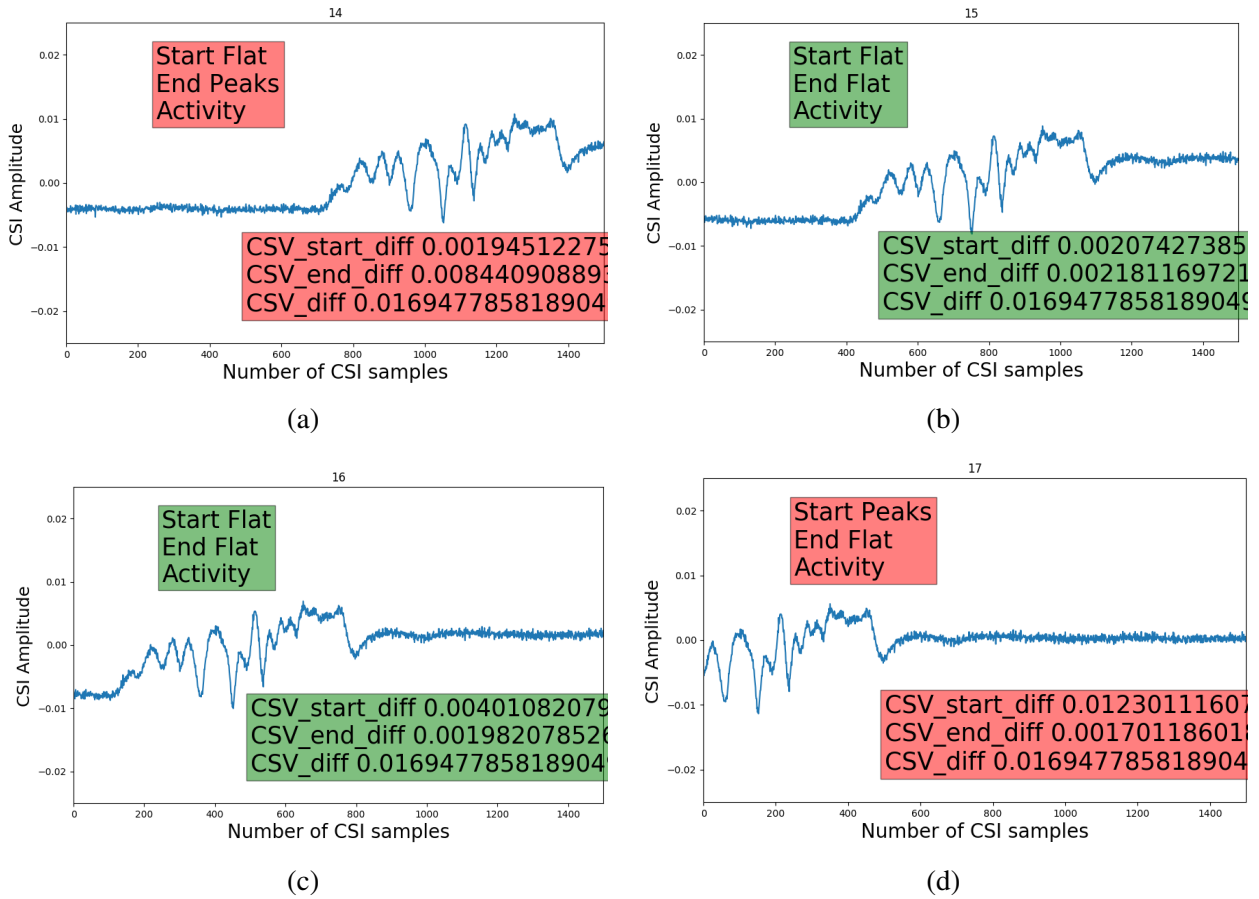


Figure 8.8: CSI Window Images Showing the Observed Values Following Data Filtering. Green Samples (b) and (c) are Passed to the Sitting and Standing AI Model and Red Samples (a) and (d) is Passed to the Walking vs No Activity AI Model.

The final rule is in place to ensure an activity did take place in the CSI window. It takes the difference of minimum and maximum amplitude values for the entire CSI window in sections of 100 samples. If any of these sections exceed 0.00449 then it can be established that an activity is present in the window. As shown in Figure 8.9. If none of the sections goes above 0.00449, as shown in Figure 8.5, then no activity has occurred.

If all of these rules are true then the data is passed to the sitting and standing AI model. If any of the rules are false then the data is passed to the walking vs no activity AI model. Figure 8.8 shows overlapping windows and the values found when applying the rules to each window. Green samples will be passed to the sitting and standing AI model and red samples are passed to the walking vs no activity AI model. All training samples of sitting and standing have been passed through these rules to test the functionality of the values set for these rules with no samples incorrectly rejected. As the data has been normalised, the difference in amplitude values is consistent during data collection.
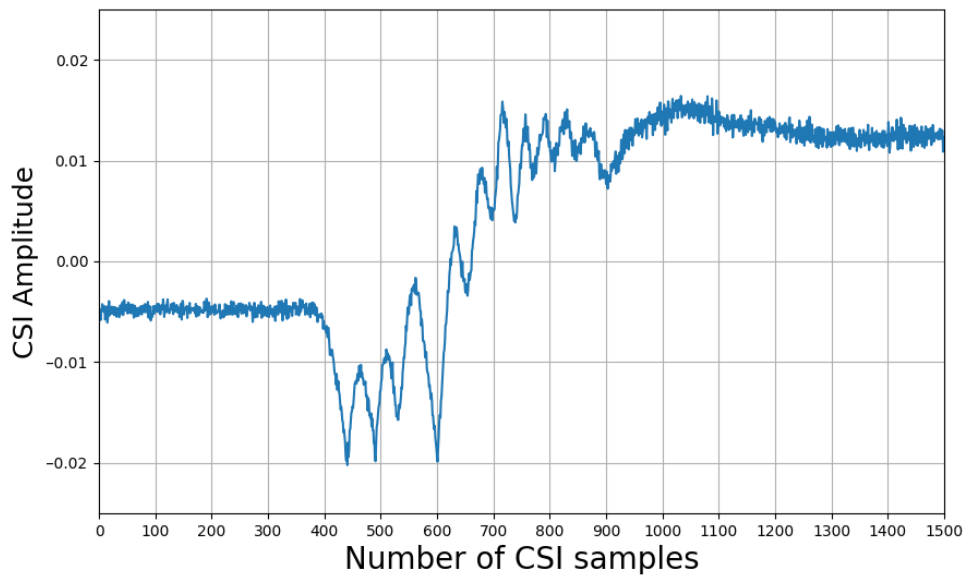
Figure 8.9: CSI Window Showing Entire Movement.

**Training Data**

The training data is collected using the same data filtering rules. For sitting and standing training, a stream of CSI is collected while RF signals are transmitted. The person will then sit and stand from various areas within the room so that training data will contain samples from across the monitored area. The CSI stream is then divided into smaller overlapping CSI amplitude windows of 1500 CSI samples in size as described in the above section 8.2.2 and saved in CSV format. The rules are then applied to the CSV files and accepted files are passed into folders for sitting and standing. This is achieved by having the person initially sit. Then the first movement action is standing and stored as such. The second movement will be sitting and this will continue for the collection of sitting and standing data. Over 600 samples of sitting and standing in various points of the room are collected and compiled into a training dataset for the sitting and standing AI model.

The collection of walking data is taken while a person walks from one corner of the room to the other continuously. The CSI stream of the walking data is then divided into the sample window size of 1500 samples with the same overlapping of 80 % applied. All of these windows are stored in CSV format for walking data. All of the other rejected samples marked as red by applying the rules to the sitting and standing training data are marked as no activity. Then all walking and no activity samples are compiled into a dataset for the walking vs no activity AI model.

### 8.2.3 Machine Learning

The finalised system makes use of ML techniques to make classifications on received CSI data. This is achieved by training AI models. Before received CSI data is passed to an AI model or the training data is used to train an AI model, data processing techniques are applied. The data processing techniques consist of applying a denoising filter and then feature extraction. A low pass Butterworth filter is applied to the CSI window, which reduces some of the noise in the CSI amplitude [268]. Then with the denoised CSI window, features can be extracted. The chosen features to extract from the CSI window are the mean, maximum, minimum, kurtosis, skew, standard deviation, and the difference between the maximum and minimum values. These 7 features are taken for the entire sample and 5 other subgroups of the sample. The subgroups are 0-500 samples, 250-750 samples, 500-1000 samples, 750 - 1250 samples and 1000 - 1500 samples and the total CSI window is 0 - 1500 samples. which gives a total of 42 features represented in the training and new unseen data.

### 8.2.4 Dashboard and Cloud Computing
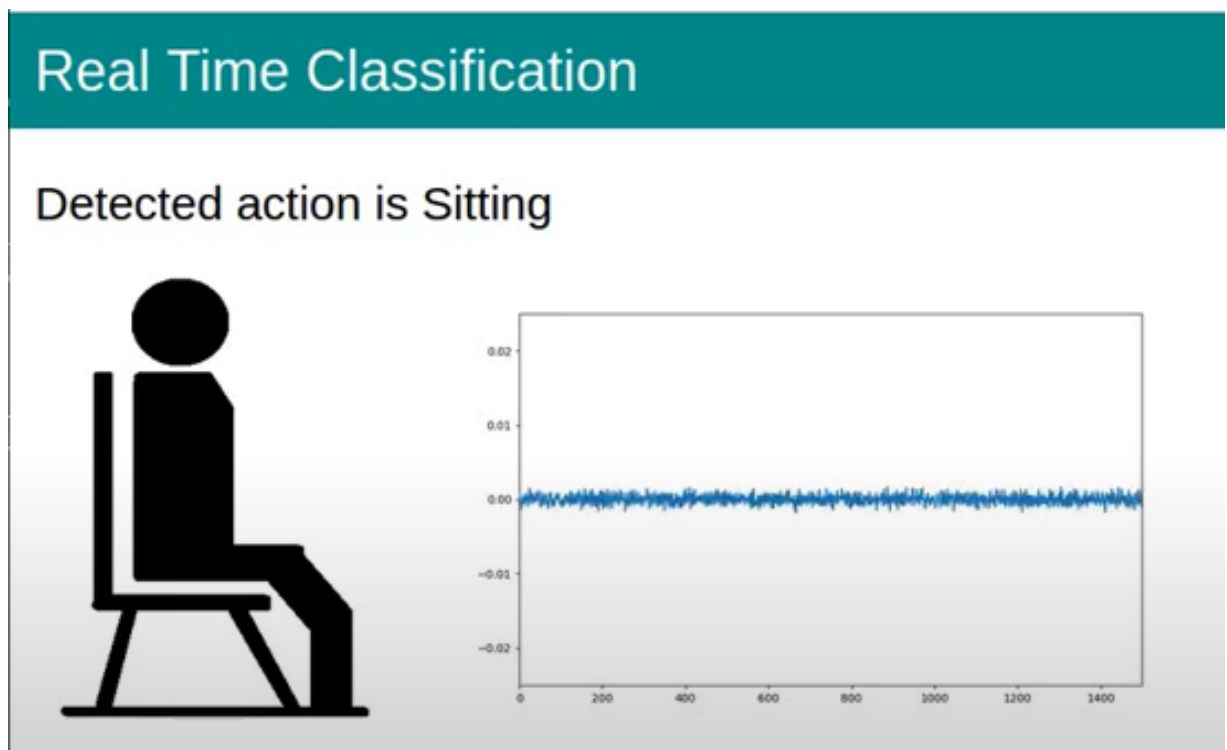


Figure 8.10: Dashboard Layout When the System Detects Subject is Sitting.
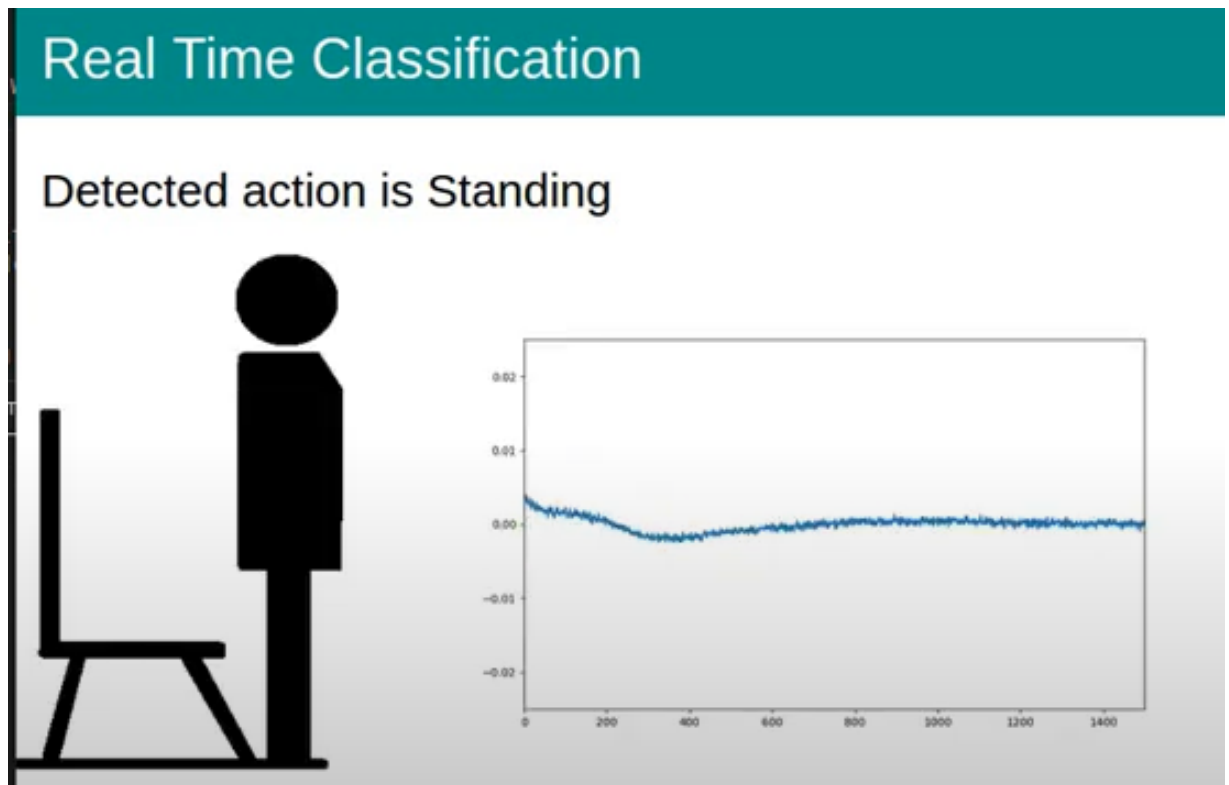
Figure 8.11: Dashboard Layout When the System Detects Subject is Standing.
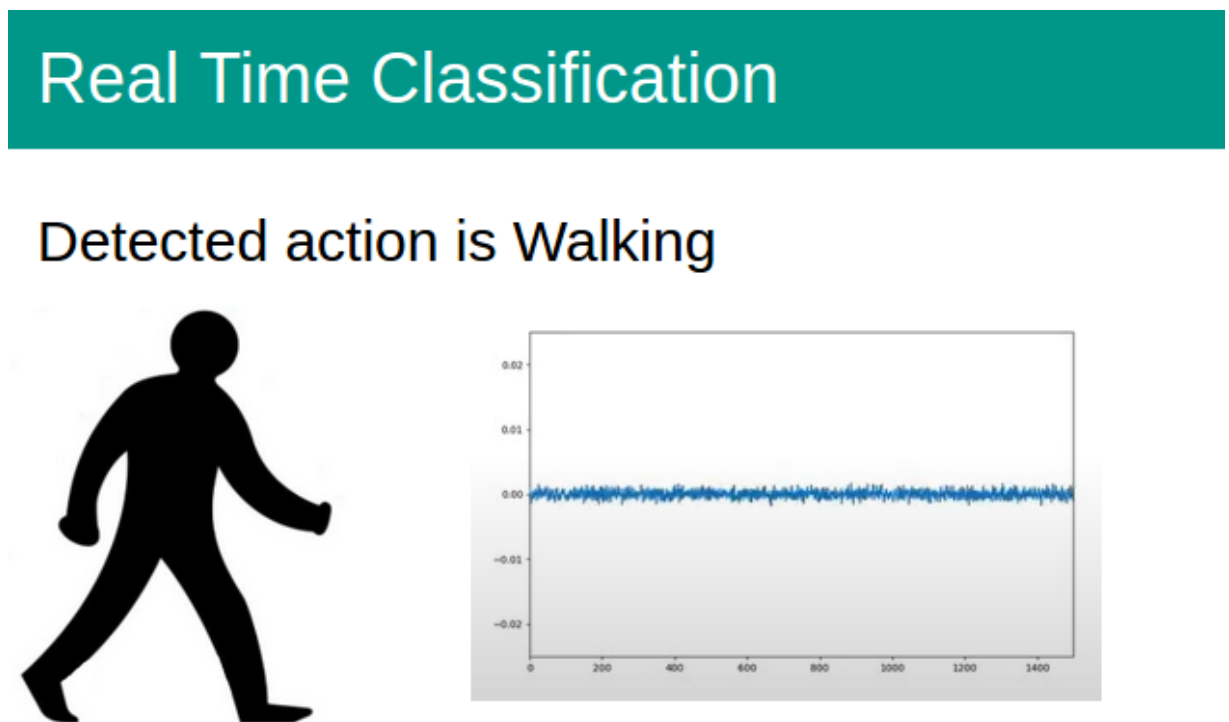


Figure 8.12: Dashboard Layout When the System Detects Subject is Walking.

For the real-time system, a dashboard is used where the output of the system can be viewed by family members and/or caregivers. The dashboard is in the format of a web page using

the Python Flask web framework as the back end. The dashboard is designed to be clear and show the user exactly the current detected activity. The last activity is consistently shown on the dashboard. For example, if a sitting action is detected by the dashboard the sitting action will be shown on the interface until a stand action is detected to change the interface image. The dashboard will display the output of the AI models and shows an image of the current CSI window and a graphical representation of the latest detected activity. The dashboard collects the CSI amplitude data from the cloud. When the receiving PC collects the CSI from the RF communication, it will encrypt and upload the raw amplitude data to the cloud. The MongoDB cloud service is used to store the data. The dashboard downloads the CSI data from MongoDB and creates an image of the raw CSI amplitude data. it then applies the rules to incoming data, processing and passing the data to the appropriate AI model. The AI model will then produce a prediction. The prediction is used to select the graphical representation image file which matches the prediction. The prediction, graphical representation, and image of the raw CSI amplitude window are displayed on the web interface. Figure 8.10 shows the layout of the dashboard for sitting and Figure 8.11 shows the layout of the dashboard for standing and 8.12 shows the layout of the dashboard for walking. The Figures show the AI prediction in text format, The graphical representation and the raw CSI amplitude data.

### 8.2.5 Encryption

As this chapter proposes a monitoring system in the application of healthcare of vulnerable people, it is essential to consider data protection [269]. The need for data protection is further required due to the use of third-party cloud providers. If there was any data breach of the cloud provider, then data that indicates the movement of a vulnerable person could be leaked. Therefore this chapter makes use of encryption to ensure that any data uploaded to the cloud is encrypted. This mitigates the risk of data leakage as the leaked data will be unreadable. The encryption method used is the well-known RSA public-key cryptosystem [270]. RSA is considered to be one of the best advances in the field of public-key encryption [271]. Various papers have implemented RSA encryption when storing sensitive data on the cloud [263, 264, 265]. The RSA algorithm is applied using Python to generate a public and private key pair for encryption and decryption [272]. Before data is uploaded to the cloud, it is encrypted by the public key. The data stored on the cloud will then be unreadable and will require the private key to decrypt. The private key is present on the web server hosting the dashboard interface. The dashboard contains the credentials required to download the encrypted data from the cloud. Once downloaded it applies the private key to decrypt the data. The data can then be processed and passed to the appropriate AI model for classification. This encryption method ensures that data is not exposed while transferring between the onsite monitoring system and the web server providing the dashboard interface. Figure 8.13 shows how the data is encrypted and then decrypted in the proposed system.
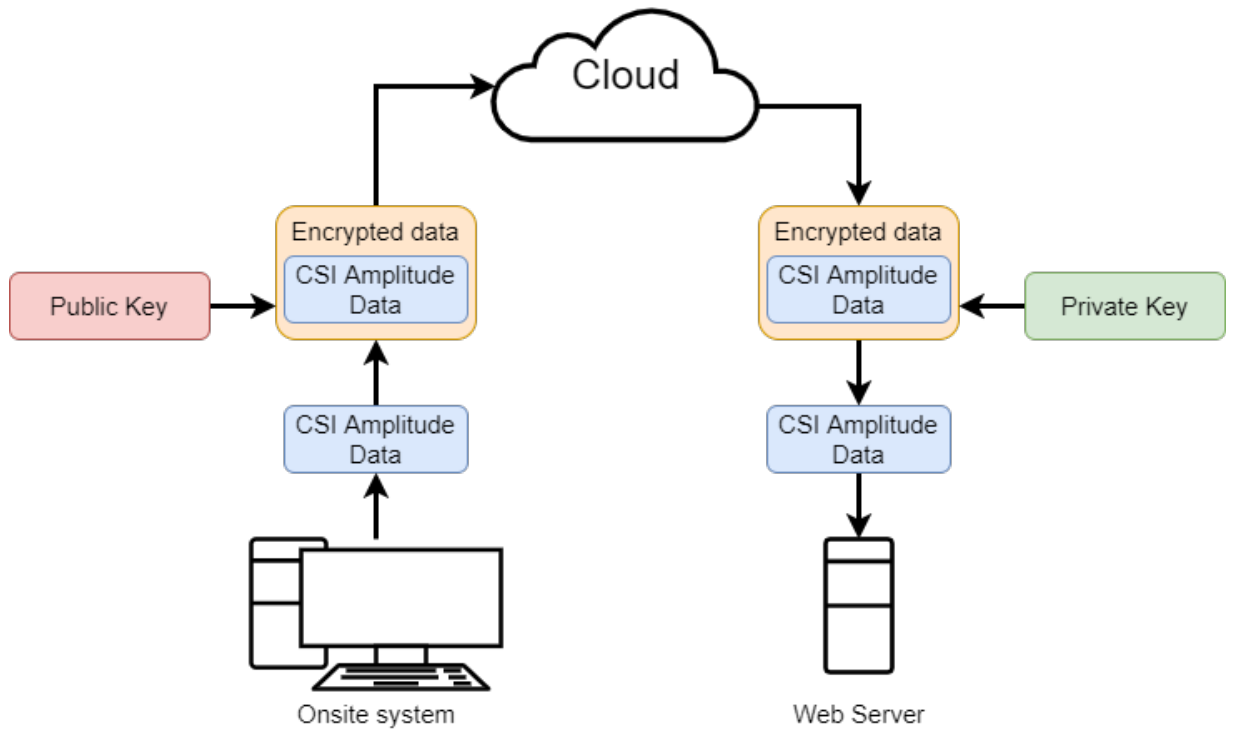
Figure 8.13: Flow Diagram of How Data Is Encrypted.

### 8.2.6   Notification System
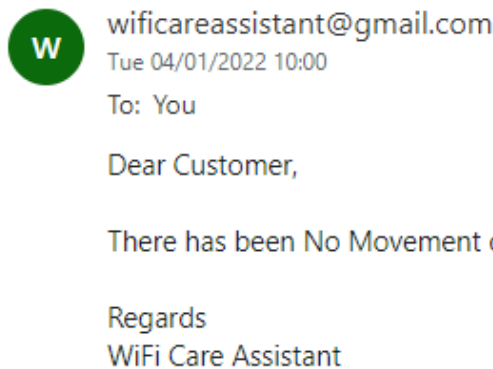


Figure 8.14: Automated Email Sent Out When No Movement Has Been Detected.

The dashboard also includes a notification system that provides family members and/or care-givers notifications if no movement is detected during times of expected movement. The notification system is configured to send automated emails to alert if no movements are detected within the last hour during the daytime. This works by recording the output of the classification from the system for each hour of the day. Once the hour changes, the classifications of the previous hour are read by the script. If the number of entries all matches the "No Activity" classification then an automated email will be sent out. At night times when a person is expected to be sleeping, the notification system is disabled. Night-time monitoring can seek to include vital

sign detection using RF signals. Vital sign monitoring with RF signals is part of the planned future work related to the monitoring of vulnerable people. To disable the notification at night, the times when the vulnerable person is expected to wake up and go to bed are entered into the system. If the hour is between the time the person goes to bed and then wakes up then no notification email is automated. Figure 8.14 shows an example of the automated email sent out if no movement has been detected in the last hour.

## 8.3  Results

This section will describe the results obtained when testing the Random Forest ML algorithm against the two datasets created for training. Namely the sitting vs standing dataset and the walking vs no activity dataset. The datasets are tested using 10-fold cross-validation to indicate how the Random Forest ML algorithm can distinguish between the two classes of each dataset. An AI model is created using the entire dataset and can be recalled later to make classifications of new data.

### 8.3.1  Sitting vs Standing

The sitting vs standing dataset had an accuracy score of 90.75 % when using the Random Forest algorithm with 10-fold cross-validation. Figure 8.15 shows the confusion matrix of the classifications made during 10-fold cross-validation.



Figure 8.15: Confusion Matrix of Sitting vs Standing Dataset.

It can be seen that the majority of the samples have been classified correctly. out of the 600 sitting samples, 540 were correctly classified. The standing samples included 51 incorrectly classified samples with 549 correctly classified samples.

### 8.3.2 Walking vs No Activity

The walking vs no activity dataset provided an accuracy of 99.83 % when using the Random Forest algorithm with 10-fold cross-validation. Figure 8.16 shows the confusion matrix of how the samples were classified.



|                | Non Walking | Walking |
| -------------- | ----------- | ------- |
| Non Walking    | 7684        | 3       |
| Walking        | 10          | 397     |

Figure 8.16: Confusion Matrix of Walking vs No Activity Dataset.

The results show that out of the 407 walking samples used for training, 397 of them were classified correctly. There are a total of 7687 no activity samples. This high number is due to the many samples taken during data collection which did not meet the rules for further classification. The high number of samples can be attributed to the overlapping nature of data collection. Only 3 of the no activity samples were incorrectly classified as walking.

## 8.4 Discussion

The results of the created AI models show that the movements of sitting, standing, and walking can be detected by observing the CSI of the received RF signals. Therefore with the implementation of the real-time system proposed in this chapter, these models can be applied to new unseen incoming data. As the system is run with CSI amplitude data streaming through the predefined rules, any CSI windows that meet the rules are passed to the sitting and standing AI model. All other CSI windows are passed to the walking and no activity AI model. Testing of the real-time system using new unseen data collected via real-time transmission found that the AI models were able to identify when movement took place between the transmitter and receiver devices correctly. This shows that the CSI can represent patterns when specific human movements disturb the signal propagation and the use of ML can recognise these patterns and identify the activity.

## 8.5   Summary

The work of this chapter has presented a real-time human activity monitoring system using RF signals. ML has been applied using the Random Forest algorithm to distinguish between different patterns of signal propagation of the RF signals to classify them as specific human movements. The specific movements the system is trained to detect are sitting, standing, and walking. This is accomplished by using two AI models. One model is used for differentiating between sitting and standing and the other model to define walking. The sitting and standing model was able to achieve an accuracy score of 90.75 % and the walking AI model had an accuracy of 99.83 %. Although the sitting and standing AI model had high accuracy, there is still 10 % inaccuracy. This inaccuracy is only a risk in defining sitting or standing. The main goal of the system is to identify movements and alert them of no movements. This is reflected in the higher accuracy of the walking and no activity AI model which has close to 100 % accuracy. This signifies the low risk of false alerts being sent to family members and/or caregivers. Additionally, the system made use of encryption to protect data that is sensitive due to the healthcare application and monitoring nature of the system. The system output can be viewed on a web page dashboard for the benefit of family members and/or caregivers. The alert system is in the format of an automated email notification used to notify caregivers and/or family members if there has been no movement detected during times of expected movement. Future work will seek to improve the overall accuracy of the system and implement additional activities which can be detected from the system. Research is being conducted to integrate vital sign monitoring with the use of RF signals in addition to activity monitoring.

# Chapter 9

# Real-time Monitoring of Vital Signs of Multiple Subjects using RF Signals

Work detailed in this thesis has detailed using RF signals to detect large body movements such as sitting and standing as a proof of concept for detecting falls. RF signals can however be used to detect smaller body movements such as chest movements. These movements can be used to provide an estimation of the vital signs of a person. In this chapter, RF signals are used to estimate the vital signs of one, two, and three subjects in real-time. This is achieved by using a directional antenna as a transmitter and two omnidirectional antennas to serve as receiver antennas. Subjects are placed between the transmitter and receiver antennas. As RF signals are sent across to the receiver antennas, the signal will reflect off the small movements of the chest produced by breathing and heart pulses. The vital signs are estimated by using the CSI of each of the receiving antennas and then calculating the phase of the signals. The difference in the phase from each antenna is then calculated. From this information, the peaks in the power spectrum of the signal can be used to estimate the vital signs of the subjects placed between the transmitter and receiver antennas. Each subject is wearing contact-based devices which can provide ground truth values for their actual breathing rate and heart rate. A web interface is used as a dashboard to display the contact-based sensor reading and the contactless RF sensing reading and the power spectrum density.

## 9.1   Introduction

Vital signs of humans are used by healthcare professionals as a tool to provide a quick assessment of the health status of an individual [273, 274]. Vital signs include respiration rate, heart rate, temperature and blood pressure [275]. Monitoring expected vital signs can ensure that individuals are in good health [276]. Abnormal vital signs are indicative of deteriorating health and the potential requirement for medical intervention [277]. Technology can provide monitoring of vital signs in patients [278]. Currently, contact-based devices can be used to detect vital

signs for both medical and fitness applications [85]. Contact-based technology is in the form of a belt or wrist band which can provide monitoring of breathing and heart rates [279]. The devices use an accelerometer to measure the movements of the body to detect heart and respiratory rates [280, 281, 282]. For example, a breathing belt will be worn around the torso area and chest movements will indicate breathing. Heart rate can be calculated by the pulse which can be found throughout the body. For example, the pulse can be felt in the wrist or neck. As RF signals can be used to replicate contact-based devices with accelerometers used to detect large-scale movements, then it can be possible to use RF signals to detect smaller movements of the chest to provide a contactless breathing rate and heart rate detection. Examples of contactless vital sign detection include radar technology [95, 283] and RFID technology [80, 284]. This chapter details how RF signals can be used to detect breathing and heart rate for up to three subjects. RF signals have the advantage of being cheaper to implement than radars and without the need to wear RFID tags which are needed for RFID vital sign detection methods.

## 9.2 Methodology

This section will detail the methodology used to perform vital sign detection of up to three subjects.
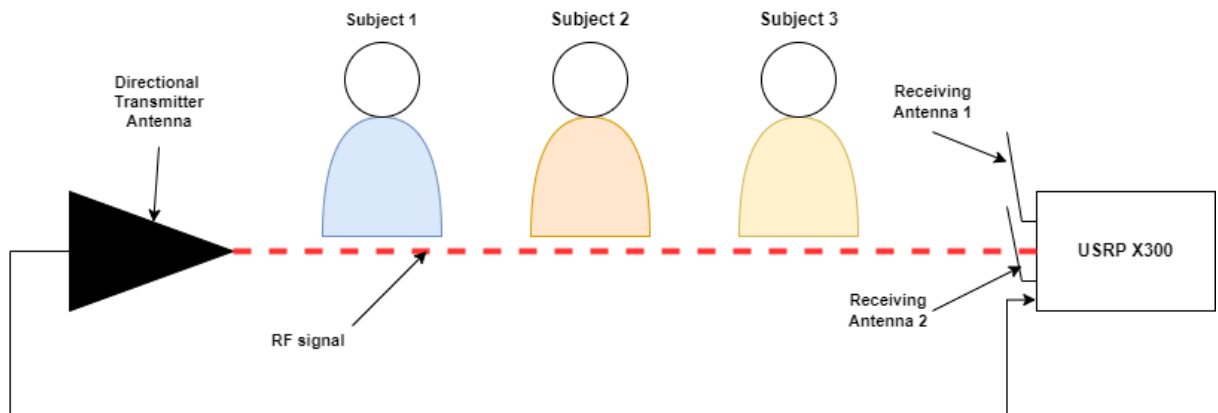


Figure 9.1: Experimental Setup of RF Vital Sign Detection of Multiple Subjects

The experimental setup used to detect vital signs involves using a USRP X300 model to produce CSI. Attached to the USRP is a directional antenna to serve as the transmitter. The directional antenna transmits RF signals similar to already existing Wi-Fi signals so there is no risk to the health of the subjects. The reason a directional antenna is used as it improves the power of the reflected signal from the chest [285]. Then there are two receiver antennas attached to the USRP device. Figure 9.1 shows the setup of the equipment with the position of three subjects. Each receiver collects CSI and from the CSI the phase of the signal can be extracted. The phase information is very sensitive and therefore contains the smaller movements

of the chest during breathing and heart rate [286]. Each antenna's phase values are then used to calculate the difference in phase between each antenna. This difference in phase is what is used to calculate the vital signs as this method can remove noise and ensure the breathing and heart rate can be observed in the signal [287, 288]. The RF signal transmission is configured by using the GNU Radio toolkit to serve as the software for the USRP device. A sample rate of 400 kHz with a 1 GHz centre frequency is used as the wireless properties of the RF channel. These settings proved the best to achieve consistent communication between antennas. The breathing and heart rate is estimated when each receiving antenna receives 4000 CSI packets. Which is approximately 10 seconds. Therefore every 10 seconds an estimation of breathing and heart rates can be produced. This is to ensure there is enough data to give reliable readings. Two arrays are then passed to functions to calculate the phase difference. Butterworth filters are applied to the data to remove noise from the data [289, 290] and then the power spectrum of the signals is calculated. As the CSI has multiple subcarriers, the mean power spectrum of all subcarriers is taken. Then by taking the highest power spectrum values for the number of subjects, the frequency values of the highest power spectrum values relate to the breathing and heart rates of the subjects. A limitation of this system is the inability to associate readings with a particular subject. The number of subjects must be predefined for the system to be able to select the number of peaks that match the number of subjects. Subjects in this experiment wear contact-based heart rate and breathing sensor belts to provide ground truth. The ground truth values are matched to the closest value detected by using the contactless method. However, without the contact-based, there is no way to match and assign vital readings to a particular subject. A dashboard is used to show the vital signs estimated from the RF signals and the vital signs estimated from the sensors so that a comparison can be drawn between the two readings.

## 9.3   Results

The results show that the vital signs estimated from the RF signals are close to the readings of the vital sign sensors for all three subjects. Table 9.1 shows the actual values from ground truth contact-based sensors with the predicted breathing and heart rates from the proposed contactless RF vital sign sensing system. There are outliers for some of the readings as expected. This is because both contactless RF sensing and commercial sensors estimate vital signs. Both methods are susceptible to noise from the environment and human movements can disturb readings [291]. Figure 9.2 shows the dashboard output for three subjects. The text in red shows the estimated breathing and heart rate from the RF signal and the text in black is the breathing and heart rate estimated from the contact-based sensors.

Table 9.1: Comparison of RF Predicted Vital Signs and Contact-based Actual Vital Signs.

| Breathing rate Predicted | Breathing rate Actual | Breathing rate Accuracy | Heartrate Predicted | Heartrate Actual | Heartrate Accuracy |
|---|---|---|---|---|---|
| 6 | 7.43 | 80.75 | 64.2 | 65 | 98.77 |
| 11.4 | 12.1 | 94.21 | 81.6 | 82 | 99.51 |
| 23.4 | 20.01 | 83.06 | 87.6 | 86 | 98.14 |
| 10.8 | 7.39 | 53.86 | 63 | 60 | 95.00 |
| 15.6 | 16.84 | 92.64 | 73.8 | 74 | 99.73 |
| 21 | 19.49 | 92.25 | 84 | 85 | 98.82 |
| 9 | 12.73 | 70.70 | 63.6 | 61 | 95.74 |
| 13.6 | 18.05 | 75.35 | 77.4 | 69 | 87.83 |
| 22.8 | 19.46 | 82.84 | 82.2 | 81 | 98.52 |
| 4.8 | 7.83 | 61.30 | 63.6 | 62 | 97.42 |
| 9 | 15.41 | 58.40 | 68.4 | 67 | 97.91 |
| 13.8 | 19.09 | 72.29 | 77.4 | 75 | 96.80 |
| **Average Accuracy** | | **76.47 %** | **Average Accuracy** | | **97.02 %** |

## Real Time Vitals Demo

### Heart Rate Readings

USRP Heart Rate BPM reading 01: 64.2 bpm

Sensor Heart Rate BPM reading 01: 65 bpm

USRP Heart Rate BPM reading 02: 81.6 bpm

Sensor Heart Rate BPM reading 02: 82 bpm

USRP Heart Rate BPM reading 03: 87.6 bpm

Sensor Heart Rate BPM reading 03: 86 bpm

### Breathing Rate Readings :

USRP Breathing Rate BPM reading 01: 6.0 bpm

Sensor Breathing Rate BPM reading 01: 7.43 bpm

USRP Breathing Rate BPM reading 02: 11.4 bpm

Sensor Breathing Rate BPM reading 02: 12.10 bpm

USRP Breathing Rate BPM reading 03: 23.4 bpm

Sensor Breathing Rate BPM reading 03: 20.01 bpm
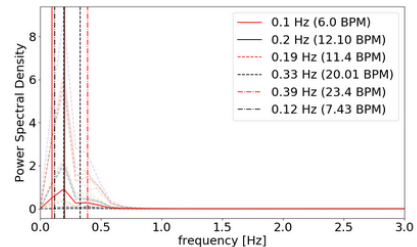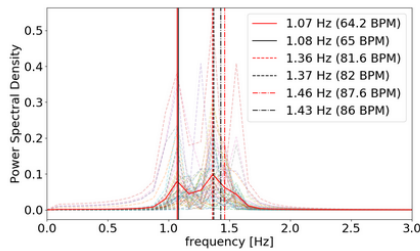
Figure 9.2: Web Dashboard Showing Estimated Vital Signs for Three Subjects

## 9.4   Summary

This chapter has detailed the work done to implement real-time vital sign detection using RF signals for multiple subjects. The experiment is effective for one, two, and three subjects. The work makes use of CSI phase data to detect the smaller movements of the chest of subjects

to give an estimation of the breathing and heart rates. The breathing and heart rates detected using the RF signal are compared to readings from contact-based sensors so that ground truth is used to validate the system. A web interface is used as a dashboard to display both breathing and heart rates from the RF signal and contact-based sensors. The dashboard also displays the power spectrum density of the signal. The RF signal was able to provide close readings with the contact-based sensors for up to three subjects.

# Chapter 10

# Conclusion and Future Work

## 10.1 Conclusion

The main contribution of this thesis is to implement RF sensing into a real-time monitoring system capable of detecting human movements with the assistance of machine learning. The thesis details the current literature in the field of human activity monitoring by using contact and contactless methods. Contact-based methods include wearable sensors. Although contact-based sensors provide good accuracy, they come with disadvantages such as being uncomfortable, battery capacity issues, and human forgetfulness to wear the device. In the application of elderly care, forgetting to wear the device is of real concern due to an increased risk of memory impairments in elderly people. If users do not wear the device then it will be useless. Contactless methods include cameras, radar, and RF technology. Camera technology is effective at monitoring human activities but using cameras in the home can be discomforting to vulnerable people as privacy is not being upheld. Radar technology is also an effective method to monitor human movements and preserve the privacy of vulnerable people but it will however include the introduction of new technology in the home. Which could be unappealing to some individuals. RF sensing is effective for human monitoring because it preserves privacy and RF signals are already present in most homes that have Wi-Fi networks installed. Wi-Fi transmits data between devices wirelessly using RF signals. When there are human movements between an RF transmitter and receiver, the signal propagation is impacted. This impact can be viewed by looking at the CSI. This thesis demonstrates a monitoring system using RF signals to detect human movements in real-time. The work has looked at using machine learning to recognise the CSI patterns that can be associated with specific movements in real-time. The thesis has analysed different machine-learning algorithms by observing accuracy and timing to ensure that the real-time component can be met. The chapters of the thesis detail how the real-time aspect of RF sensing has been achieved. From initial applications successfully detecting human motion to eventually being able to detect specific motions in a CSI data stream and use machine learning to accurately classify which specific motion occurred. This provides proof of concept that RF

109

signals would be able to detect if an elderly or vulnerable person was to suffer a fall. The work of the thesis has progressed to detail a prototype RF monitoring system that is able to detect if a person is sitting, standing, or walking with additional features such as secure cloud storage and a working alert system. The monitoring system takes the CSI data and then encrypts the data. This ensures that data is protected on the cloud. Then a web server can download the data from the cloud and perform decryption. The data is then processed to search for movements contained in the CSI. If there are movements then machine learning can be applied to classify the movement into sitting, standing, or walking. If there are no expected movements within a specified time frame then an email is sent out to alert a family member and/or caregiver that expected movements have not occurred. The thesis also presents a working prototype for using RF signals to detect the vital signs of multiple subjects. RF signals can be used to detect the small movements of the chest created by a person breathing and their heart beating. This information can be used to estimate the breathing rate and heart rate of the person. The work detailed in this thesis makes use of RF signals to estimate the vital signs of three subjects. Each subject wears a contact-based device to detect their breathing and heart rate and to serve as ground truth. The vital signs are then estimated for the three subjects in real-time. The output of both the RF estimation and contact-based estimation are displayed to show a direct comparison between the two methods. The results showed the RF vital sign estimation was close in value to the detected estimation of the commercial contact-based devices.

## 10.2   Future Work

This thesis presents a working real-time monitoring system for human activity detection using RF signals however there is still scope for improvements. The experiments detailed in this thesis were very controlled where CSI was collected in a set number of fixed locations. Future work would seek to improve the detection system by building a diverse dataset that includes samples of data in a wide range of positions and orientations. Further work on signal processing should be considered for future work as it can help to reduce noise in the CSI and ensure that activities can be clearly classified. Environmental noise reduction will also help to enable the system to work in different environments which can cover a wide range of different homes which will vary greatly in terms of furniture and floor plan layout. The work detailed in this thesis has made use of SDRs to create RF signals configured to simulate Wi-Fi signals. Future work will seek to implement actual Wi-Fi devices which can connect to existing Wi-Fi networks and capture the CSI used to make classifications using RF signals. Software-defined radios are expensive and over-engineered for the sole process of RF sensing. Cheaper devices such as Raspberry Pis can be used to capture RF signals and provide the CSI data needed to provide RF sensing. Further work can be done in the machine learning aspect to further improve the accuracy of RF sensing. Especially as CSI will become more complex due to more varied dataset collection. Analysis

of Deep learning performance can be carried out to assess their appropriateness for applications of RF sensing. Accuracy and speed of classification are two major requirements of real-time applications.

# Bibliography

[1]    Mohammad Mehedi Hassan et al. "A Smartphone-Enabled Fall Detection Framework for Elderly People in Connected Home Healthcare". In: *IEEE Network* 33.6 (2019), pp. 58–63.

[2]    Marco Mercuri et al. "Healthcare system for non-invasive fall detection in indoor environment". In: *Applications in Electronics Pervading Industry, Environment and Society*. Springer, 2016, pp. 145–152.

[3]    Daniyal Haider et al. "An efficient monitoring of eclamptic seizures in wireless sensors networks". In: *Computers & Electrical Engineering* 75 (2019), pp. 16–30.

[4]    Ying Liu et al. "A novel cloud-based framework for the elderly healthcare services using digital twin". In: *IEEE Access* 7 (2019), pp. 49088–49101.

[5]    Cuijuan Shang et al. "BIA: Behavior Identification Algorithm using Unsupervised Learning Based on Sensor Data for Home Elderly". In: *IEEE Journal of Biomedical and Health Informatics* (2019).

[6]    Xinyue Yang et al. "Human Posture Recognition in Intelligent Healthcare". In: *Journal of Physics: Conference Series*. Vol. 1437. 1. IOP Publishing. 2020, p. 012014.

[7]    Qammer H Abbasi et al. *Advances in body-centric wireless communication: Applications and state-of-the-art*. Institution of Engineering and Technology, 2016.

[8]    Tao Zhang et al. "WiGrus: A Wifi-Based Gesture Recognition System Using Software-Defined Radio". In: *IEEE Access* 7 (2019), pp. 131102–131113.

[9]    Ahsen Tahir et al. "WiFreeze: Multiresolution Scalograms for Freezing of Gait Detection in Parkinsons Leveraging 5G Spectrum with Deep Learning". In: *Electronics* 8.12 (2019), p. 1433.

[10]   Ali Rizwan et al. "Non-invasive hydration level estimation in human body using Galvanic Skin Response". In: *IEEE Sensors Journal* (2020).

[11]   Ahmad Jalal, Majid AK Quaid, and MA Sidduqi. "A Triaxial acceleration-based human motion detection for ambient smart home system". In: *2019 16th International Bhurban Conference on Applied Sciences and Technology (IBCAST)*. IEEE. 2019, pp. 353–358.

[12] Ali Fatih Demir et al. "Anatomical region-specific in vivo wireless communication channel characterization". In: *IEEE journal of biomedical and health informatics* 21.5 (2016), pp. 1254–1262.

[13] Guto Leoni Santos et al. "Accelerometer-based human fall detection using convolutional neural networks". In: *Sensors* 19.7 (2019), p. 1644.

[14] Syeda Fizzah Jilani et al. "Millimeter-wave liquid crystal polymer based conformal antenna array for 5G applications". In: *IEEE Antennas and Wireless Propagation Letters* 18.1 (2018), pp. 84–88.

[15] J Pena Queralta et al. "Edge-AI in LoRa-based health monitoring: fall detection system with fog computing and LSTM recurrent neural networks". In: *2019 42nd International Conference on Telecommunications and Signal Processing (TSP)*. IEEE. 2019, pp. 601–604.

[16] Ipsit Vahia et al. "IDENTIFICATION AND EVALUATION OF BEHAVIORAL SYMPTOMS IN DEMENTIA USING PASSIVE RADIO SENSING AND MACHINE LEARNING". In: *The American Journal of Geriatric Psychiatry* 27.3 (2019), S126–S127.

[17] Xin Yao, Aftab Khan, and Yichao Jin. "Energy Efficient Communication among Wearable Devices using Optimized Motion Detection". In: *2019 IEEE Symposium on Computers and Communications (ISCC)*. IEEE. 2019, pp. 1–6.

[18] Xiao Dong Yang et al. "Spatial correlation analysis of on-body radio channels considering statistical significance". In: *IEEE Antennas and Wireless Propagation Letters* 10 (2011), pp. 780–783.

[19] Ahmet Cengizhan DIrican and Selim Aksoy. "Step counting using smartphone accelerometer and fast fourier transform". In: *Sigma J. Eng. Nat. Sci* 8 (2017), pp. 175–182.

[20] Alexis Nez et al. "Comparison of calibration methods for accelerometers used in human motion analysis". In: *Medical engineering & physics* 38.11 (2016), pp. 1289–1299.

[21] Andrey D Ignatov and Vadim V Strijov. "Human activity recognition using quasiperiodic time series collected from a single tri-axial accelerometer". In: *Multimedia tools and applications* 75.12 (2016), pp. 7257–7270.

[22] Zhen Yang et al. "Graphene textile strain sensor with negative resistance variation for human motion detection". In: *ACS nano* 12.9 (2018), pp. 9134–9141.

[23] Xiaoliang Fang et al. "High-performance wearable strain sensors based on fragmented carbonized melamine sponges for human motion detection". In: *Nanoscale* 9.45 (2017), pp. 17948–17956.

[24] Yanjun Zheng et al. "The effect of filler dimensionality on the electromechanical performance of polydimethylsiloxane based conductive nanocomposites for flexible strain sensors". In: *Composites Science and Technology* 139 (2017), pp. 64–73.

[25]  Jingjing Guo, Mengxuan Niu, and Changxi Yang. "Highly flexible and stretchable opti-
      cal strain sensing for human motion detection". In: *Optica* 4.10 (2017), pp. 1285–1288.

[26]  Shuaitao Yang et al. "Facile Fabrication of High Performance Pen-Ink Decorated Textile
      Strain Sensor for Human Motion Detection". In: *ACS Applied Materials & Interfaces*
      (2020).

[27]  Shaowei Lu et al. "Wearable graphene film strain sensors encapsulated with nylon fab-
      ric for human motion monitoring". In: *Sensors and Actuators A: Physical* 295 (2019),
      pp. 200–209.

[28]  Shu Wang et al. "Environmentally-Friendly and Multifunctional Graphene-Silk Fabric
      Strain Sensor for Human-Motion Detection". In: *Advanced Materials Interfaces* (2019),
      p. 1901507.

[29]  Seyed Reza Larimi et al. "Low-cost ultra-stretchable strain sensors for monitoring hu-
      man motion and bio-signals". In: *Sensors and Actuators A: Physical* 271 (2018), pp. 182–
      191.

[30]  Katsunori Suzuki et al. "Rapid-response, widely stretchable sensor of aligned MWCNT/elastomer
      composites for human motion detection". In: *Acs Sensors* 1.6 (2016), pp. 817–825.

[31]  Shi Qiang Liu, Jun Chang Zhang, and Rong Zhu. "A Wearable Human Motion Tracking
      Device Using Micro Flow Sensor Incorporating with Micro Accelerometer". In: *IEEE
      Transactions on Biomedical Engineering* (2019).

[32]  Zi Hau Chin et al. "Daily Activities Classification on Human Motion Primitives Detec-
      tion Dataset". In: *Computational Science and Technology*. Springer, 2019, pp. 117–125.

[33]  Ahmad Jalal, Majid Ali Khan Quaid, and Kibum Kim. "A wrist worn acceleration based
      human motion analysis and classification for ambient smart home system". In: *Journal
      of Electrical Engineering & Technology* 14.4 (2019), pp. 1733–1739.

[34]  Heng Zhang, Zengjun Fu, and Kuang-I Shu. "Recognizing Ping-Pong Motions Using
      Inertial Data Based on Machine Learning Classification Algorithms". In: *IEEE Access*
      7 (2019), pp. 167055–167064.

[35]  Božidara Cvetković et al. "Real-time activity monitoring with a wristband and a smart-
      phone". In: *Information Fusion* 43 (2018), pp. 77–93.

[36]  Shengke Wang et al. "Human fall detection in surveillance video based on PCANet". In:
      *Multimedia tools and applications* 75.19 (2016), pp. 11603–11613.

[37]  O Dorgham, Sanad Abu Rass, and Habes Alkhraisat. "Improved Elderly Fall Detec-
      tion by Surveillance Video using Real-Time Human Motion Analysis". In: *International
      Journal of Soft Computing* 12.4 (2017), pp. 253–262.

[38]  Md Islam et al. "Human Activity Recognition Using Tools of Convolutional Neural Networks: A State of the Art Review, Data Sets, Challenges and Future Prospects". In: *arXiv preprint arXiv:2202.03274* (2022).

[39]  Sahil Waqar, Muhammad Muaaz, and Matthias Pätzold. "Human Activity Signatures Captured under Different Directions Using SISO and MIMO Radar Systems". In: *Applied Sciences* 12.4 (2022), p. 1825.

[40]  Chengxi Yu et al. "Noninvasive human activity recognition using millimeter-wave radar". In: *IEEE Systems Journal* (2022).

[41]  Xinyu Li, Yuan He, and Xiaojun Jing. "A survey of deep learning-based human activity recognition in radar". In: *Remote Sensing* 11.9 (2019), p. 1068.

[42]  Baris Erol and Moeness G Amin. "Radar data cube processing for human activity recognition using multisubspace learning". In: *IEEE Transactions on Aerospace and Electronic Systems* 55.6 (2019), pp. 3617–3628.

[43]  Ying Luo et al. "Doppler effect and micro-Doppler effect of vortex-electromagnetic-wave-based radar". In: *IET Radar, Sonar & Navigation* 14.1 (2020), pp. 2–9.

[44]  Huseyin Duysak, Umut Ozkaya, and Enes Yigit. "Determination of the amount of grain in silos with deep learning methods based on radar spectrogram data". In: *IEEE Transactions on Instrumentation and Measurement* 70 (2021), pp. 1–10.

[45]  Fei Luo, Stefan Poslad, and Eliane Bodanese. "Human activity detection and coarse localization outdoors using micro-Doppler signatures". In: *IEEE Sensors Journal* 19.18 (2019), pp. 8079–8094.

[46]  Chuanwei Ding et al. "Fall detection with multi-domain features by a portable FMCW radar". In: *2019 IEEE MTT-S International Wireless Symposium (IWS)*. IEEE. 2019, pp. 1–3.

[47]  Syed Aziz Shah and Francesco Fioranelli. "Human Activity Recognition: Preliminary Results for Dataset Portability using FMCW Radar". In: (2019).

[48]  Branka Jokanovic, Moeness Amin, and Fauzia Ahmad. "Radar fall motion detection using deep learning". In: *2016 IEEE radar conference (RadarConf)*. IEEE. 2016, pp. 1–6.

[49]  Baris Erol et al. "Wideband radar based fall motion detection for a generic elderly". In: *2016 50th Asilomar Conference on Signals, Systems and Computers*. IEEE. 2016, pp. 1768–1772.

[50]  Mingyang Wang, Yimin D Zhang, and Guolong Cui. "Human motion recognition exploiting radar with stacked recurrent neural network". In: *Digital Signal Processing* 87 (2019), pp. 125–131.

[51] Baris Erol and Moeness Amin. "Generalized pca fusion for improved radar human motion recognition". In: *2019 IEEE Radar Conference (RadarConf)*. IEEE. 2019, pp. 1–5.

[52] Rui Qi et al. "Multi-Classification Algorithm for Human Motion Recognition Based on IR-UWB Radar". In: *IEEE Sensors Journal* 20.21 (2020), pp. 12848–12858.

[53] Taekjin Han, Wonho Kang, and Gyunghyun Choi. "IR-UWB Sensor Based Fall Detection Method Using CNN Algorithm". In: *Sensors* 20.20 (2020), p. 5948.

[54] Kevin Bouchard et al. "Activity recognition in smart homes using UWB radars". In: *Procedia Computer Science* 170 (2020), pp. 10–17.

[55] Arijit Chowdhury et al. "Activity recognition using ultra wide band range-time scan". In: *2020 28th European Signal Processing Conference (EUSIPCO)*. IEEE. 2021, pp. 1338–1342.

[56] Julien Maitre et al. "Recognizing activities of daily living from UWB radars and deep learning". In: *Expert Systems with Applications* 164 (2021), p. 113994.

[57] Ghassem Mokhtari, Qing Zhang, and Amir Fazlollahi. "Non-wearable UWB sensor to detect falls in smart home environment". In: *2017 IEEE International Conference on Pervasive Computing and Communications Workshops (PerCom Workshops)*. IEEE. 2017, pp. 274–278.

[58] Jijun Zhao et al. "R-DEHM: CSI-based robust duration estimation of human motion with WiFi". In: *Sensors* 19.6 (2019), p. 1421.

[59] Nishtha Chopra et al. "THz time-domain spectroscopy of human skin tissue for in-body nanonetworks". In: *IEEE Transactions on Terahertz Science and Technology* 6.6 (2016), pp. 803–809.

[60] Sadhana Lolla and Amy Zhao. "WiFi motion detection: a study into efficacy and classification". In: *2019 IEEE Integrated STEM Education Conference (ISEC)*. IEEE. 2019, pp. 375–378.

[61] Tao Wang et al. "Wi-Alarm: Low-Cost Passive Intrusion Detection Using WiFi". In: *Sensors* 19.10 (2019), p. 2335.

[62] Pengyu Zhang et al. "Complex Motion Detection Based on Channel State Information and LSTM-RNN". In: *2020 10th Annual Computing and Communication Workshop and Conference (CCWC)*. IEEE. 2020, pp. 0756–0760.

[63] Md Nafiul Alam Nipu et al. "Human identification using wifi signal". In: *2018 Joint 7th International Conference on Informatics, Electronics & Vision (ICIEV) and 2018 2nd International Conference on Imaging, Vision & Pattern Recognition (icIVPR)*. IEEE. 2018, pp. 300–304.

[64] B Tan et al. "Monitoring Health Using Wifi Sensing and Machine Learning". In: *EngineerIT* 2018.March (2018).

[65] Syed Aziz Shah et al. "Posture recognition to prevent bedsores for multiple patients using leaking coaxial cable". In: *IEEE Access* 4 (2016), pp. 8065–8072.

[66] Asif Hanif, Mazher Iqbal, and Farasat Munir. "WiSpy: Through-wall movement sensing and person counting using commodity WiFi signals". In: *2018 IEEE SENSORS*. IEEE. 2018, pp. 1–4.

[67] Shirley Minola et al. "Human motion detection using channel property of wireless communication link". In: *International Journal of Pure and Applied Mathematics* 119.12 (2018), pp. 13165–13169.

[68] Zhanjun Hao et al. "CSI-HC: a WiFi-based indoor complex human motion recognition method". In: *Mobile Information Systems* 2020 (2020).

[69] Sameer Ahmad Bhat et al. "Human Recognition using Single-Input-Single-Output Channel Model and Support Vector Machines". In: ().

[70] MOHAMMED Al-Khafajiy et al. "Intelligent Control and Security of Fog Resources in Healthcare Systems via a Cognitive Fog Model". In: *ACM Transactions on Internet Technology* ().

[71] Soraia Oueida et al. "An edge computing based smart healthcare framework for resource management". In: *Sensors* 18.12 (2018), p. 4307.

[72] Fazel Anjomshoa et al. "Social behaviometrics for personalized devices in the internet of things era". In: *IEEE Access* 5 (2017), pp. 12199–12213.

[73] "5g-enabled contactless multi-user presence and activity detection for independent assisted living". In: *Scientific Reports* 11.1 (2021), pp. 1–15.

[74] Syed Aziz Shah et al. "Privacy-preserving non-wearable occupancy monitoring system exploiting Wi-Fi imaging for next-generation body centric communication". In: *Micromachines* 11.4 (2020), p. 379.

[75] Daqing Zhang et al. "Anti-fall: A non-intrusive and real-time fall detector leveraging CSI from commodity WiFi devices". In: *International Conference on Smart Homes and Health Telematics*. Springer. 2015, pp. 181–193.

[76] Yao Ge et al. "Real-Time Human Activity Recognition System Exploiting Ubiquitous Wi-Fi Signals". In: *2021 IEEE International Symposium on Antennas and Propagation and USNC-URSI Radio Science Meeting (APS/URSI)*. IEEE. 2021, pp. 1033–1034.

[77] Aryan Sharma et al. "Passive WiFi CSI sensing based machine learning framework for COVID-Safe occupancy monitoring". In: *2021 IEEE International Conference on Communications Workshops (ICC Workshops)*. IEEE. 2021, pp. 1–6.

[78] Munder Abdulatef Al-Hashem, Ali Mohammad Alqudah, and Qasem Qananwah. "Performance Evaluation of Different Machine Learning Classification Algorithms for Disease Diagnosis". In: *International Journal of E-Health and Medical Communications (IJEHMC)* 12.6 (2021), pp. 1–28.

[79] Keming Tang, Yong Xu, and Wei Guo. "An indoor human motion detection algorithm based on channel state information". In: *2017 International Smart Cities Conference (ISC2)*. IEEE. 2017, pp. 1–6.

[80] Xuan Liu et al. "Vital signs monitoring with RFID: Opportunities and challenges". In: *IEEE Network* 33.4 (2019), pp. 126–132.

[81] Martine JM Breteler et al. "Vital Signs Monitoring with Wearable Sensors in High-risk Surgical PatientsA Clinical Validation Study". In: *Anesthesiology: The Journal of the American Society of Anesthesiologists* 132.3 (2020), pp. 424–439.

[82] Tonny Heng Yew Ling, Lim Jin Wong, and Raymond Moore. "IoT Fitness Device with Real Time Health Assessment and Cloud Storage". In: *2019 7th International Conference on Smart Computing & Communications (ICSCC)*. IEEE. 2019, pp. 1–5.

[83] Bandana Mallick and Ajit Kumar Patro. "Heart rate monitoring system using finger tip through arduino and processing software". In: *International Journal of Science, Engineering and Technology Research (IJSETR)* 5.1 (2016), pp. 84–89.

[84] Jiacheng Shang and Jie Wu. "Fine-grained vital signs estimation using commercial wi-fi devices". In: *Proceedings of the Eighth Wireless of the Students, by the Students, and for the Students Workshop*. 2016, pp. 30–32.

[85] Yasser Khan et al. "Monitoring of vital signs with flexible and wearable medical devices". In: *Advanced Materials* 28.22 (2016), pp. 4373–4395.

[86] Zhihua Wang, Zhaochu Yang, and Tao Dong. "A review of wearable technologies for elderly care that can accurately track indoor position, recognize physical activities and monitor vital signs in real time". In: *Sensors* 17.2 (2017), p. 341.

[87] Alexandru Cismas, Eduard Cismas, and Decebal Popescu. "Detecting Vital Signs Using Inertial Measurement Unit Sensors in Military Applications". In: *2019 22nd International Conference on Control Systems and Computer Science (CSCS)*. IEEE. 2019, pp. 86–90.

[88] Felician Alecu, Paul Pocatilu, and Sergiu Capisizu. "An IoT project for Vital Signs Monitoring." In: *Informatica Economica* 21.2 (2017).

[89] Kafil M Razeeb et al. "SmartVista: Smart Autonomous Multi Modal Sensors for Vital Signs Monitoring". In: *Smart Systems Integration; 13th International Conference and Exhibition on Integration Issues of Miniaturized Systems*. VDE. 2019, pp. 1–8.

[90] Yihao Chen et al. "Biocompatible and ultra-flexible inorganic strain sensors attached to skin for long-term vital signs monitoring". In: *IEEE Electron Device Letters* 37.4 (2016), pp. 496–499.

[91] Sitthichok Chaichulee et al. "Cardio-respiratory signal extraction from video camera data for continuous non-contact vital sign monitoring using deep learning". In: *Physiological measurement* 40.11 (2019), p. 115001.

[92] Ruchika Sinhal, Kavita Singh, and MM Raghuwanshi. "An Overview of Remote Photoplethysmography Methods for Vital Sign Monitoring". In: *Computer Vision and Machine Intelligence in Medical Image Analysis*. Springer, 2020, pp. 21–31.

[93] Mauricio Villarroel et al. "Non-contact vital sign monitoring in the clinic". In: *2017 12th IEEE International Conference on Automatic Face & Gesture Recognition (FG 2017)*. IEEE. 2017, pp. 278–285.

[94] Hamideh Ghanadian, Mohammad Ghodratigohar, and Hussein Al Osman. "A machine learning method to improve non-contact heart rate monitoring using an RGB camera". In: *IEEE Access* 6 (2018), pp. 57085–57094.

[95] Mamady Kebe et al. "Human vital signs detection methods and potential using radars: A review". In: *Sensors* 20.5 (2020), p. 1454.

[96] Emanuele Cardillo, Changzhi Li, and Alina Caddemi. "Vital sign detection and radar self-motion cancellation through clutter identification". In: *IEEE Transactions on Microwave Theory and Techniques* 69.3 (2021), pp. 1932–1942.

[97] Jian Liu et al. "Monitoring vital signs and postures during sleep using WiFi signals". In: *IEEE Internet of Things Journal* 5.3 (2018), pp. 2071–2084.

[98] Jian Liu et al. "Tracking vital signs during sleep leveraging off-the-shelf wifi". In: *Proceedings of the 16th ACM International Symposium on Mobile Ad Hoc Networking and Computing*. 2015, pp. 267–276.

[99] Jin Zhang et al. "WiCare: Towards In-Situ Breath Monitoring". In: *Proceedings of the 14th EAI International Conference on Mobile and Ubiquitous Systems: Computing, Networking and Services*. 2017, pp. 126–135.

[100] Syed Aziz Shah and Francesco Fioranelli. "RF sensing technologies for assisted daily living in healthcare: A comprehensive review". In: *IEEE Aerospace and Electronic Systems Magazine* 34.11 (2019), pp. 26–44.

[101] Yunlu Wang et al. "Abnormal respiratory patterns classifier may contribute to large-scale screening of people infected with COVID-19 in an accurate and unobtrusive manner". In: *arXiv preprint arXiv:2002.05534* (2020).

[102] Youwei Zeng et al. "FarSense: Pushing the range limit of WiFi-based respiration sensing with CSI ratio of two antennas". In: *Proceedings of the ACM on Interactive, Mobile, Wearable and Ubiquitous Technologies* 3.3 (2019), pp. 1–26.

[103] Josyl Rocamora et al. "Survey of CSI Fingerprinting-based indoor positioning and mobility tracking systems". In: *IET Signal Processing* (2020).

[104] Mohammed AA Al-qaness et al. "Channel state information from pure communication to sense and track human motion: A survey". In: *Sensors* 19.15 (2019), p. 3329.

[105] Xuyu Wang, Chao Yang, and Shiwen Mao. "ResBeat: Resilient breathing beats monitoring with realtime bimodal CSI data". In: *GLOBECOM 2017-2017 IEEE Global Communications Conference*. IEEE. 2017, pp. 1–6.

[106] Joe G Greener et al. "A guide to machine learning for biologists". In: *Nature Reviews Molecular Cell Biology* 23.1 (2022), pp. 40–55.

[107] Ramon Mayor Martins and Christiane Gresse Von Wangenheim. "Findings on Teaching Machine Learning in High School: A Ten-Year Systematic Literature Review". In: *Informatics in Education* (2022).

[108] Jafar Alzubi, Anand Nayyar, and Akshi Kumar. "Machine learning from theory to algorithms: an overview". In: *Journal of physics: conference series*. Vol. 1142. 1. IOP Publishing. 2018, p. 012012.

[109] Ku Chhaya A Khanzode and Ravindra D Sarode. "Advantages and Disadvantages of Artificial Intelligence and Machine Learning: A Literature Review". In: *International Journal of Library & Information Science (IJLIS)* 9.1 (2020), p. 3.

[110] Thorsten Wuest et al. "Machine learning in manufacturing: advantages, challenges, and applications". In: *Production & Manufacturing Research* 4.1 (2016), pp. 23–45.

[111] Batta Mahesh. "Machine learning algorithms-a review". In: *International Journal of Science and Research (IJSR).[Internet]* 9 (2020), pp. 381–386.

[112] Mohamed Alloghani et al. "A systematic review on supervised and unsupervised machine learning algorithms for data science". In: *Supervised and unsupervised learning for data science* (2020), pp. 3–21.

[113] Sergey Levine et al. "Offline reinforcement learning: Tutorial, review, and perspectives on open problems". In: *arXiv preprint arXiv:2005.01643* (2020).

[114] Ian Osband et al. "Behaviour suite for reinforcement learning". In: *arXiv preprint arXiv:1908.0356* (2019).

[115] Adam C Mater and Michelle L Coote. "Deep learning in chemistry". In: *Journal of chemical information and modeling* 59.6 (2019), pp. 2545–2559.

[116] Timothy P Lillicrap et al. "Random synaptic feedback weights support error backpropagation for deep learning". In: *Nature communications* 7.1 (2016), pp. 1–10.

[117] Abul Bashar et al. "Survey on evolving deep learning neural network architectures". In: *Journal of Artificial Intelligence* 1.02 (2019), pp. 73–82.

[118] Ochin Sharma. "Deep challenges associated with deep learning". In: *2019 international conference on machine learning, big data, cloud and parallel computing (COMITCon)*. IEEE. 2019, pp. 72–75.

[119] Ajay Shrestha and Ausif Mahmood. "Review of deep learning algorithms and architectures". In: *IEEE access* 7 (2019), pp. 53040–53065.

[120] Musab Coşkun et al. "An overview of popular deep learning methods". In: *European Journal of Technique (EJT)* 7.2 (2017), pp. 165–176.

[121] Yann LeCun, Yoshua Bengio, and Geoffrey Hinton. "Deep learning". In: *nature* 521.7553 (2015), pp. 436–444.

[122] Tobias Gruber et al. "On deep learning-based channel decoding". In: *2017 51st Annual Conference on Information Sciences and Systems (CISS)*. IEEE. 2017, pp. 1–6.

[123] Tanu Singhal. "A review of coronavirus disease-2019 (COVID-19)". In: *The Indian Journal of Pediatrics* (2020), pp. 1–6.

[124] Lei Pan et al. "Clinical characteristics of COVID-19 patients with digestive symptoms in Hubei, China: a descriptive, cross-sectional, multicenter study". In: *The American journal of gastroenterology* 115 (2020).

[125] Neo Poyiadji et al. "COVID-19–associated acute hemorrhagic necrotizing encephalopathy: CT and MRI features". In: *Radiology* (2020), p. 201187.

[126] Zhe Xu et al. "Pathological findings of COVID-19 associated with acute respiratory distress syndrome". In: *The Lancet respiratory medicine* 8.4 (2020), pp. 420–422.

[127] John Willan et al. *Challenges for NHS hospitals during covid-19 epidemic*. 2020.

[128] William Taylor et al. "An intelligent non-invasive real-time human activity recognition system for next-generation healthcare". In: *Sensors* 20.9 (2020), p. 2653.

[129] Bo Tan et al. "Exploiting WiFi channel state information for residential healthcare informatics". In: *IEEE Communications Magazine* 56.5 (2018), pp. 130–137.

[130] John J Marini and Luciano Gattinoni. "Management of COVID-19 respiratory distress". In: *Jama* (2020).

[131] Dou Fan et al. "Breathing rhythm analysis in body centric networks". In: *IEEE Access* 6 (2018), pp. 32507–32513.

[132] Ying-Ying Zheng et al. "COVID-19 and the cardiovascular system". In: *Nature Reviews Cardiology* 17.5 (2020), pp. 259–260.

[133] URL: `https://www.nhs.uk/conditions/coronavirus-covid-19/testing-and-tracing/what-your-test-result-means/`.

[134] Feng Shi et al. "Review of artificial intelligence techniques in imaging data acquisition, segmentation and diagnosis for covid-19". In: *IEEE Reviews in Biomedical Engineering* (2020).

[135] Linda Wang and Alexander Wong. "COVID-Net: A Tailored Deep Convolutional Neural Network Design for Detection of COVID-19 Cases from Chest X-Ray Images". In: *arXiv preprint arXiv:2003.09871* (2020).

[136] Biraja Ghoshal and Allan Tucker. "Estimating uncertainty and interpretability in deep learning for coronavirus (COVID-19) detection". In: *arXiv preprint arXiv:2003.10769* (2020).

[137] Zheng Jiang et al. "Combining Visible Light and Infrared Imaging for Efficient Detection of Respiratory Infections such as COVID-19 on Portable Device". In: *arXiv preprint arXiv:2004.06912* (2020).

[138] Jannis Born et al. "POCOVID-Net: automatic detection of COVID-19 from a new lung ultrasound imaging dataset (POCUS)". In: *arXiv preprint arXiv:2004.12084* (2020).

[139] Mostafa Alizadeh et al. "Remote monitoring of human vital signs using mm-Wave FMCW radar". In: *IEEE Access* 7 (2019), pp. 54958–54968.

[140] Francesco Fioranelli, Julien Le Kernec, and Syed Aziz Shah. "Radar for Health Care: Recognizing Human Activities and Monitoring Vital Signs". In: *IEEE Potentials* 38.4 (2019), pp. 16–23.

[141] Binbin Dong et al. "Monitoring of atopic dermatitis using leaky coaxial cable". In: *Healthcare technology letters* 4.6 (2017), pp. 244–248.

[142] Daniyal Haider et al. "Utilizing a 5G spectrum for health care to detect the tremors and breathing activity for multiple sclerosis". In: *Transactions on Emerging Telecommunications Technologies* 29.10 (2018), e3454.

[143] Xiaodong Yang et al. "Detection of essential tremor at the *s*-band". In: *IEEE journal of translational engineering in health and medicine* 6 (2018), pp. 1–7.

[144] Xiaodong Yang et al. "Monitoring of patients suffering from REM sleep behavior disorder". In: *IEEE Journal of Electromagnetics, RF and Microwaves in Medicine and Biology* 2.2 (2018), pp. 138–143.

[145] Valmir Oliveira Silvino et al. "IDENTIFYING FEBRILE HUMANS USING INFRARED THERMOGRAPHY SCREENING: POSSIBLE APPLICATIONS DURING COVID-19 OUTBREAK". In: *Revista Contexto & Saúde* 20.38 (2020), pp. 5–9.

[146] Yu Rong et al. "Cardiac Sensing Exploiting an Ultra-Wideband Terahertz Sensing System". In: *2020 IEEE International Radar Conference (RADAR)*. IEEE. 2020, pp. 1002–1006.

[147] Hironori Matsumoto et al. "Integrated terahertz radar based on leaky-wave coherence tomography". In: *Nature Electronics* 3.2 (2020), pp. 122–129.

[148] Lin Li et al. "Artificial intelligence distinguishes COVID-19 from community acquired pneumonia on chest CT". In: *Radiology* (2020), p. 200905.

[149] Ali Narin, Ceren Kaya, and Ziynet Pamuk. "Automatic detection of coronavirus disease (covid-19) using x-ray images and deep convolutional neural networks". In: *arXiv preprint arXiv:2003.10849* (2020).

[150] Tulin Ozturk et al. "Automated detection of COVID-19 cases using deep neural networks with X-ray images". In: *Computers in Biology and Medicine* (2020), p. 103792.

[151] Shekh MM Islam. "Can Radar Remote Life Sensing Technology Help to Combat COVID-19?" In: (2020).

[152] Mucahid Barstugan, Umut Ozkaya, and Saban Ozturk. "Coronavirus (covid-19) classification using ct images by machine learning methods". In: *arXiv preprint arXiv:2003.09424* (2020).

[153] Adam Conner-Simons. *CSAIL device lets doctors monitor COVID-19 patients from a distance*. Apr. 2020. URL: https://www.csail.mit.edu/news/csail-device-lets-doctors-monitor-covid-19-patients-distance.

[154] Jianpeng Zhang et al. "Covid-19 screening on chest x-ray images using deep learning based anomaly detection". In: *arXiv preprint arXiv:2003.12338* (2020).

[155] Fei Shan et al. "Lung infection quantification of covid-19 in ct images with deep learning". In: *arXiv preprint arXiv:2003.04655* (2020).

[156] Wenjing Yang et al. "The role of imaging in 2019 novel coronavirus pneumonia (COVID-19)". In: *European Radiology* (2020), pp. 1–9.

[157] Buddhisha Udugama et al. "Diagnosing COVID-19: the disease and tools for detection". In: *ACS nano* 14.4 (2020), pp. 3822–3835.

[158] Guilherme Duprat Ceniccola et al. "Current technologies in body composition assessment: advantages and disadvantages". In: *Nutrition* 62 (2019), pp. 25–31.

[159] David J Brenner. "Radiation risks potentially associated with low-dose CT screening of adult smokers for lung cancer". In: *Radiology* 231.2 (2004), pp. 440–445.

[160] Prabira Kumar Sethy and Santi Kumari Behera. "Detection of coronavirus disease (covid-19) based on deep features". In: *Preprints* 2020030300 (2020), p. 2020.

[161]  Yunyoung Nam et al. "Monitoring of heart and breathing rates using dual cameras on a smartphone". In: *PloS one* 11.3 (2016), e0151013.

[162]  Abhijit Bhattacharya and Rodney Vaughan. "Deep Learning Radar Design for Breathing and Fall Detection". In: *IEEE Sensors Journal* 20.9 (2020), pp. 5072–5085.

[163]  Heather E Elphick et al. "Exploratory study to evaluate respiratory rate using a thermal imaging camera". In: *Respiration* 97.3 (2019), pp. 205–212.

[164]  Alexander EJ Powles et al. "Physics of ultrasound". In: *Anaesthesia & Intensive Care Medicine* 19.4 (2018), pp. 202–205.

[165]  Francesco Mojoli et al. "Lung ultrasound for critically ill patients". In: *American journal of respiratory and critical care medicine* 199.6 (2019), pp. 701–714.

[166]  Gino Soldati et al. "Is there a role for lung ultrasound during the COVID-19 pandemic?" In: *Journal of Ultrasound in Medicine* (2020).

[167]  Danilo Buonsenso, Davide Pata, and Antonio Chiaretti. "COVID-19 outbreak: less stethoscope, more ultrasound". In: *The Lancet Respiratory Medicine* 8.5 (2020), e27.

[168]  Philippe Arlotto et al. "An ultrasonic contactless sensor for breathing monitoring". In: *Sensors* 14.8 (2014), pp. 15371–15386.

[169]  Ali Al-Naji et al. "A system for monitoring breathing activity using an ultrasonic radar detection with low power consumption". In: *Journal of Sensor and Actuator Networks* 8.2 (2019), p. 32.

[170]  Tianben Wang et al. "Contactless respiration monitoring using ultrasound signal with off-the-shelf audio devices". In: *IEEE Internet of Things Journal* 6.2 (2018), pp. 2959–2973.

[171]  Kyu Cheol Kim et al. "Smartphone-based portable ultrasound imaging system: A primary result". In: *2013 IEEE International Ultrasonics Symposium (IUS)*. IEEE. 2013, pp. 2061–2063.

[172]  Alicja Genc et al. "Ultrasound imaging in the general practitioner's office–a literature review". In: *Journal of ultrasonography* 16.64 (2016), p. 78.

[173]  Syed Aziz Shah, Xiaodong Yang, and Qammer H Abbasi. "Cognitive health care system and its application in pill-rolling assessment". In: *International Journal of Numerical Modelling: Electronic Networks, Devices and Fields* 32.6 (2019), e2632.

[174]  Xiaodong Yang et al. "Diagnosis of the Hypopnea syndrome in the early stage". In: *Neural Computing and Applications* 32.3 (2020), pp. 855–866.

[175]  Syed Aziz Shah et al. "Sensor Fusion for Identification of Freezing of Gait Episodes using Wi-Fi and Radar Imaging". In: *IEEE Sensors Journal* (2020).

[176] Francesco Fioranelli et al. "Radar sensing for healthcare". In: *Electronics Letters* 55.19 (2019), pp. 1022–1024.

[177] Gianluca Gennarelli, Giovanni Ludeno, and Francesco Soldovieri. "Real-time through-wall situation awareness using a microwave Doppler radar sensor". In: *Remote Sensing* 8.8 (2016), p. 621.

[178] Seong-Hoon Kim and Gi-Tae Han. "1D CNN Based Human Respiration Pattern Recognition using Ultra Wideband Radar". In: *2019 International Conference on Artificial Intelligence in Information and Communication (ICAIIC)*. IEEE. 2019, pp. 411–414.

[179] Paul D Christenson, Cai Xia Yang, and Naima Kaabouch. "A Low Cost Through-Wall Radar for Vital Signs Monitoring". In: *2019 IEEE International Conference on Electro Information Technology (EIT)*. IEEE. 2019, pp. 567–571.

[180] Sami Ekici and Hushang Jawzal. "Breast cancer diagnosis using thermography and convolutional neural networks". In: *Medical Hypotheses* 137 (2020), p. 109542.

[181] Xingliang Liu et al. "Non-Contact Degradation Evaluation for IGBT Modules Using Eddy Current Pulsed Thermography Approach". In: *Energies* 13.10 (2020), p. 2613.

[182] Thiago Alves Elias da Silva et al. "A Computational Method to Assist the Diagnosis of Breast Disease Using Dynamic Thermography". In: *Sensors* 20.14 (2020), p. 3866.

[183] BB Lahiri et al. "Medical applications of infrared thermography: a review". In: *Infrared Physics & Technology* 55.4 (2012), pp. 221–235.

[184] Haiyan Qiu et al. "Clinical and epidemiological features of 36 children with coronavirus disease 2019 (COVID-19) in Zhejiang, China: an observational cohort study". In: *The Lancet Infectious Diseases* (2020).

[185] Jun Chen et al. "Clinical progression of patients with COVID-19 in Shanghai, China". In: *Journal of Infection* (2020).

[186] Preeti Jagadev and Lalat Indu Giri. "Non-contact monitoring of human respiration using infrared thermography and machine learning". In: *Infrared Physics & Technology* 104 (2020), p. 103117.

[187] Anwaar Ulhaq et al. "Computer Vision for COVID-19 Control: A Survey". In: *arXiv preprint arXiv:2004.09420* (2020).

[188] Muhammad Ali Farooq and Peter Corcoran. "Infrared Imaging for Human Thermography and Breast Tumor Classification using Thermal Images". In: *2020 31st Irish Signals and Systems Conference (ISSC)*. IEEE. 2020, pp. 1–6.

[189] Francisco J Rodriguez-Lozano et al. "Non-Invasive forehead segmentation in thermographic imaging". In: *Sensors* 19.19 (2019), p. 4096.

[190] Yu Heng Tao, Anthony J Fitzgerald, and Vincent P Wallace. "Non-contact, non-destructive testing in various industrial sectors with terahertz technology". In: *Sensors* 20.3 (2020), p. 712.

[191] Douglas T Petkie et al. "Remote respiration and heart rate monitoring with millimeter-wave/terahertz radars". In: *Millimetre Wave and Terahertz Sensors and Technology*. Vol. 7117. International Society for Optics and Photonics. 2008, p. 71170I.

[192] Weizhong Yan et al. "FDTD Simulation of Terahertz Wave Propagation in Time-varying Plasma". In: *2019 Photonics & Electromagnetics Research Symposium-Fall (PIERS-Fall)*. IEEE. 2019, pp. 699–701.

[193] Nasir Saeed et al. "Body-Centric Terahertz Networks: Prospects and Challenges". In: (2020).

[194] Sheetal Punia and Hitendra K Malik. "THz radiation generation in axially magnetized collisional pair plasma". In: *Physics Letters A* 383.15 (2019), pp. 1772–1777.

[195] Nick Rothbart et al. "Analysis of human breath by millimeter-wave/terahertz spectroscopy". In: *Sensors* 19.12 (2019), p. 2719.

[196] Catherine Dinh-Le et al. "Wearable health technology and electronic health record integration: scoping review and future directions". In: *JMIR mHealth and uHealth* 7.9 (2019), e12861.

[197] Hui-Jing Qiu et al. "A calibration-free self-powered sensor for vital sign monitoring and finger tap communication based on wearable triboelectric nanogenerator". In: *Nano Energy* 58 (2019), pp. 536–542.

[198] Hyoyoung Jeong, John A Rogers, and Shuai Xu. "Continuous on-body sensing for the COVID-19 pandemic: Gaps and opportunities". In: *Science Advances* 6.36 (2020), eabd4794.

[199] Aditya Kapoor et al. "Digital healthcare: The only solution for better healthcare during COVID-19 pandemic?" In: *Indian Heart Journal* (2020).

[200] Dhruv R Seshadri et al. "Wearable sensors for COVID-19: A call to action to harness our digital infrastructure for remote patient monitoring and virtual assessments". In: *Frontiers in Digital Health* 2 (2020), p. 8.

[201] Anita Woll and Tone Bratteteig. "A trajectory for technology-supported elderly care work". In: *Computer Supported Cooperative Work (CSCW)* 28.1-2 (2019), pp. 127–168.

[202] Giuliano Grossi et al. "Positive technology for elderly well-being: A review". In: *Pattern Recognition Letters* (2019).

[203] Koldo De Miguel et al. "Home camera-based fall detection system for the elderly". In: *Sensors* 17.12 (2017), p. 2864.

[204] Lei Yang, Yanyun Ren, and Wenqiang Zhang. "3D depth image analysis for indoor fall detection of elderly people". In: *Digital Communications and Networks* 2.1 (2016), pp. 24–34.

[205] Carla Taramasco et al. "A novel monitoring system for fall detection in older people". In: *Ieee Access* 6 (2018), pp. 43563–43574.

[206] Panagiotis Tsinganos and Athanassios Skodras. "A smartphone-based fall detection system for the elderly". In: *Proceedings of the 10th International Symposium on Image and Signal Processing and Analysis*. IEEE. 2017, pp. 53–58.

[207] Yafei Ou et al. "Automatic Radiographic Quantification of Joint Space Narrowing Progression in Rheumatoid Arthritis Using POC". In: *2019 IEEE 16th International Symposium on Biomedical Imaging (ISBI 2019)*. IEEE. 2019, pp. 1183–1187.

[208] Faisal Hussain et al. "An Efficient Machine Learning-based Elderly Fall Detection Algorithm". In: *arXiv preprint arXiv:1911.11976* (2019).

[209] Joseph Santiago et al. "Fall detection system for the elderly". In: *2017 IEEE 7th Annual Computing and Communication Workshop and Conference (CCWC)*. IEEE. 2017, pp. 1–4.

[210] Kamal Sehairi, Fatima Chouireb, and Jean Meunier. "Elderly fall detection system based on multiple shape features and motion analysis". In: *2018 International Conference on Intelligent Systems and Computer Vision (ISCV)*. IEEE. 2018, pp. 1–8.

[211] Mohamad Daher et al. "Elder tracking and fall detection system using smart tiles". In: *IEEE Sensors Journal* 17.2 (2016), pp. 469–479.

[212] Noriyuki Okumura et al. "Fall detection and walking estimation using floor vibration for solitary elderly people". In: *2019 IEEE International Conference on Systems, Man and Cybernetics (SMC)*. IEEE. 2019, pp. 1437–1442.

[213] Pramod Kumar Soni and Ayesha Choudhary. "Automated Fall Detection From a Camera Using Support Vector Machine". In: *2019 Second International Conference on Advanced Computational and Communication Paradigms (ICACCP)*. IEEE. 2019, pp. 1–6.

[214] Baris Erol, Moeness G Amin, and Boualem Boashash. "Range-Doppler radar sensor fusion for fall detection". In: *2017 IEEE Radar Conference (RadarConf)*. IEEE. 2017, pp. 0819–0824.

[215] Stéfan van der Walt et al. "scikit-image: image processing in Python". In: *PeerJ* 2 (June 2014), e453. ISSN: 2167-8359. DOI: 10.7717/peerj.453. URL: https://doi.org/10.7717/peerj.453.

[216]  Ali Güneş, Habil Kalkan, and Efkan Durmuş. "Optimizing the color-to-grayscale conversion for image classification". In: *Signal, Image and Video Processing* 10.5 (2016), pp. 853–860.

[217]  Hieu Minh Bui et al. "Using grayscale images for object recognition with convolutional-recursive neural network". In: *2016 IEEE Sixth International Conference on Communications and Electronics (ICCE)*. IEEE. 2016, pp. 321–325.

[218]  Takuya Sakamoto. "Personal identification using ultrawideband radar measurement of walking and sitting motions and a convolutional neural network". In: *arXiv preprint arXiv:2008.02182* (2020).

[219]  Ian T Jolliffe and Jorge Cadima. "Principal component analysis: a review and recent developments". In: *Philosophical Transactions of the Royal Society A: Mathematical, Physical and Engineering Sciences* 374.2065 (2016), p. 20150202.

[220]  Yacine Aıt-Sahalia and Dacheng Xiu. "Principal component analysis of high-frequency data". In: *Journal of the American Statistical Association* 114.525 (2019), pp. 287–303.

[221]  Qizhe Xie et al. "Unsupervised data augmentation". In: *arXiv preprint arXiv:1904.12848* (2019).

[222]  Jiangang Hao and Tin Kam Ho. "Machine Learning Made Easy: A Review of Scikit-learn Package in Python Programming Language". In: *Journal of Educational and Behavioral Statistics* 44.3 (2019), pp. 348–361.

[223]  B Likith Vishal et al. "Image Classification Using Neural Networks and Tensor-flow". In: (2020).

[224]  Torgyn Shaikhina et al. "Decision tree and random forest models for outcome prediction in antibody incompatible kidney transplantation". In: *Biomedical Signal Processing and Control* 52 (2019), pp. 456–462.

[225]  Banu Saçlı et al. "Microwave dielectric property based classification of renal calculi: Application of a kNN algorithm". In: *Computers in biology and medicine* 112 (2019), p. 103366.

[226]  Kunming Li et al. "Research on KNN Algorithm in Malicious PDF Files Classification under Adversarial Environment". In: *Proceedings of the 2019 4th International Conference on Big Data and Computing*. 2019, pp. 156–159.

[227]  Shujun Huang et al. "Applications of support vector machine (SVM) learning in cancer genomics". In: *Cancer Genomics-Proteomics* 15.1 (2018), pp. 41–51.

[228]  Manas Jain et al. "Speech emotion recognition using support vector machine". In: *arXiv preprint arXiv:2002.07590* (2020).

[229] Jiang Wang et al. "Cnn-rnn: A unified framework for multi-label image classification". In: *Proceedings of the IEEE conference on computer vision and pattern recognition.* 2016, pp. 2285–2294.

[230] Shouxiang Wang et al. "Bi-directional long short-term memory method based on attention mechanism and rolling update for short-term load forecasting". In: *International Journal of Electrical Power & Energy Systems* 109 (2019), pp. 470–479.

[231] Peter D Chang et al. "Hybrid 3D/2D convolutional neural network for hemorrhage evaluation on head CT". In: *American Journal of Neuroradiology* 39.9 (2018), pp. 1609–1616.

[232] Aifeng Ren et al. "Machine learning driven approach towards the quality assessment of fresh fruits using non-invasive sensing". In: *IEEE Sensors Journal* 20.4 (2019), pp. 2075–2083.

[233] Maha Elbayad, Laurent Besacier, and Jakob Verbeek. "Pervasive attention: 2d convolutional neural networks for sequence-to-sequence prediction". In: *arXiv preprint arXiv:1808.03867* (2018).

[234] Moslem Azamfar et al. "Multisensor data fusion for gearbox fault diagnosis using 2-D convolutional neural network and motor current signature analysis". In: *Mechanical Systems and Signal Processing* 144 (2020), p. 106861.

[235] Jonas Myhre Christiansen and Graeme E Smith. "Development and Calibration of a Low-Cost Radar Testbed Based on the Universal Software Radio Peripheral". In: *IEEE Aerospace and Electronic Systems Magazine* 34.12 (2019), pp. 50–60.

[236] Sang-Chul Kim. "Device-free activity recognition using CSI & big data analysis: A survey". In: *2017 Ninth International Conference on Ubiquitous and Future Networks (ICUFN)*. IEEE. 2017, pp. 539–541.

[237] Marek Tichy and Karel Ulovec. "OFDM system implementation using a USRP unit for testing purposes". In: *Proceedings of 22nd International Conference Radioelektronika 2012*. IEEE. 2012, pp. 1–4.

[238] Aboajeila Ashleibta et al. "Software Defined Radio Based Testbed for Large Scale Body Movements". In: (2020).

[239] Shujaat Ali Khan Tanoli et al. "An experimental channel capacity analysis of cooperative networks using Universal Software Radio Peripheral (USRP)". In: *Sustainability* 10.6 (2018), p. 1983.

[240] Luca Pappalardo. "SCIKIT-MOBILITY: A PYTHON LIBRARY FOR THE ANALYSIS, GENERATION AND RISK ASSESSMENT OF MOBILITY DATA". In: *arXiv preprint arXiv:1907.07062* (2019).

[241] Yasir Hamid, M Sugumaran, and VR Balasaraswathi. "Ids using machine learning-current state of art and future directions". In: *Current Journal of Applied Science and Technology* (2016), pp. 1–22.

[242] Asma Abbas Hassan, Alaa F Sheta, and Talaat M Wahbi. "Intrusion Detection System Using Weka Data Mining Tool". In: *Internaitonal Journal of Science and Research (IJSR)* 6.9 (2017), pp. 2319–7064.

[243] Saroj Kr Biswas. "Intrusion detection using machine learning: A comparison study". In: *International Journal of Pure and Applied Mathematics* 118.19 (2018), pp. 101–114.

[244] Sakshi Tandon et al. "Bitcoin Price Forecasting using LSTM and 10-Fold Cross validation". In: *2019 International Conference on Signal Processing and Communication (ICSC)*. IEEE. 2019, pp. 323–328.

[245] Thanasis Vafeiadis et al. "A comparison of machine learning techniques for customer churn prediction". In: *Simulation Modelling Practice and Theory* 55 (2015), pp. 1–9.

[246] Davide Anguita et al. "A public domain dataset for human activity recognition using smartphones." In: *Esann*. 2013.

[247] Yu Taso et al. "Subcarrier selection for efficient CSI-based indoor localization". In: *IOP Conference Series: Materials Science and Engineering*. Vol. 383. 1. IOP Publishing. 2018, p. 012017.

[248] Mehran Soltani et al. "Deep learning-based channel estimation". In: *IEEE Communications Letters* 23.4 (2019), pp. 652–655.

[249] Yan Wang et al. "E-eyes: device-free location-oriented activity identification using fine-grained wifi signatures". In: *Proceedings of the 20th annual international conference on Mobile computing and networking*. 2014, pp. 617–628.

[250] Itaf Omar Joudeh et al. "Location Independence in Machine Learning Classification of Sitting-Down and Standing-Up Actions using Wi-Fi Sensors". In: *2021 IEEE International Symposium on Medical Measurements and Applications (MeMeA)*. IEEE. 2021, pp. 1–6.

[251] Yanzhao Wang et al. "WiFi indoor localization with CSI fingerprinting-based random forest". In: *Sensors* 18.9 (2018), p. 2869.

[252] Robert M Keenan and Le-Nam Tran. "Fall detection using Wi-Fi signals and threshold-based activity segmentation". In: *2020 IEEE 31st Annual International Symposium on Personal, Indoor and Mobile Radio Communications*. IEEE. 2020, pp. 1–6.

[253] Sheheryar Arshad et al. "Wi-chase: A WiFi based human activity recognition system for sensorless environments". In: *2017 IEEE 18th International Symposium on A World of Wireless, Mobile and Multimedia Networks (WoWMoM)*. IEEE. 2017, pp. 1–6.

[254] Baha A Alsaify et al. "A CSI-Based Multi-Environment Human Activity Recognition Framework". In: *Applied Sciences* 12.2 (2022), p. 930.

[255] Renzo Phellan et al. "Real-time biomechanics using the finite element method and machine learning: Review and perspective". In: *Medical Physics* 48.1 (2021), pp. 7–18.

[256] Jieming Yang et al. "A framework for human activity recognition based on WiFi CSI signal enhancement". In: *International Journal of Antennas and Propagation* 2021 (2021).

[257] Shunuo Shang et al. "LSTM-CNN network for human activity recognition using WiFi CSI data". In: *Journal of Physics: Conference Series*. Vol. 1883. 1. IOP Publishing. 2021, p. 012139.

[258] Qinyi Xu et al. "Indoor events monitoring using channel state information time series". In: *IEEE Internet of Things Journal* 6.3 (2019), pp. 4977–4990.

[259] Rita Murri et al. "A real-time integrated framework to support clinical decision making for covid-19 patients". In: *Computer Methods and Programs in Biomedicine* 217 (2022), p. 106655.

[260] Omar H Salman et al. "A review on utilizing machine learning technology in the fields of electronic emergency triage and patient priority systems in telemedicine: Coherent taxonomy, motivations, open research challenges and recommendations for intelligent future work". In: *Computer Methods and Programs in Biomedicine* 209 (2021), p. 106357.

[261] Senzhong Gan, Qingbin Zhuang, and Bingyan Gong. "Human-computer interaction based interface design of intelligent health detection using PCANet and multi-sensor information fusion". In: *Computer Methods and Programs in Biomedicine* (2022), p. 106637.

[262] Bogdan Kwolek and Michal Kepski. "Human fall detection on embedded platform using depth maps and wireless accelerometer". In: *Computer methods and programs in biomedicine* 117.3 (2014), pp. 489–501.

[263] Yong Wang et al. "An Encryption Method of Power Cloud Data Based on n-RSA". In: *Advances in Intelligent Information Hiding and Multimedia Signal Processing: Proceeding of the 16th International Conference on IIHMSP in conjunction with the 13th international conference on FITAT, November 5-7, 2020, Ho Chi Minh City, Vietnam, Volume 1*. Vol. 211. Springer. 2021, p. 416.

[264] K Jaspin et al. "Efficient and Secure File Transfer in Cloud Through Double Encryption Using AES and RSA Algorithm". In: *2021 International Conference on Emerging Smart Computing and Informatics (ESCI)*. IEEE. 2021, pp. 791–796.

[265] Muhammad Faraz Hyder, Syeda Tooba, et al. "Performance Evaluation of RSA-based Secure Cloud Storage Protocol using OpenStack". In: *Engineering, Technology & Applied Science Research* 11.4 (2021), pp. 7321–7325.

[266] Raghav Sharma et al. "Electrically connected spin-torque oscillators array for 2.4 GHz WiFi band transmission and energy harvesting". In: *Nature communications* 12.1 (2021), pp. 1–10.

[267] Sriram Ramgopal et al. "Use of a metalearner to predict emergency medical services demand in an urban setting". In: *Computer Methods and Programs in Biomedicine* 207 (2021), p. 106201.

[268] Yaowen Mei et al. "WiWave: WiFi-based Human Activity Recognition Using the Wavelet Integrated CNN". In: *2021 IEEE/CIC International Conference on Communications in China (ICCC Workshops)*. IEEE. 2021, pp. 100–105.

[269] Darius Nahavandi et al. "Application of artificial intelligence in wearable devices: Opportunities and challenges". In: *Computer Methods and Programs in Biomedicine* 213 (2022), p. 106541.

[270] Umar Hussain Mir, Deep Singh, and Parveiz Nazir Lone. "Color image encryption using RSA cryptosystem with a chaotic map in Hartley domain". In: *Information Security Journal: A Global Perspective* (2021), pp. 1–15.

[271] KL Neela and V Kavitha. "An Improved RSA Technique with Efficient Data Integrity Verification for Outsourcing Database in Cloud". In: *Wireless Personal Communications* (2022), pp. 1–18.

[272] Guodong Ye et al. "An asymmetric image encryption algorithm based on a fractional-order chaotic system and the RSA public-key cryptosystem". In: *International Journal of Bifurcation and Chaos* 30.15 (2020), p. 2050233.

[273] Jennifer Gonik Chester and James L Rudolph. "Vital signs in older patients: age-related changes". In: *Journal of the American Medical Directors Association* 12.5 (2011), pp. 337–343.

[274] Cristiano André Da Costa et al. "Internet of health things: toward intelligent vital signs monitoring in hospital wards". In: *Artificial intelligence in medicine* 89 (2018), pp. 61–69.

[275] Ali M Ansary, Joseph N Martinez, and John D Scott. "The virtual physical exam in the 21st century". In: *Journal of Telemedicine and Telecare* 27.6 (2021), pp. 382–392.

[276] Cristiane Chagas Teixeira et al. "Vital signs measurement: an indicator of safe care delivered to elderly patients". In: *Texto & Contexto-Enfermagem* 24 (2015), pp. 1071–1078.

[277] Una Kyriacos, J Jelsma, and S Jordan. "Monitoring vital signs using early warning scoring systems: a review of the literature". In: *Journal of nursing management* 19.3 (2011), pp. 311–330.

[278]   Ahmed Youssef Ali Amer et al. "Vital signs prediction and early warning score calcu-
        lation based on continuous monitoring of hospitalised patients using wearable technol-
        ogy". In: *Sensors* 20.22 (2020), p. 6593.

[279]   Jie Li et al. "Low-cost wearable device based D-shaped single mode fiber curvature
        sensor for vital signs monitoring". In: *Sensors and Actuators A: Physical* 337 (2022),
        p. 113429.

[280]   Fleur Jacobs et al. "Reliability of heart rate and respiration rate measurements with a
        wireless accelerometer in postbariatric recovery". In: *PLoS One* 16.4 (2021), e0247903.

[281]   Gordon B Drummond et al. "Classifying signals from a wearable accelerometer device
        to measure respiratory rate". In: *ERJ Open Research* 7.2 (2021).

[282]   Atefeh Valipour and Keivan Maghooli. "Vital Signs Monitoring based on a Developed
        Accelerometer Sensor for Sporty Purposes". In: *Journal of Orthopaedics and Sports
        Medicine* 1.3 (2019), pp. 51–59.

[283]   Adeel Ahmad et al. "Vital signs monitoring of multiple people using a FMCW millimeter-
        wave sensor". In: *2018 IEEE Radar Conference (RadarConf18)*. IEEE. 2018, pp. 1450–
        1455.

[284]   Yuanqing Zheng and Yanwen Wang. "RFID-based vital signs monitoring". In: *Contact-
        less Vital Signs Monitoring* (2022), pp. 257–279.

[285]   Xuyu Wang, Chao Yang, and Shiwen Mao. "On CSI-based vital sign monitoring us-
        ing commodity WiFi". In: *ACM Transactions on Computing for Healthcare* 1.3 (2020),
        pp. 1–27.

[286]   Xiaonan Hui and Edwin C Kan. "Monitoring vital signs over multiplexed radio by near-
        field coherent sensing". In: *Nature Electronics* 1.1 (2018), pp. 74–78.

[287]   Xuyu Wang, Chao Yang, and Shiwen Mao. "PhaseBeat: Exploiting CSI phase data for
        vital sign monitoring with commodity WiFi devices". In: *2017 IEEE 37th International
        Conference on Distributed Computing Systems (ICDCS)*. IEEE. 2017, pp. 1230–1239.

[288]   Julio CH Soto et al. "A survey on vital signs monitoring based on Wi-Fi CSI data". In:
        *Computer Communications* 195 (2022), pp. 99–110.

[289]   Ashikur Rahman et al. "Signal processing techniques for vital sign monitoring using mo-
        bile short range Doppler radar". In: *2015 IEEE Topical Conference on Biomedical Wire-
        less Technologies, Networks, and Sensing Systems (BioWireleSS)*. IEEE. 2015, pp. 1–
        3.

[290]   Hisham Abuella and Sabit Ekin. "Non-contact vital signs monitoring through visible
        light sensing". In: *IEEE Sensors Journal* 20.7 (2019), pp. 3859–3870.

[291]  Rahel Gilgen-Ammann, Theresa Schweizer, and Thomas Wyss. "RR interval signal quality of a heart rate monitor and an ECG Holter at rest and during exercise". In: *European journal of applied physiology* 119.7 (2019), pp. 1525–1532.